General Disclaimer

One or more of the Following Statements may affect this Document

- This document has been reproduced from the best copy furnished by the organizational source. It is being released in the interest of making available as much information as possible.

- This document may contain data, which exceeds the sheet parameters. It was furnished in this condition by the organizational source and is the best copy available.

- This document may contain tone-on-tone or color graphs, charts and/or pictures, which have been reproduced in black and white.

- This document is paginated as submitted by the original source.

- Portions of this document are not fully legible due to the historical nature of some of the material. However, it is the best reproduction available from the original submission.

NASA CR-144376
MDC E1198

EVALUATION AND STUDY OF ADVANCED OPTICAL CONTAMINATION, DEPOSITION, MEASUREMENT, AND REMOVAL TECHNIQUES

by

R.M.F. LINFORD, T.H. ALLEN AND C.F. DILLOW

MCDONNELL DOUGLAS ASTRONAUTICS COMPANY - EAST

Saint Louis, Missouri

Contract NAS 9-13606

May 1975

Final Report

prepared for

NATIONAL AERONAUTICS AND SPACE ADMINISTRATION

LYNDON B. JOHNSON SPACE CENTER

1. Report No.	2. Government Accession No.	3. Recipient's Catalog No.

4. Title and Subtitle

EVALUATION AND STUDY OF ADVANCED OPTICAL CONTAMINATION, DEPOSITION, MEASUREMENT, AND REMOVAL TECHNIQUES

5. Report Date
May 1975

6. Performing Organization Code

7. Author(s)
R. M. F. Linford, T. H. Allen, C. F. Dillow

8. Performing Organization Report No.
MDC E1198

10. Work Unit No.

9. Performing Organization Name and Address
McDonnell Douglas Astronautics Company - East
St. Louis, Missouri 63166

11. Contract or Grant No.
NAS9-13606

13. Type of Report and Period Covered
Contractor Report
June 1973 - April 1975

12. Sponsoring Agency Name and Address
National Aeronautics and Space Administration
Washington, D. C. 20546

14. Sponsoring Agency Code

15. Supplementary Notes
Contracting Officer Representative R. G. Richmond, NASA
Johnson Space Center, Houston, Texas

16. Abstract

A program is described to design, fabricate and install an experimental Work Chamber Assembly (WCA) to provide a wide range of experimental capability. The WCA incorporates several techniques for studying the kinetics of contaminant films and their effect on optical surfaces. It incorporates the capability for depositing both optical and contaminant films on temperature-controlled samples, and for in-situ measurements of the vacuum ultraviolet reflectance. Ellipsometer optics are mounted on the chamber for film thickness determinations, and other features include access ports for radiation sources and instrumentation. Several supporting studies were conducted to define specific chamber requirements, to determine the sensitivity of the measurement techniques to be incorporated in the chamber, and to establish procedures for handling samples prior to their installation in the chamber. A bibliography and literature survey of contamination-related articles is included.

17. Key Words (Suggested by Author(s))	18. Distribution Statement
Contamination - Spacecraft Facilities - Contamination Test Optics - Contamination Induced Degradation Reflection - Ultraviolet Far Ultraviolet Reflectometer Ellipsometers - Contamination Measuring Instrument	Unclassified - Unlimited

19. Security Classif. (of this report)	20. Security Classif. (of this page)	21. No. of Pages	22. Price*
Unclassified	Unclassified	70	

*For sale by the National Technical Information Service, Springfield. Virginia 22151

Copy No. 57

NASA — JSC

TABLE OF CONTENTS

TABLE OF CONTENTS (Continued)

LIST OF PAGES

Title Page

ii - vii

1 - 70

A1 - A5

B1 - B2

C1 - C19

ILLUSTRATIONS

ILLUSTRATIONS (Continued)

TABLES

1.0 INTRODUCTION

As the duration of space missions has increased and payloads have become more complex, the contamination of optical surfaces on spaceborne systems has emerged as a significant problem. Outgassed contaminants from non-metallic materials on a spacecraft generate an artificial "atmosphere" around the vehicles, and these contaminants subsequently condense on exposed or cooled surfaces. The problem is compounded if the condensed contaminants are exposed to energetic radiation (solar ultraviolet, electron and proton radiation), because such exposure can polymerize the films and inhibit the natural re-evaporation processes, which might otherwise reduce the buildup of contamination. Most space vehicles are also subjected to prelaunch testing in space simulation chambers, and during such testing there is risk of significant contamination from outgassing of polymeric materials in the chamber and from backstreaming of vacuum pump oils.

Optical surfaces are particularly sensitive to the effects of contaminant deposition as lenses, mirrors, detectors and windows can all be significantly degraded by thin organic films. The most serious effects are experienced by systems operating at ultraviolet wavelengths, where absorption and scattering of the optical radiation is very significant, even with contaminant films just a few hundred angstroms thick.[1]

Cleaning of surfaces contaminanted during space simulation testing is often difficult and expensive, and cleaning surfaces contaminated in space is usually impossible. Therefore, it is important that the dynamics of contaminants and their effects be studied and understood, so that the design and testing of space vehicles can be modified to reduce the risk of degradation.

As part of an ongoing program to study contamination phenomena, an experimental vacuum chamber has been designed and fabricated to provide a wide range of experimental capability. This Work Chamber Assembly (WCA) was conceived to establish the proof-of-principle of various techniques for studying the kinetics of contaminants and their effects. It incorporates the capability for depositing both optical and contaminant films on temperature-controlled samples, and for in-situ measurements of the vacuum ultraviolet reflectance. Ellipsometer optics are mounted on the chamber for film thickness determinations, and other features include access ports for radiation sources and instrumentation.

In support of the chamber design, several studies were conducted to define specific chamber requirements, to determine the sensitivity of the measurement techniques to be incorporated in the chamber, and to establish procedures for handling samples prior to their installation in the chamber. These studies included combined Auger electron spectroscopy and ellipsometry measurements, ultraviolet reflectance measurements on contaminated surfaces, and a study of the cleaning and storing of metal samples prior to testing.

This report includes a description of the supportive studies, the design and fabrication of the WCA, the development of an ellipsometer data reduction system and the fabrication of a vacuum ultraviolet reflectometer.

2.0 PRELIMINARY TASKS

Before embarking on the major tasks of the program, several preliminary tasks were undertaken. These included:

- o Bibliography and Literature Survey - an examination and cataloging of current literature on contamination phenomena
- o Mirror Fabrication - the vacuum deposition of quantities of small mirror samples for delivery to JSC
- o Development of the Vapor Effusion Source - an effort to improve on the design of sources for repeatable and uniform deposition of organic contaminant films.

2.1 BIBLIOGRAPHY AND LITERATURE SURVEY. A literature search was conducted at several facilities including: the McDonnell Douglas Research and Engineering Library (MDREL) in St. Louis; the Douglas Aircraft computerized data retrieval system in Long Beach, California; and the NASA Scientific and Technical Information Division's Literature Search #22974, 17 July 1973.

The MDREL search produced over 50 abstracts of papers and reports on contamination phenomena that are included in the library collection. Selected papers from this list were reviewed and/or copied. Very few references were generated by the computer search at Long Beach, but a total of 41 references were listed in NASA Literature Search #22974. Many of these references were sought for a detailed review.

The references compiled from the papers reviewed are assembled in the bibliography and included as Appendix A. Classifications were selected for the references as follows:

- o Sources
  - o rocket plumes
  - o ablators
  - o organics
  - o cryodeposits
- o Surfaces
  - o optical systems
  - o sensors
  - o thermal control coatings

- Experimental
  - measurement techniques
  - contamination monitoring
  - cleaning techniques
- Theoretical
  - analytical techniques
  - contamination kinetics
- General
  - space radiation effects

2.2 MIRROR FABRICATION. A series of vacuum-deposited mirrors were fabricated in support of contamination experiments being conducted at NASA-JSC. All the mirrors were deposited on 1-inch diameter, 1/8-inch thick fused silica substrates. Two batches of mirrors were fabricated and delivered to JSC as follows:

- 50 aluminum mirrors overcoated with magnesium fluoride to an optical thickness of 1/2 wave at 1216Å.
- 50 aluminum mirrors overcoated with magnesium fluoride to an optical thickness of 3/4 wave at 1216Å.

2.3 VAPOR EFFUSION SOURCE DEVELOPMENT. Of prime importance in the study of thin film molecular contamination of optical surfaces is the deposition of uniform thin organic films in a controlled and reproducible manner. This is accomplished using a vapor effusion source, consisting of a heated oven to produce molecular vapors, and an effusion nozzle to direct the molecular vapors toward the substrate. The original vapor effusion source (VES) design in use at MDC-St. Louis had several limitations; in particular, the single orifice nozzle limited the uniformity of the deposited films, and the shutter design resulted in excessive contamination of the vacuum system due to leakage of contaminant flux. The purpose of this task was to develop an improved version of this important component.

2.3.1 Analytical Treatment

Single Orifice. The radial thickness distribution t(r), of a deposited film from a single orifice of finite area is given by the equation:

$$t(r) = \frac{m \cos\gamma \cos\theta}{\rho \pi h^2} \qquad (2\text{-}1)$$

where m is the total mass deposited per unit solid angle, ρ is the density of the film, γ and θ are the emission and incident angles respectively, and h is the

distance between the orifice and the area deposited. These parameters are identified in Figure 2-1 and it is apparent that $\gamma = \theta$ and $h^2 = \ell^2 + r^2$, where h is the source to sample distance. Therefore, Equation 2-1 reduces to:

$$t(r) = \frac{m \cos^2 \theta}{\rho \pi (\ell^2 + r^2)} \tag{2-2}$$

At the center of the sample, r = 0:

$$t(0) = \frac{m}{\rho \pi \ell^2} \tag{2-3}$$

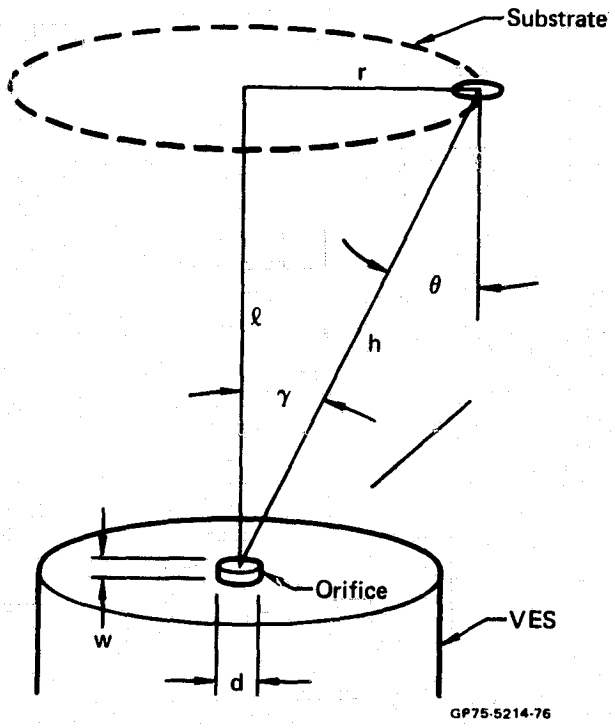

FIGURE 2-1 – GEOMETRY OF SINGLE ORIFICE SOURCES

The emission angle, γ, is limited by the finite wall thickness, w, of the orifice and is given by the expression:

$$\gamma = \tan^{-1} \left(\frac{d}{2w}\right) \tag{2-4}$$

where d is the orifice diameter.

Unfortunately, many single orifice effusion sources do not obey the cosine law as given by Equation 2-2. This is due to a number of effects such as interaction of the molecular flux with the orifice wall and the residual chamber gases. In view of the complexity of these interactions one can use the cosine law only as a first order approximation and must make experimental measurements for an accurate determination of the flux distribution. The flux at the center of the sample can be predicted from Equation 2-3 if the correction factor $W = \frac{1}{(1 + \frac{3w}{4d})}$ is applied, so that $t(0) = \frac{Wm}{\rho \pi \ell^2}$.

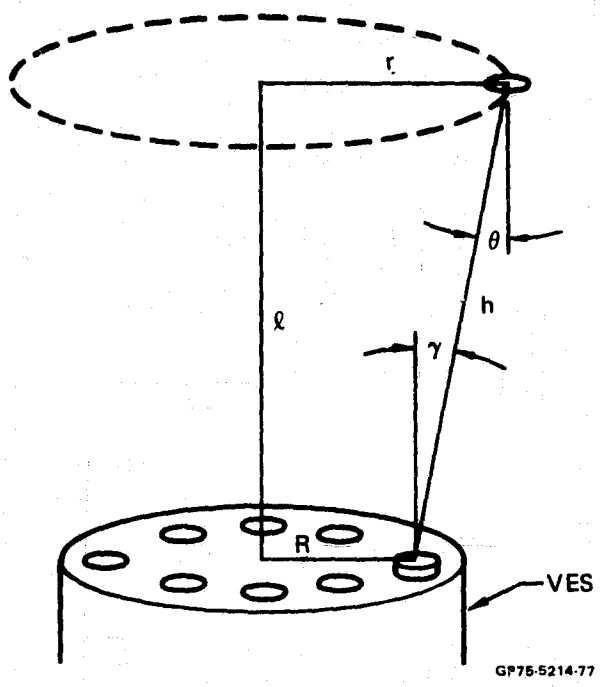

FIGURE 2-2 – GEOMETRY OF MULTIPLE ORIFICE SOURCES

Multiple Orifices. The multiple-orifice nozzle consists of a series of single orifices equally spaced around the circumference of a circle of radius R (Figure 2-2). The contribution of each orifice to the radial distribution of the deposited film is given by:

$$dt(r) = \frac{m\ell^2}{2\rho\pi^2 h^4} \, d\theta \qquad (2\text{-}5)$$

The total radial distribution can be shown to be:

$$t(r) = \frac{m\ell^2}{2\rho\pi^2} \int_0^{\pi} \frac{2\, d\theta}{[\ell^2 + (R+r)^2 - 4\, Rr \sin^2(\theta/2)]^2}$$

$$= \frac{m\ell^2}{2\rho\pi} \cdot \frac{2\ell^2 + (r+R)^2 + (r-R)^2}{[\ell^2 + (r+R)^2]^{3/2}\,[\ell^2 + (r-R)^2]^{3/2}} \qquad (2\text{-}6)$$

At the center of the sample, r = 0.

$$t(0) = \frac{m^2}{\rho\pi} \cdot \frac{1}{(\ell^2 + R^2)^2} \qquad (2\text{-}7)$$

The variations of t(r) for several values of ℓ and R are shown in Figure 2-3. As with the single nozzle equations, the wall thickness of the orifices modifies the distribution represented in Equation 2-6.

2.3.2 Selection of Nozzle Designs. The selection of any one specific type of effusion nozzle geometry depends on the type of measurement to be made. For measurements requiring thickness uniformity over a small area, as in the case of ellipsometric measurements, the choice of orifice design is not critical. However, for experiments requiring uniformity over a larger area a multiple nozzle source can be used to advantage.

Both types of effusion nozzle were selected for experimental evaluation. A single orifice was made with a diameter of 1.1 mm and a wall thickness of 1.1 mm. The field angle of this orifice, as defined by Equation 2-4, was 90° so that the vapors from the nozzle were deposited over an area 100 mm in diameter on a sample placed 50 mm from the source. The multiple-orifice nozzle consisted of ten orifices each 0.5 mm diameter, 0.5 mm wall thickness, equally spaced on a 10 mm circle. Results of the evaluation are given in paragraph 2.3.4.

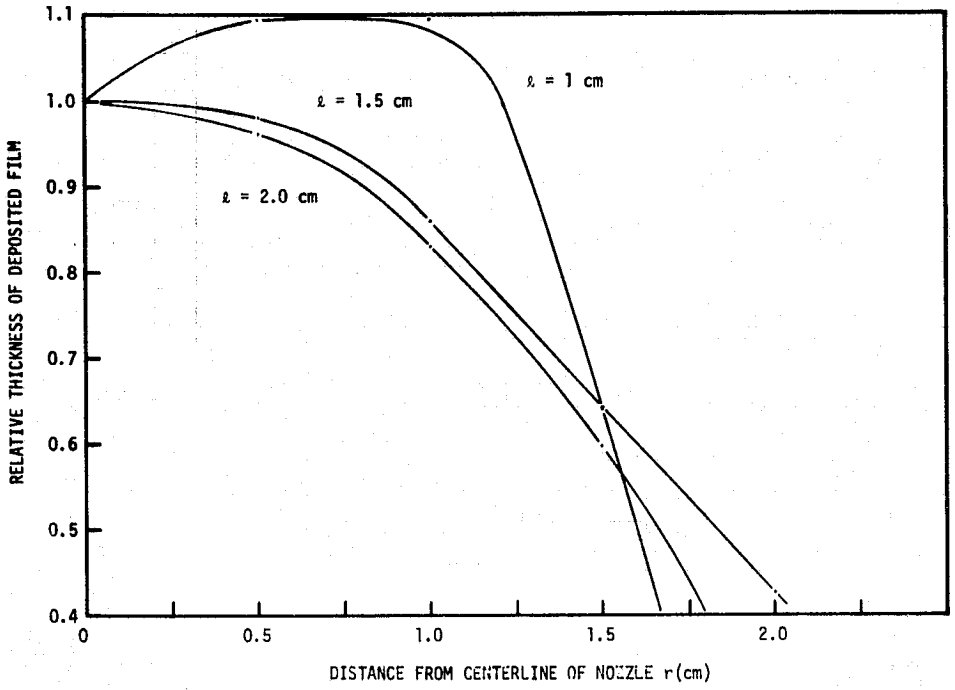

FIGURE 2-3 – PREDICTED DISTRIBUTION OF FILMS DEPOSITED WITH A MULTIPLE NOZZLE VES WITH R = 1 cm

2.3.3 Improved Vapor Effusion Source Design. A new VES design (Figure 2-4) was prepared and it included the following improved features: a shield and rotary shutter manifold which collected the contaminant fluxes between deposition cycles, a demountable effusion nozzle replacing the single fixed orifice of the original design, six heaters (compared with four previously) to ensure uniform heating, and removable components to facilitate cleaning.

A VES was manufactured to the design shown in Figure 2-4 and was installed in an ellipsometer chamber for evaluation; this installation is illustrated in Figure 2-5. The shutter manifold was supported on a rotary vacuum passthrough located in the port directly behind the VES. The tube shown extending from the front of the shutter provided a vapor bypass from the shutter/manifold to the pumping port, to remove volatiles when the shutter was closed.

2.3.4 Evaluation of the Vapor Effusion Source. An evaluation of the new VES was undertaken in the vacuum ellipsometer illustrated in Figure 2-5. A series of experiments were conducted using both the single and multi-orifice nozzles. The working fluid was Dow Corning DC-705 diffusion pump oil. Thin films of DC-705 were deposited onto a gold-coated silica substrate mounted

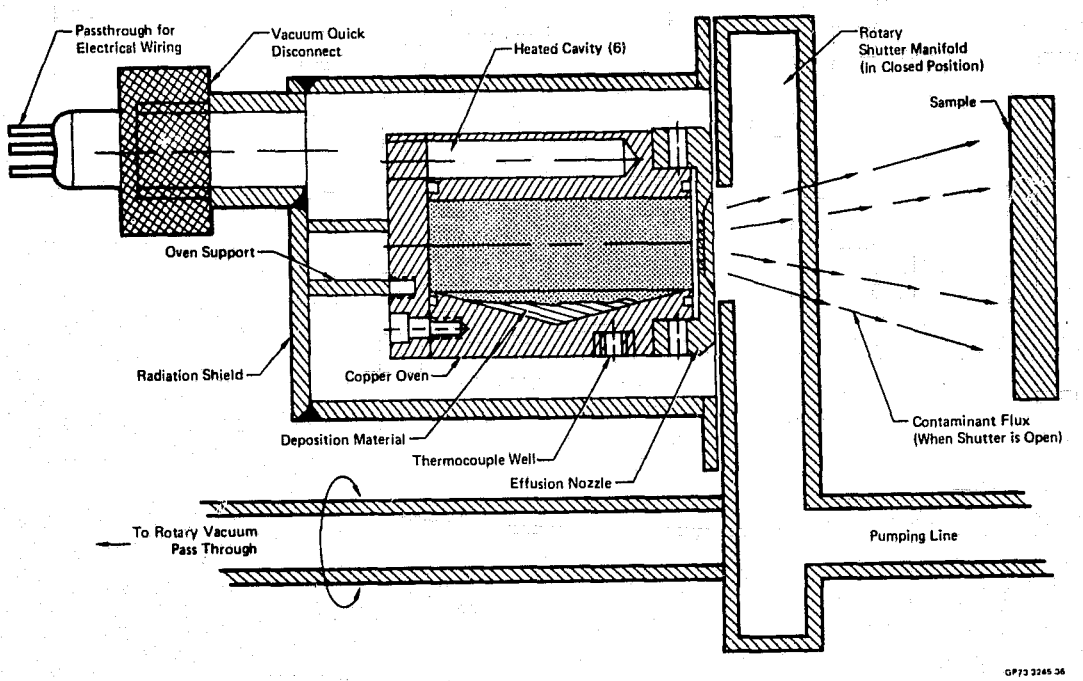

FIGURE 2-4 – IMPROVED VES DESIGN

50mm from the VES nozzle with the VES temperature set at 130°C (403K), the deposition rates were 8 and 11Å/min for the single and multiple-orifice nozzle respectively.

The uniformity of the deposited film was determined by scanning across the sample with the 2mm diameter ellipsometer laser beam. Results of these measurements are summarized in Figure 2-6. Some scatter is obvious in the data and this was probably due as much to instabilities in the DC-705 film as to measurement errors. (Prior experience in the MDAC-E laboratories has indicated that DC-705 films often take several hours to reach equilibrium) Over the central area of the sample, up to approximately 4mm radius, the single nozzle provided a uniform flux within 2 or 3%. Beyond an 8mm radius the measured thickness dropped off even more severely than the theoretical cosine distribution. In contrast the multiple orifice nozzle provided moderately good uniformity over a 12mm radius, but fell well below the theoretical curve at the 17mm radius. As discussed earlier, the departure from the theory can be attributed to the finite wall thickness of the orifices.

FIGURE 2-5 - SECOND GENERATION VES INSTALLED IN THE ELLIPSOMETER CHAMBER

The VES developed in this study has been in frequent use since this evaluation and has performed extremely well in a variety of applications. However, during the design of the Work Chamber Assembly (WCA) new design constraints were introduced and the VES assembly for the WCA was further modified. Details of the changes are discussed in Section 4.4.

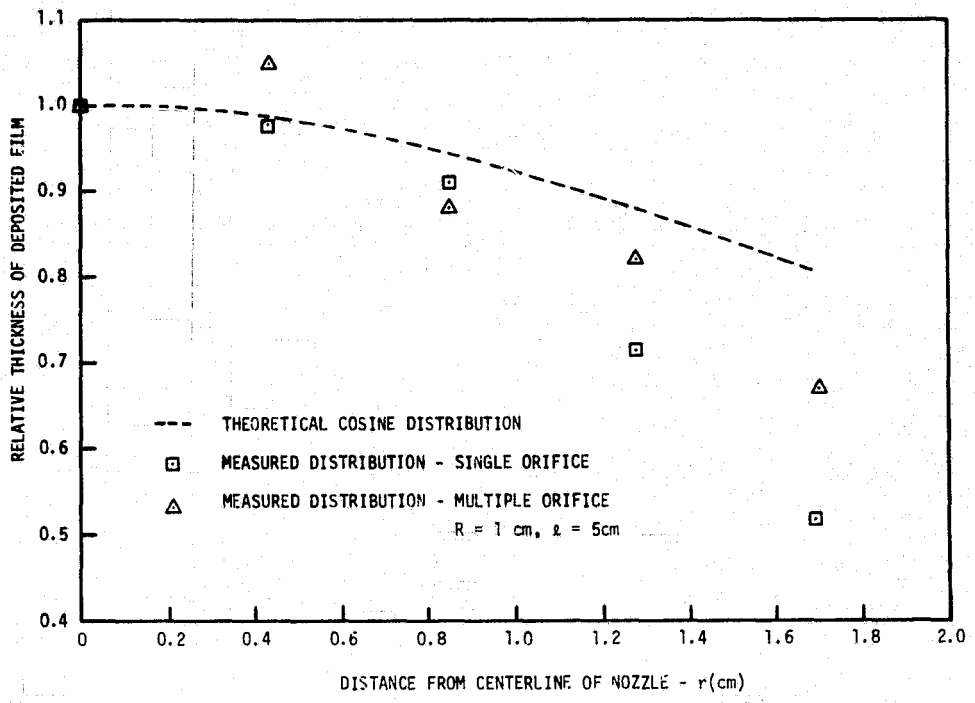

FIGURE 2-6 – MEASURED THICKNESS DISTRIBUTION OF DC-705 FILM DEPOSITED WITH VES

3.0 SUPPORTIVE STUDIES

The design requirements for the WCA included the integration of several sophisticated items of equipment, and the proposed utilization of the finished hardware also imposed severe demands on the design. To support and verify the WCA design concepts, a series of supportive studies was undertaken, and the results of these efforts became the basis of the design. In particular, the following studies were performed:

- o Inert Gas Storage Study - to examine the oxidation of metallic mirror coatings.
- o Reflectance Studies - to determine the effect of contaminant films on the reflectance of aluminum mirrors at vacuum ultraviolet, ultraviolet, and visible wavelengths, as a basis for designing a VUV reflectometer for the WCA.
- o Sensitivity Studies - to determine the sensitivity of Auger electron spectroscopy and ellipsometry for measurements on thin contaminant films, as a basis for selecting which of the instruments might be selected for integration with the WCA.
- o Optical Cleaning Studies - to examine methods of removing contaminants from optical surfaces.
- o Pumping Study - to select the optimum pumping system for the WCA.

Details of these studies are included in the sections that follow.

3.1 STORAGE STUDY. Clean aluminum surfaces are extremely active chemically and will oxidize even in a high vacuum environment. The reflectance of aluminum coated mirrors such as those used in solar simulation systems can be degraded by oxide formation and one potential use of the WCA is for studies for such phenomena. The ability to deposit metal films and measure their optical properties in-situ was to be incorporated into the WCA unless samples could be prepared, and then preserved by storage in an inert atmosphere. To examine this problem a storage study was undertaken.

Storage studies were conducted in air, argon, and nitrogen using specially designed environmental chambers, as shown in Figure 3-1. Each sample was supported on a nichrome support attached to a rubber stopper inserted in an aperture in the wall of the plexiglass box. Commercial grade argon and nitrogen gases were passed through two of the containers, over the samples, and out

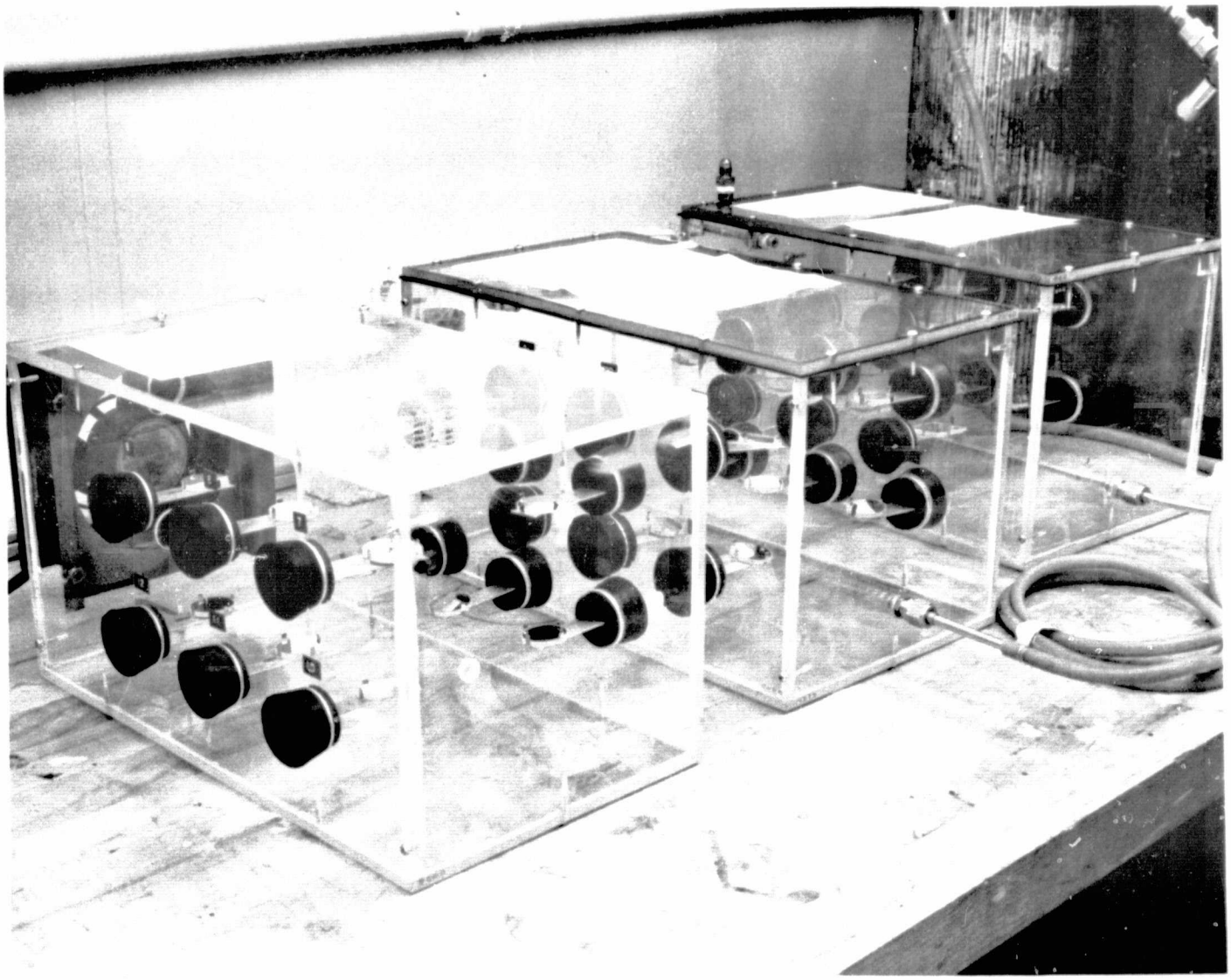

FIGURE 3-1 – STORAGE CONTAINERS

through a mercury bubbler (neither oil nor water bubblers were used because of possible contamination of the samples). Filtered air was drawn through the third box using a small fan (this container was normally kept in a laminar flow bench; it was removed for the photograph).

A total of 36 samples were prepared by vapor depositing approximately 1100 Å of aluminum onto a fused silica substrate, at 2×10^{-7} torr, in an ion-pumped vacuum chamber. Each sample substrate was cleaned with organic solvents (acetone and propanol) prior to installation in the vacuum chamber.

The samples were deposited in three separate batches, and each batch was mounted in one of the three environmental chambers. A pair of samples from each batch was measured on the ellipsometer to determine the initial film thickness prior to storage and after various elapsed storage times up to 1000 hours. The results of these measurements are summarized in Table I.

These measurements show that the final thickness after 1000 hours of storage was not significantly different for air, nitrogen or argon. Moreover, the initial ellipsometric measurements indicated that the majority of the oxide growth occurred within an hour after removal from the vapor deposition system, while the samples were being transported to the environmental chambers.

Elapsed Storage Time (Hours)	Average Measured Oxide Thickness (Å)		
	Air	Argon	Nitrogen
0	54	55	50
12	64	58	60
26	65	58	63
52	70	57	54
95	67	54	55
237	69	61	65
500	71	64	61
1000	64	60	56

GP75-5214-51

TABLE I
GROWTH OF OXIDE FILM ON ALUMINUM FILMS IN VARIOUS STORAGE ENVIRONMENTS

The results of the study demonstrate the extreme difficulty in preserving an oxide-free surface if a sample is handled in the laboratory environment, even for a brief period. It was evident from the tests that fresh films must be deposited and measured in-situ without breaking the vacuum. The WCA was subsequently designed to provide this feature.

3.2 REFLECTANCE STUDIES. Thin contaminant films can severely degrade the reflectance properties of optical surfaces, especially at vacuum ultraviolet and ultraviolet wavelengths. The capability for studying such phenomena was to be included in the WCA design, and the reflectance studies were undertaken as a basis for selecting the design parameters. A series of experiments were performed on the reflectance of mirror substrates contaminanted with organic films of varying thickness. The results of these measurements led to the selection of an integrating-sphere reflectometer design.

3.2.1 Experimental Procedure. The vacuum reflectometer assembled for this study is illustrated diagrammatically in Figure 3-2. A 16-inch diameter stainless steel chamber was fabricated and equipped with a vapor effusion source (VES), shutter and liquid nitrogen cooled baffles. A lead-screw sample translation stage, driven through a magnetically-coupled rotary pass through, allowed the movement of an optical sample behind the baffles for contaminant deposition. This arrangement restricted the organic vapors to the annex which was connected directly to the pumping line of a turbomolecular pump. For reflectance measurements the sample was returned to the center of the chamber where a spring-loaded device rotated the sample to a preselected angle relative to the incident light. A small, rugged photomultiplier (RCA 8571) was mounted on a swivel arm supported on a rotary pass through in the base of the chamber. The acceptance angle of this detector was 3°, allowing angular reflectance measurements of moderate resolution. For measurements at wavelengths below 350 nm a sodium salicylate coated silica window was installed directly in front of the photocathode; for measurements at longer wavelengths a silica diffuser plate was used to ensure uniform illumination of the photocathode.

Radiation from the exit slit of a McPherson Model 225 Scanning Monochromator was focussed on the surface of the sample with an f/3.2 mirror in the vacuum elbow. An 800 Hz tuning fork chopper modulated the radiation in the plane of the exit slit and a lock-in amplifier was used to monitor the output of the photomultiplier detector. To cover the spectral range required, 120nm to 600 nm,

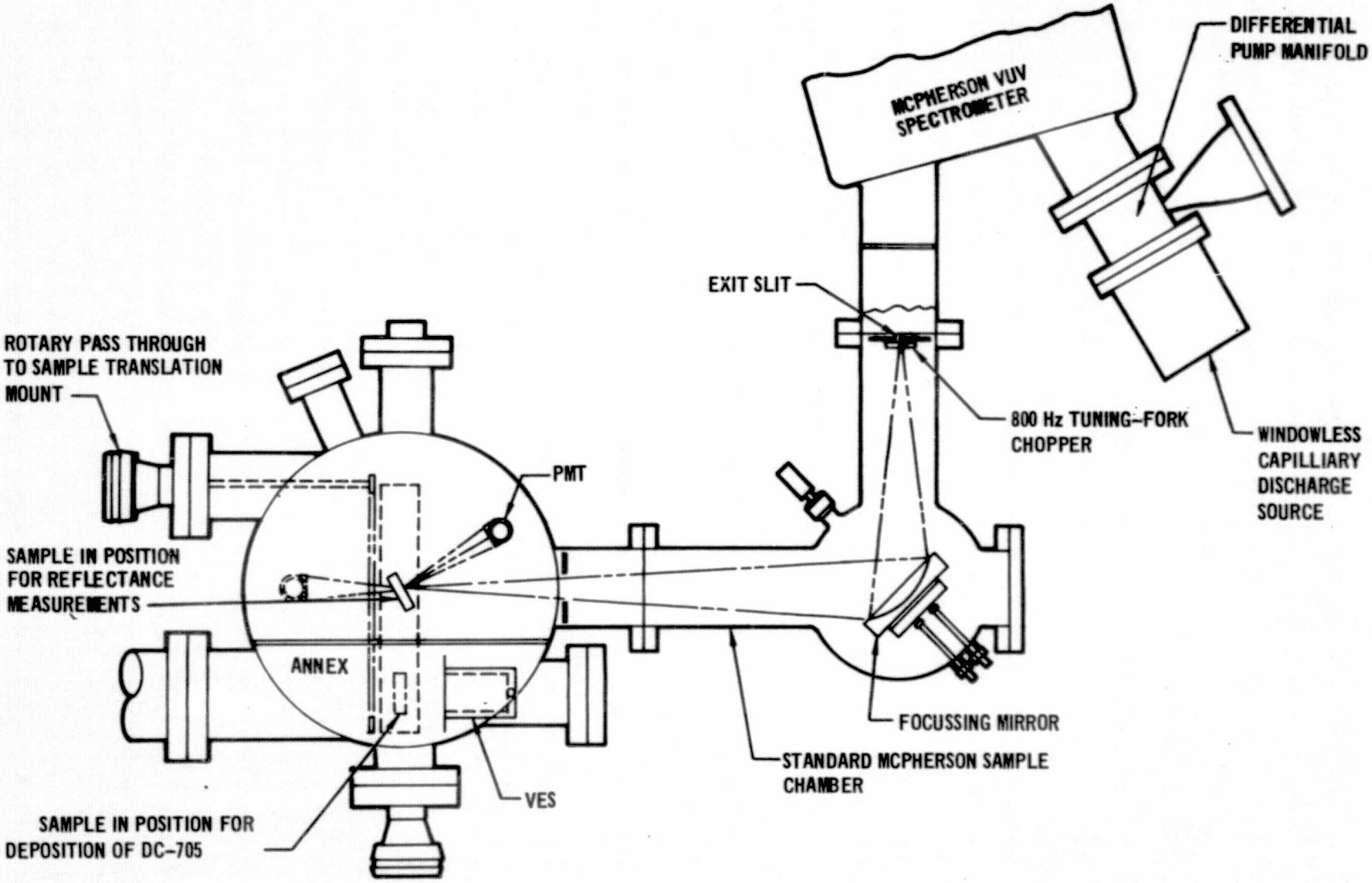

FIGURE 3-2 – VACUUM ULTRAVIOLET REFLECTOMETER

three light sources were used:

- o Hinteregger Capillary Discharge Source using hydrogen gas - 120nm to 200nm
- o Mercury Vapor Lamp - 200 nm to 350 nm
- o Quartz Halogen Lamp - 350nm to 600nm

Contaminant films were deposited from a VES with a single 0.5mm diameter nozzle, 35mm from the sample. With the VES charged with DC705 diffusion pump oil, a deposition rate of approximately 40 $\mathring{A}\ min^{-1}$ was measured in a separate experiment using an ellipsometer. Some problems were experienced with maintaining a steady deposition rate, and with making accurate measurements of the thickness of the DC-705 films. These problems are discussed later in this section.

3.2.2 Experimental Results. In the initial experiments the effect of DC-705 films on the reflectance of both over-coated and bare aluminum mirrors was investigated, over the wavelength range 350nm to 600nm. The sample mirror in this case was a vacuum-deposited aluminum mirror overcoated with magnesium fluoride equivalent to a 1/2-wave at 121.6nm; the sample was prepared concurrently with those mirrors fabricated and delivered to JSC (Section 2.2).

Data illustrated in Figure 3-3 shows the effect of varying film thicknesses for a 30° angle of incidence. The degradation is most marked at the lower wavelengths, but even at 600nm a 100$\mathring{A}$ thick film results in a 20% reduction in reflectance. The variation of reflectance with film thickness, at three wavelengths, is illustrated in Figure 3-4.

Visual inspection of the samples suggested that the degradation in reflectance of the contaminated samples was caused by scattering rather than by absorption of radiation. To confirm this phenomenon, the hemispherical reflectance of a contaminated sample was measured on a Beckman DK-2A spectrophotometer equipped with an integrating sphere. Results of these measurements are illustrated in Figure 3-5 and it is apparent that the hemispherical reflectance was barely influenced by a 400$\mathring{A}$ film of DC-705, yet the specular reflectance was halved. Similar results were obtained for an uncoated aluminum surface, indicating that scattering was the predominant mechanism degrading mirror performance.

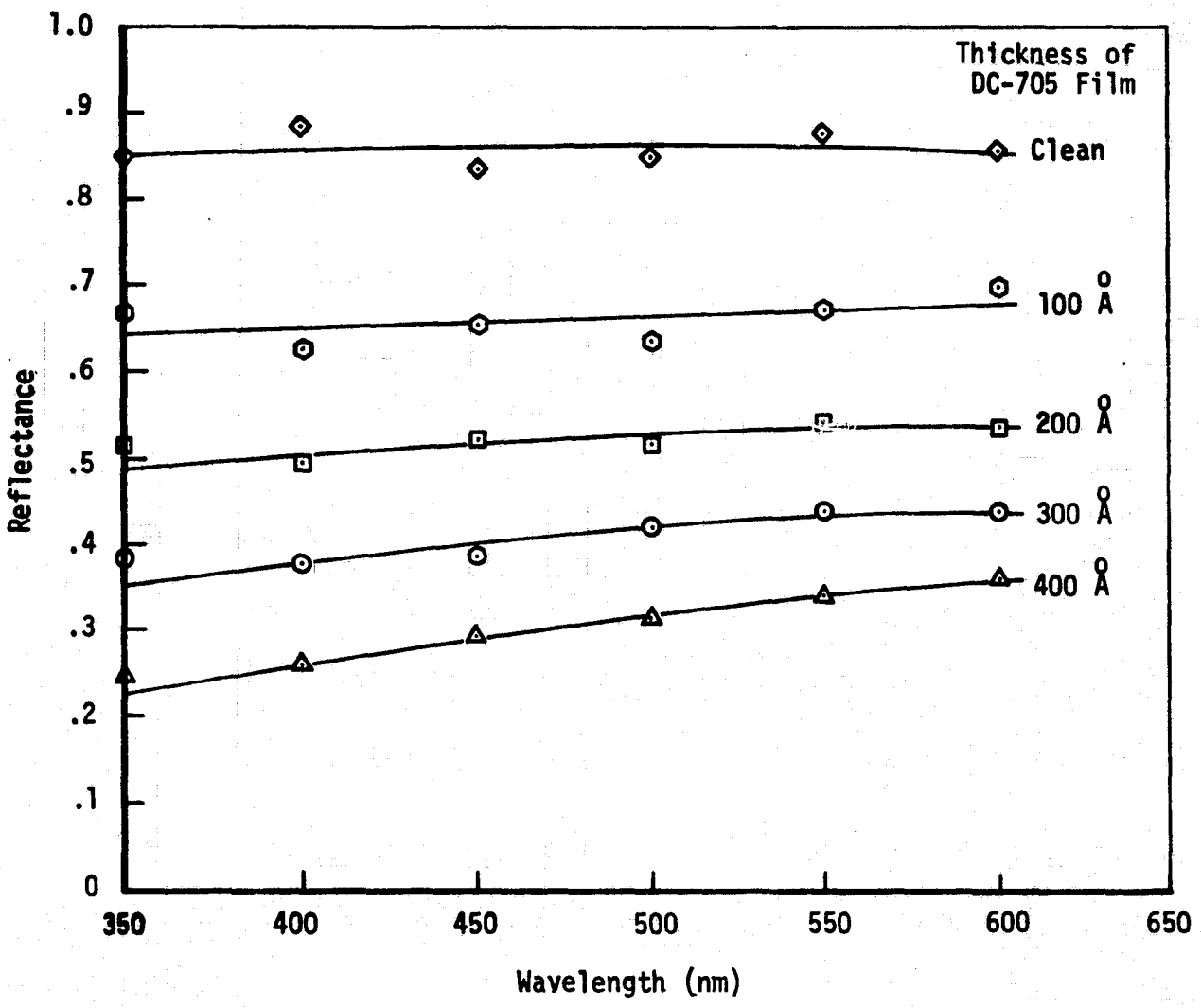

FIGURE 3-3 – EFFECT OF DC-705 FILM ON REFLECTANCE OF 1/2-WAVE MgF_2/AL MIRROR

The angular distribution of scattered 490nm radiation was investigated using the rotating photomultiplier detector with its acceptance angle of approximately 3°. The result of such a measurement is shown in Figure 3-6. Lorenz-Mie scattering theory predicts such an intensity distribution when the particle dimensions are much greater than the wavelength of the radiation. This suggests that the contaminant particles are several microns in diameter. Although the scope of this supportive study did not permit further investigation of this phenomenon, results of recent experiments on related MDAC programs have confirmed this scattering effect.

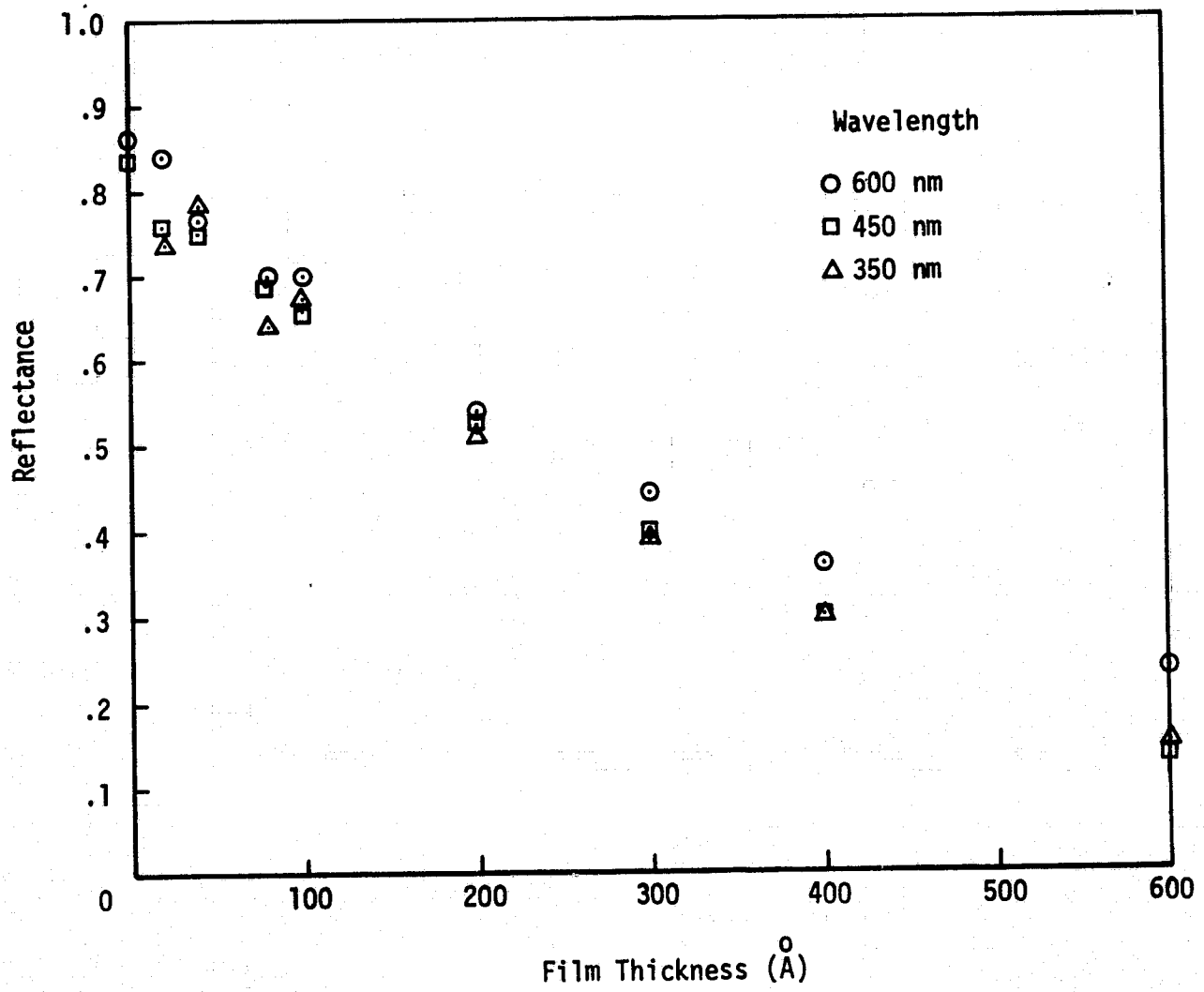

FIGURE 3-4 – EFFECT OF THICKNESS OF DC-705 FILMS ON REFLECTANCE OF 1/2-WAVE MgF_2/AL MIRROR

Later experiments were conducted at ultraviolet and vacuum ultraviolet wavelengths (120 to 350nm). In these tests a 1.5mg cm^{-2} coating of sodium salicylate scintillator was deposited on the window in front of the photomultiplier.

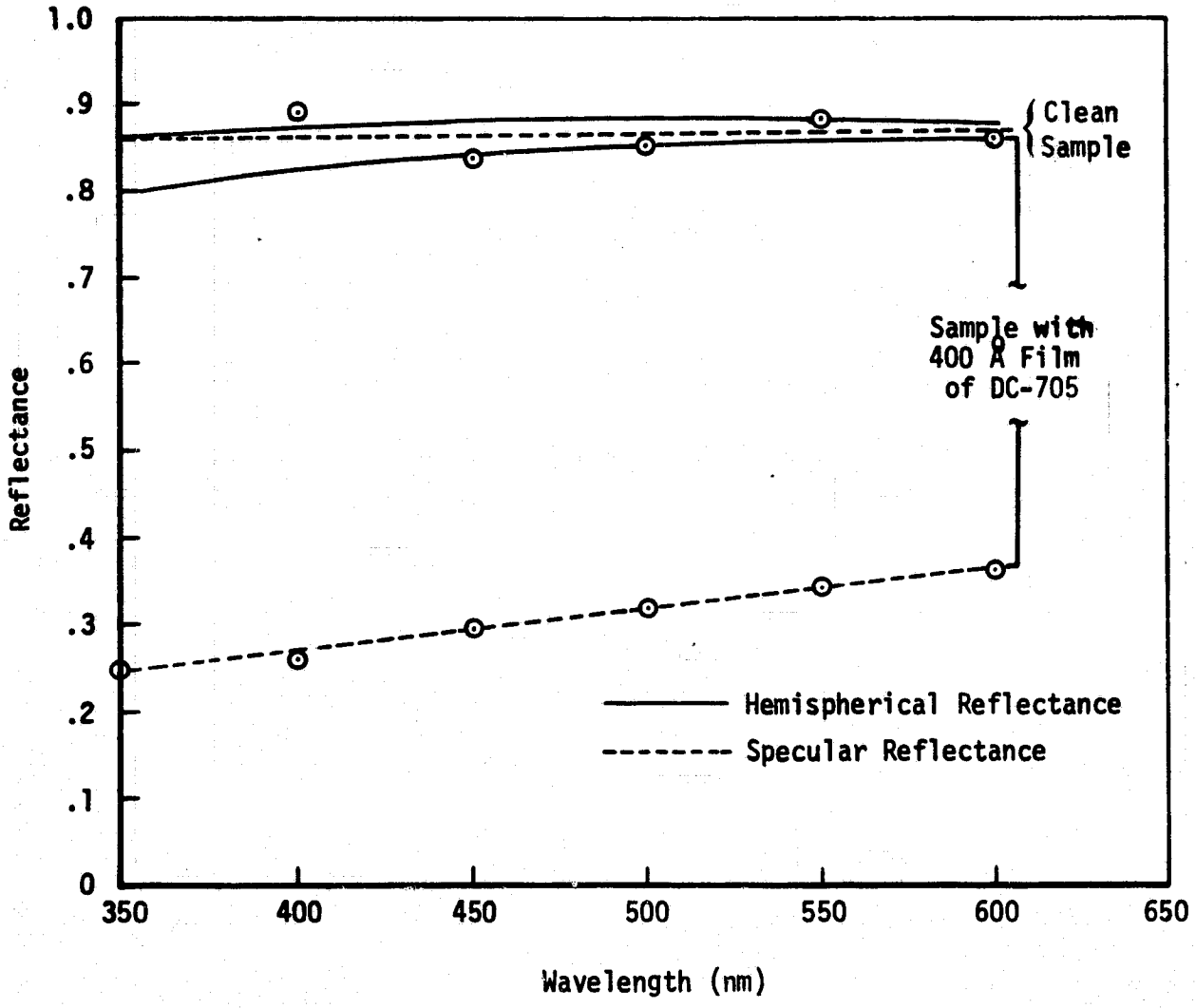

FIGURE 3-5 – EFFECT OF DC-705 FILM ON THE SPECULAR AND HEMISPHERICAL REFLECTANCE OF 1/2-WAVE MgF_2/AL MIRROR

Data from the UV/VUV runs is shown in Figures 3-7 and 3-8 where they have been integrated with the results of the earlier experiments (Figure 3-3). Results from bare aluminum samples (presumably covered with approximately 50Å film of aluminum oxide) showed significant degradation at all wavelengths after deposition of 400Å of DC-705. Similar results were obtained for aluminum samples with a 1/2-wave (at 121.6nm) overcoating of magnesium fluoride. Degradation similar to that of the bare aluminum can be observed but the MgF_2 overcoat has enhanced the reflectance of the samples below 200nm.

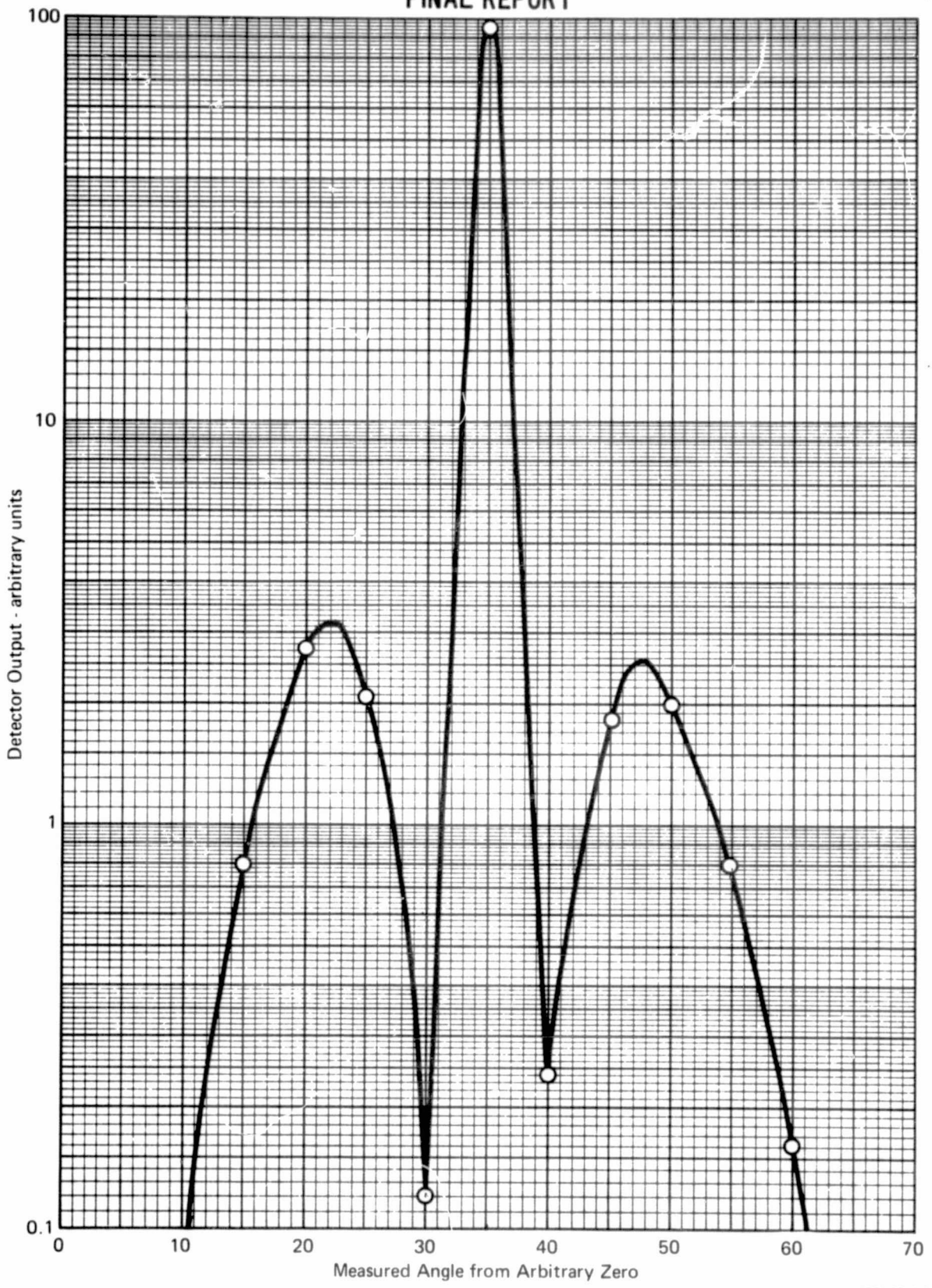

FIGURE 3-6 – ANGULAR DISTRIBUTION OF 490 NM SCATTERED RADIATION FROM 1/2-WAVE MgF_2/AL MIRROR CONTAMINATED WITH 400 Å OF DC-705

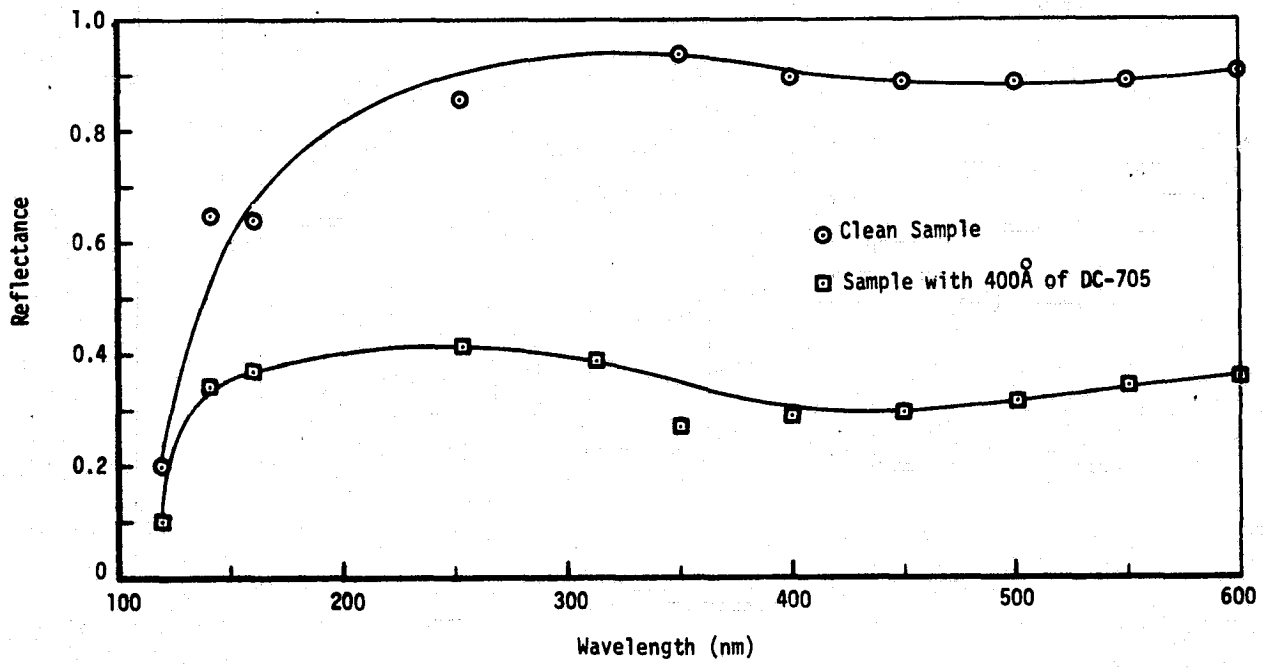

FIGURE 3-7 – EFFECT OF A DC-705 FILM ON THE REFLECTANCE OF A 1/2-WAVE MgF_2 OVERCOATED ALUMINUM MIRROR

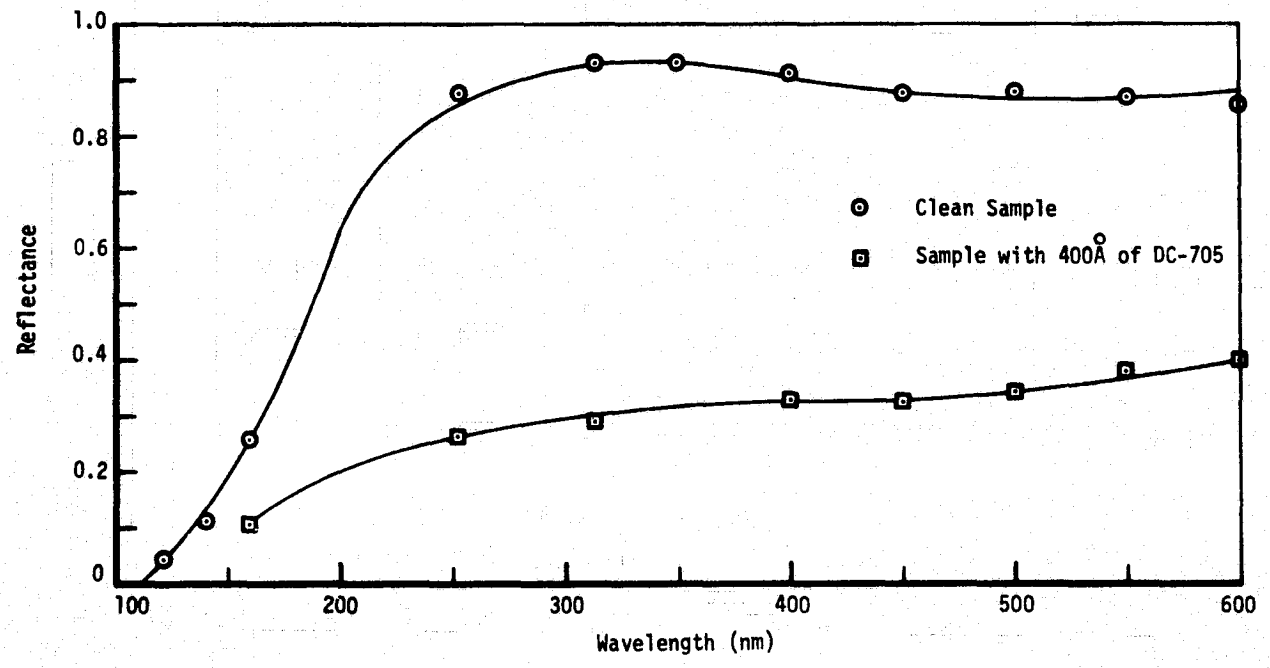

FIGURE 3-8 – EFFECT OF A DC-705 FILM ON THE REFLECTANCE OF AN UNCOATED ALUMINUM MIRROR

The effect of the film thickness for three wavelengths across the range studied is illustrated in Figures 3-9 and 3-10.

3.2.3 Conclusions of Study. Both the results of the optical measurements and the experience gained during the study influenced the design of the WCA and of the VUV reflectometer. The problems encountered with determining the thickness of the DC-705 films demonstrated the advantages of ellipsometer measurements concurrent with the reflectance measurements. Therefore in the design of the WCA, ellipsometer windows were set at 70° incident angle, either side of the reflectometer ports at 45°.

Scattering of optical radiation by contaminant films was shown to be a significant and sometimes predominant degradation mechanism for reflective and transmitting optics. Therefore two options were designed into the WCA for reflectance measurements; an integrating sphere for hemispherical reflectance measurements, and provision for angular reflectance measurements.

The results of the reflectance study demonstrated the need for precision sample temperature control and measurement, and these features were incorporated in the WCA sample holder.

3.3 SENSITIVITY STUDY. The primary purpose of this study was to determine sensitivities of Auger electron spectroscopy and ellipsometry, when applied to the study of the oxidation kinetics of clean aluminum surfaces. These measurements were also used as a basis for defining the WCA vacuum requirements for oxidation studies and to generate information on the short term storage of aluminum mirrors.

3.3.1 Auger Electron Spectroscopy. Auger electron spectroscopy (AES) has been developed in recent years as one of the most sensitive techniques for studying the contamination of surfaces. Auger or secondary electrons are those ejected during the process of autoionization of excited-ionized atoms. Symbolically, this can be represented as:

$$\text{excitation:} \quad e_0 + A \rightarrow A^{+*} + e_1 + e_2$$

$$\text{relaxation:} \quad A^{+*} \longrightarrow A^{++} + e_A$$

where e_0, e_1, e_2 and e_A refer to the incident, inelastically scattered, primary and Auger electrons, respectively. A, A^{+*}, and A^{++} refer to the unexcited, neutral atom, the atom singly-ionized and excited and the unexcited, doubly ionized atom. Excitation is accomplished by

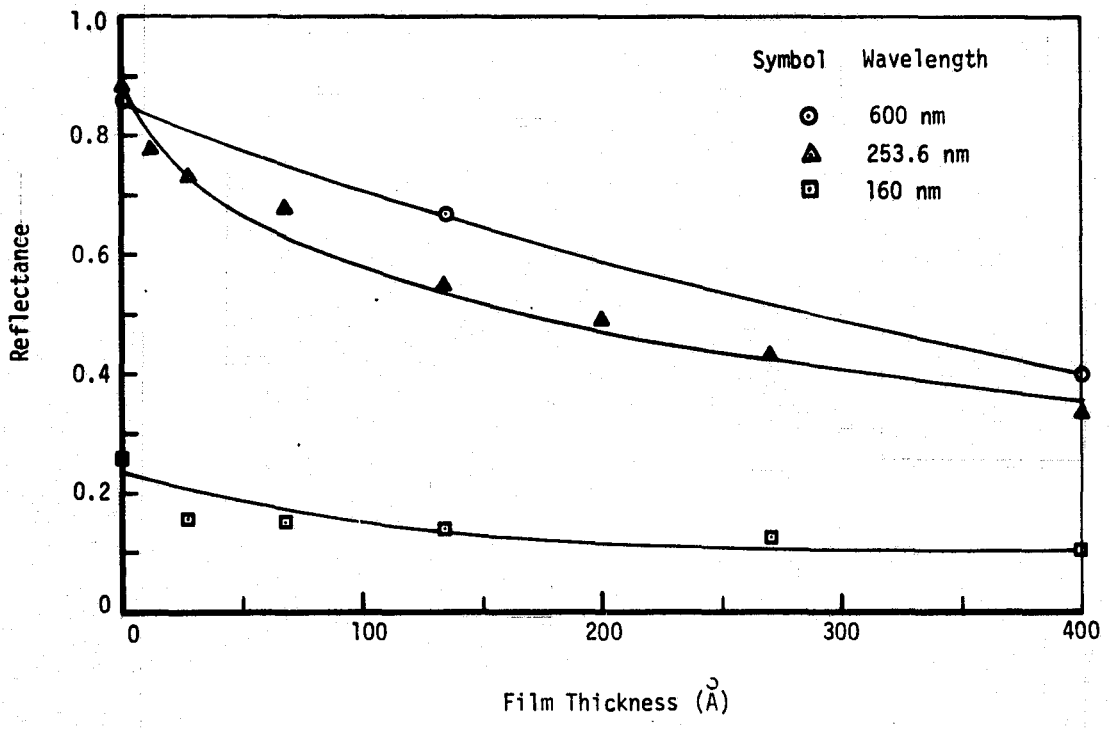

FIGURE 3-9 – EFFECT OF THE THICKNESS OF DC-705 FILMS ON THE REFLECTANCE OF AN UNCOATED ALUMINUM MIRROR

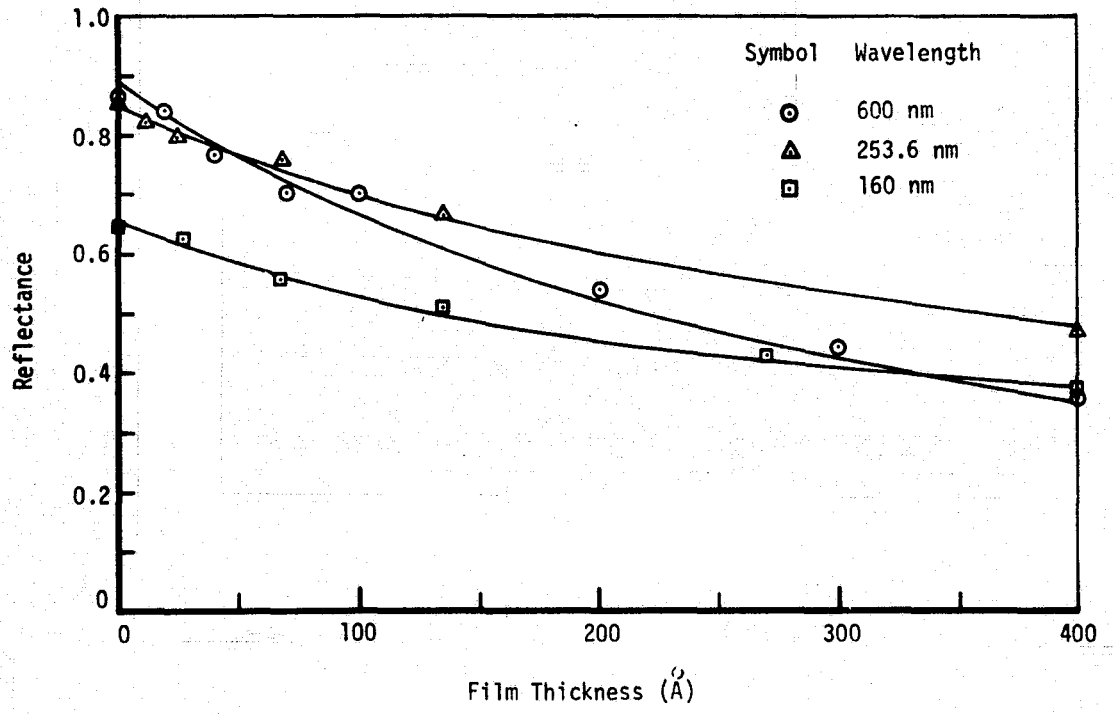

FIGURE 3-10 – EFFECT OF THE THICKNESS OF DC-705 FILMS ON THE REFLECTANCE OF A 1/2-WAVE MgF_2 OVERCOATED ALUMINUM MIRROR

irradiating the sample surface with energetic electrons, e_0, having energies ranging from 2 to 3 keV. Since the energy of the Auger electron is dependent upon the electron structure of the host atom, it can be used to determine the atomic number and hence its chemical identification. The extreme sensitivity of this technique is a consequence of the fact that the Auger electrons originate from the first few monolayers because of the limited mean free path Calculations have indicated that surface atomic densities of 10^{10} atoms cm^{-2} can be detected using this technique.

3.3.2 Ellipsometry. The ellipsometer measures Δ(deg.) and ψ(deg.) which corresponds to the phase shift and relative attenuation of the electric field vectors of light reflected at an optical surface. Mathematically, the relationship between Δ and ψ and the optical properties of the surface can be expressed as:

$$\frac{R_p}{R_s} = \tan(\psi)\, e^{i\Delta} \qquad (3.1)$$

where R_p and R_s are the reflectance coefficients for light with its electric vector parallel and perpendicular to the plane of incidence, respectively.

The optical constants of a film free surface can be related to Δ and ψ by:

$$2\,nk = \frac{\sin^2\theta \tan^2\theta \sin 4\psi \sin\Delta}{(1 + \sin 2\psi \cos\Delta)^2} \qquad (3.2)$$

$$n^2 - k^2 = \frac{(\sin^2\theta \tan^2\theta)(\cos^2 2\psi - \sin^2 2\psi \sin^2\Delta)}{(1 + \sin 2\psi \cos\Delta)^2} + \sin^2\theta \qquad 3.3$$

where θ is the angle of incidence.

Ellipsometric measurements at a single wavelength can be reduced by finding solutions to Equation 3.2 and 3.3 using a digital computer, to yield values of n and k. If the surface is covered with an oxide or contaminant film the ellipsometer data can be reduced to determine the thickness of the film in addition to its optical properties.

3.3.3 Experimental Measurements. Measurements were made on both bulk and vapor deposited aluminum to study the oxidation kinetics and to compare the sensitivity of AES and ellipsometry for measuring thin oxide films.

The measurements were made in an all-metal ion-pumped vacuum chamber

designed to permit simultaneous Auger and ellipsometric measurements on the sample. This system was also equipped with an ion sputtering source to clean sample surfaces, and a vapor deposition station to deposit metal films for in-situ measurements. The chamber was capable of pressures of 10^{-9} torr.

A sample of 99.999% aluminum was mechanically polished to a 0.5μm finish before installation in the AES vacuum chamber; at this stage there was approximately 10Å of oxide on the surface, as measured with the ellipsometer. This oxide layer was then completely removed with a sputter ion source using Argon at 10^{-5} torr, with the chamber continually pumped with an ion pump to ensure an extremely low partial pressure of oxygen, while maintaining the argon atmosphere.

An AES scan was recorded to verify the chemical integrity of the oxide free aluminum surface, and the ellipsometer was used to determine the intrinsic optical properties of the pure aluminum. The results of the optical measurements are shown in Table II and are in good agreement with those measured by Fane[2] for vacuum deposited aluminum.

Auger spectra recorded on the sputtered samples as they gradually oxidized showed that the amplitude of the oxygen peak (513eV) increased steadily from the onset of oxidation while the Al_2O_3 (53eV) peak did not appear for some time. These data indicate that oxygen is both physically and chemically adsorbed on the aluminum surface and that both phenomena affect the ellipsometer

TABLE II
OPTICAL CONSTANTS FOR ALUMINUM

Material	n	k	Source
Vac Deposited Al	1.420	7.719	MDC
Cleaned Bulk Al	1.566	7.938	MDC
Vac Deposited Al	1.570	8.046	Fane et al, Reference 2
Vac Deposited Al	1.158	6.190	Hass, Reference 3
Vac Deposited Al	1.212	6.924	Hass et al, Reference 4
Vac Deposited Al	1.417	6.393	Heavens, Reference 5
Aluminum Oxide	1.635	0.000	MDC

GP75-5214-71

readings. The contribution to the variation in Δ attributable to the formation of aluminum oxide, did not appear until the film was approximately a monolayer thick (1.0Å). This is the apparent limit to the sensitivity of the ellipsometer as applied to the study of oxidized aluminum films.

An estimate of the sensitivity of the AES technique was also made from these measurements. Using the linear relationship established between the height of the 513 eV Auger peak for absorbed oxygen, and the film thickness as measured on the ellipsometer, it was calculated that the ultimate sensitivity of the Auger spectrometer is approximately 10^{11} molecules cm^{-2}, or less than 1/100th of a monolayer.

The optical properties of vapor deposited aluminum were studied using the in-situ deposition source. This source consisted of tungsten spiral filaments wetted with high purity aluminum. During normal operation the pressure in the chamber was 10^{-9} torr but it rose to 10^{-7} torr during the deposition cycles. An Auger spectrum recorded for a freshly deposited aluminum film is included as Figure 3-11, and the size of the 513 eV oxygen peak indicates that a relatively oxygen-free film was prepared. The absence of the 53 eV peak associated with aluminum oxide and the strength of the 67 eV aluminum peak also indicate that pure aluminum films were deposited. Furthermore, the Auger peaks associated with tungsten around 160 eV were never detected, indicating that the tungsten filament did not evaporate.

Ellipsometer measurements at 632nm on such a freshly deposited aluminum film yielded values for the optical constants of aluminum in this form, and of the aluminum oxide layers that develop, even under ultra-high vacuum. These values are summarized in Table II together with other values quoted in the literature.

There is considerable variance between the results of the different authors and this can be correlated with the pressure at which the aluminum surfaces were prepared. Our work and that of Fane were conducted at pressures of 10^{-7} torr and below; others operated at 10^{-5} to 10^{-6} torr, at which pressures the risk of oxidation is increased.

Experiments were conducted to study the effect of oxygen partial pressure on film thickness. The ellipsometer was used to measure film thickness and the results of these measurements are shown in Table III. They indicate that the equilibrium film thickness is dependent on the oxygen partial pressure,

TABLE III
ELLIPSOMETERS MEASUREMENTS OF THE GROWTH OF OXIDE FILM ON VACUUM DEPOSITED ALUMINUM

System Pressure (torr)	Elapsed Exposure Time (Minutes)	Oxide Film Thickness (Å)	Remarks
2×10^{-8}	10	0	
2×10^{-8}	20	0.5	
2×10^{-8}	36	0.5	
2×10^{-8}	50	1.1	
2×10^{-8}	75	1.2	
2×10^{-7}	14	0.5	Backfilled with Oxygen
2×10^{-7}	70	3.5	
2×10^{-6}	13	5.7	Backfilled with Oxygen
2×10^{-6}	28	6.1	
2×10^{-6}	43	6.3	
2×10^{-6}	53	6.3	
2×10^{-6}	68	6.3	
755	13	17.3	Backfilled with Air
755	28	17.8	
755	43	18.1	
755	58	18.6	
755	73	18.8	
755	25.7 hr	22.1	

GP75-5214-78

with a final thickness of 22Å when exposed to air. The AES spectrum of the freshly deposited aluminum film, reproduced in Figure 3-11, shows a large aluminum peak at 67eV with a residual trace of oxygen and carbon. A similar AES spectrum for an oxidized sample, Figure 3-12 shows not only a well developed oxygen peak at 513eV but also an Al_2O_3 peak at 53eV. In addition, a carbon peak at 277eV was detected. This peak is probably due to the physical absorption of CO and CO_2 from the residual gases in the vacuum chamber or was present in the oxygen used to backfill the chamber.

These results show that extreme precautions must be taken with regard to the vacuum integrity of the chamber for this type of study, and that impurity gases such as CO and CO_2 must be removed by proper outgassing procedures before valid oxidation measurements can be conducted.

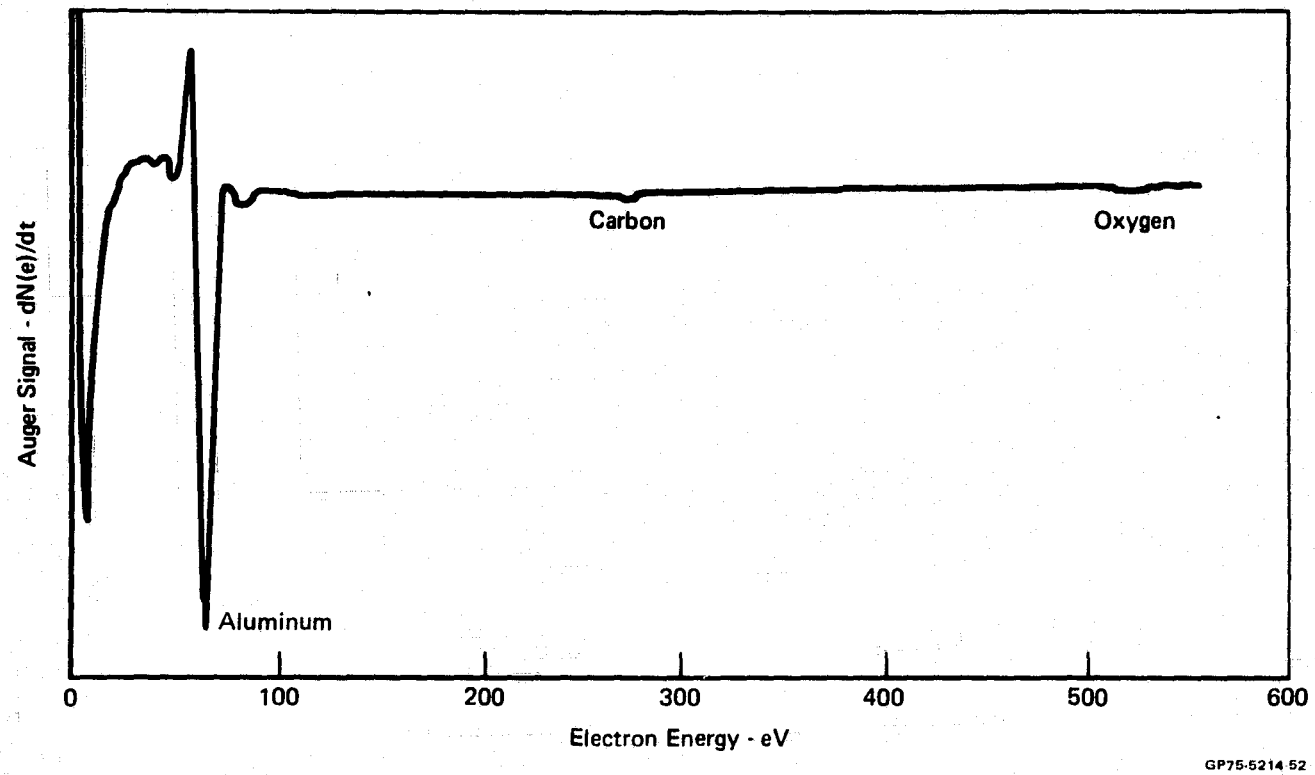

FIGURE 3-11 – AUGER ELECTRON SPECTRUM OF FRESHLY VACUUM DEPOSITED ALUMINUM FILM

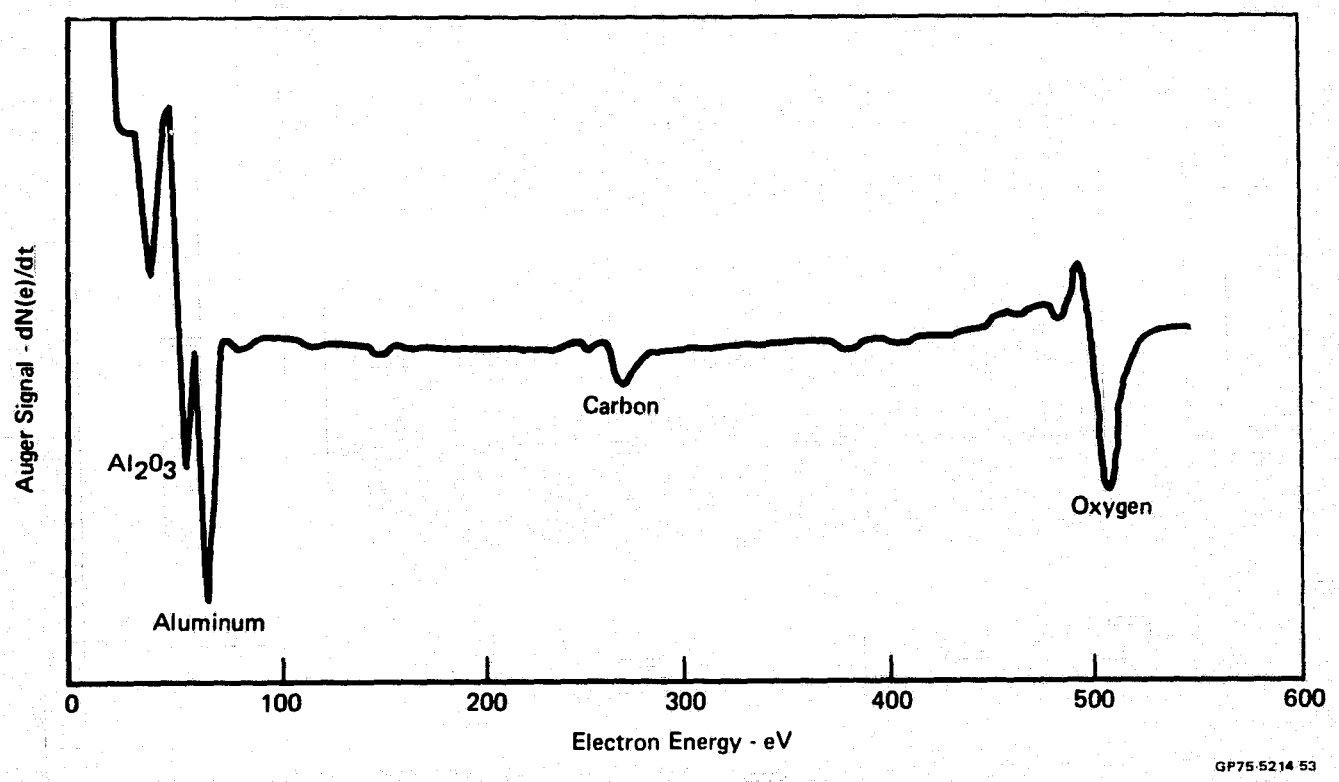

FIGURE 3-12 – AUGER ELECTRON SPECTRUM OF PARTIALLY OXIDIZED ALUMINUM FILM

3.4 CLEANING STUDY. The purpose of this study was to determine the effectiveness of various techniques for removing organic contaminants from the surface of an optical element. The organic material used for this study was DC-705 diffusion pump oil. Small quantities of the fluid (0.05 cm^3) were deposited on the gold-coated mirror, and the film was mechanically spread over the entire surface. After the cleaning experiments, ellipsometer measurements were made to determine the thickness of the residual film.

3.4.1 Cleaning Techniques Evaluated. Two categories of cleaning techniques were evaluated, solvent cleaning and cleaning by substrate heating.

The specific cleaning techniques used in this study were:

- o Sample immersion in a solvent, at ambient temperature, with some mechanical agitation.
- o Sample immersion in an ultrasonic cleaner charged with the particular solvent, at ambient temperature.
- o Vapor degreasing by exposing the mirror to hot vapors of the solvent.
- o Substrate heating in a vacuum environment.

The commercially available solvents used are summarized in Table IV.

TABLE IV

SOLVENTS USED IN THE CLEANING STUDY

Acetone	99 Mole % Pure
2-Propanol (Isopropyl Alcohol)	99 Mole % Pure
Benzene	Commercially Pure
MEK (Methyl Ethyl Ketone)	Commercially Pure

3.4.2 Results of the Study. The results of the solvent cleaning study are shown in Table V. In the case of ultrasonic cleaning, both acetone, and propanol completely removed the DC-705 while the other two solvents, benzene and MEK, left a residue of approximately one monolayer. A cleaning time of 10 minutes was required to completely remove the contaminant. The results for sample immersion with some mechanical agitation of the solvent produced similar results. The last cleaning technique, vapor degreasing, appears to

TABLE V
RESULTS OF THE CLEANING STUDY

Solvent	Cleaning Technique			
	Ultrasonic Cleaning		Immersion and Agitation (5 min)	Vapor Degreasing (5 min)
	Cleaning Time	Film Thickness (Å)	Film Thickness (Å)	Film Thickness (Å)
Acetone	5	24	<1	<1
	10	<1		
MEK	5	12	4	<1
	10	6		
	15	2		
Benzene	5	10	<1	<1
	10	2		
	15	3		
Propanol	5	<1	<1	<1
	10	<1		

GP75-5214-70

be the best approach to solvent cleaning of metal optical surfaces.

Organic contaminants can also be removed from a substrate by heating in vacuum, to raise the vapor pressure to a point at which the contaminant vaporizes at a significant rate. To determine the range of temperatures required for such cleaning a series of evaporation tests were conducted with DC-705 films on a gold-coated polished aluminum substrate. Several evaporation runs were conducted; at 25°C, 40°C, and 50°C. The results are summarized in Figure 3-13. To achieve significant evaporation rates, the sample should be heated to at least 50°C, at which temperature a DC-705 film will evaporate at approximately 8Å min^{-1}.

3.4.3 Cleaning System for the WCA. Though solvent cleaning methods are seen to be quite effective, they are not practical for use inside the WCA. Two techniques which are compatible with the vacuum environment and have been provided for in the WCA are:

- o Substrate heating; the sample heater will be capable of attaining temperatures up to 100°C for removal of organic contaminants.
- o Glow discharge; the sample holder will be electrically isolated from ground so that glow discharge techniques can be used to prepare

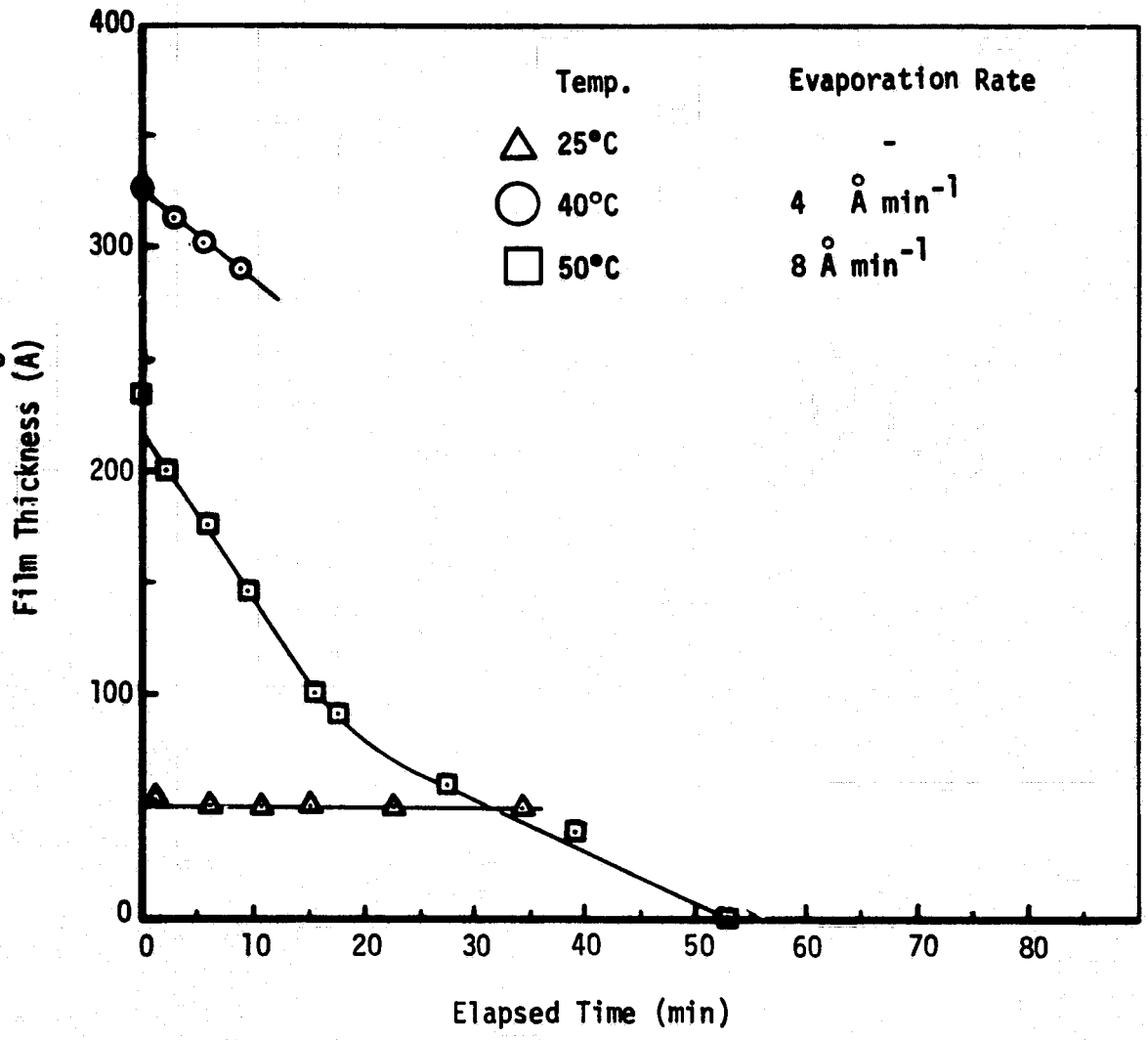

FIGURE 3-13 – RE-EVAPORATION OF DC-705 FILMS FOR VARIOUS SUBSTRATE TEMPERATURES

surfaces prior to vapor deposition of optical films.

3.5 PUMPING REQUIREMENTS FOR THE WCA. The Work Chamber Assembly (WCA) was designed to fulfill a wide variety of roles. These ranged from measurements on optical surfaces contaminated with organic materials deposited from a vapor effusion source, to studies of freshly vapor deposited optical thin films. Such diverse applications would place severe demands on any pumping system. For measurements involving organic films, the pumping system had to provide

pressures in the 10^{-6} to 10^{-7} torr range in the WCA, yet its performance could not be degraded by the organic materials. For the deposition of oxide-free reactive films, such as aluminum, the oxygen partial pressure had to be 10^{-9} torr or less. In other applications a fast turnaround time from atmospheric pressure was required. The addition of a VUV Reflectometer resulted in a large helium gas load from the discharge source and further impacted the pumping system design.

Several types of pumping were considered for this application; diffusion pumps, turbomolecular pumps, sputter ion pumps, sublimation pumps, cryogenic absorption pumps and helium-cooled fingers. Diffusion pumps suffer the disadvantage of backstreaming and, even with a cryogenic baffle, organic contamination could enter the main vacuum chamber. Sputter ion pumps and titanium sublimation pumps have excellent low ultimate pressures but their efficiency may be impaired by organic contamination. Contamination of optical surfaces by titanium from such pumps can also be significant. Cryogenic pumps offer several advantages at low pressures, but they should be operated in conjunction with other pumps to remove the bulk of the system gases which could saturate and reduce the effectiveness of the cooled surfaces.

A turbomolecular pump was identified as the best pump to evacuate the WCA, for several reasons:

- o Wide range of operating pressures.
- o Low ultimate pressures; 10^{-8} - 10^{-9} torr.
- o Good pumping speed 250 - 800 ls^{-1}.
- o Negligible backstreaming of organic contaminants.
- o Pumping efficiency approximately constant for noble gases, common gases, and organic vapors.

3.5.1 Proposed Pumping System for the WCA. A combination of pumps were required to rough the WCA, to back the turbomolecular pump, and to remove the residual gases from the chamber to achieve 10^{-9} torr or less. The following arrangement was selected for the WCA.

- o Roughing System: A simple aspirator pump (Varian 942-9000) run on dry nitrogen gas, was selected to remove the bulk of the gas load in the WCA. This would reduce the system pressure to approximately 150 torr; below this pressure molecular sieve sorption pumps were chosen to lower the system pressure to less than 1 torr.

- Main Pump: A turbomolecular pump with a pumping speed of 500 ls^{-1} was recommended to pump the WCA, through a large diameter gate valve and a short, large diameter pumping line.
- Ultra High Vacuum Pump: For ultimate performance of the vacuum system, with the WCA sealed with a metal top plate, an ion pump was preferred.

3.5.2 Outcome of Study. At the request of NASA-JSC, the WCA was designed to be compatible with a 400 ls^{-1} ULTEK Model 206-4000 Differential Ion Pump, equipped with a stainless steel gate valve. The aspirator/sorption pump combination was used for roughing the chamber, and provision was made for coupling the WCA to a Welch turbomolecular pump.

4.0 DESIGN OF THE WORK CHAMBER ASSEMBLY

The design of the WCA was based on a set of requirements defined by NASA-JSC. These included a wide range of experimental capability, and a series of general design requirements.

Experimental capability designed into the system included the following:

- o Vacuum deposition of thin optical films onto a sample surface, with precise control of the film thickness.
- o Measurement of the thin film growth rates using ellipsometry.
- o Deposition of thin organic contaminant films on the sample surface in a controlled manner.
- o Determination of the effects of contamination on the reflectance of an optical surface using a NASA-furnished vacuum ultraviolet scanning monochromator.
- o Evaluation of sample cleaning techniques such as ion bombardment and substrate heating.
- o Irradiation of samples with ultraviolet and particulate fluxes to simulate the natural space radiation environment.

In addition, certain components in the system were specified in more detail as follows:

- o A single stainless steel vacuum chamber with a minimum inside diameter of 18 inches and a maximum height of 30 inches.
- o Vacuum bakeout capability.
- o Provision for cooling the sample assembly.
- o Up to four spare ports on the WCA.
- o A stable stand to support the WCA and associated equipment.
- o Compatibility with NASA-furnished pumping equipment.
- o Compatibility with other NASA equipment such as a Welch turbomolecular pump and a Cockroft-Walton type proton/electron accelerator.

4.1 MAIN VACUUM CHAMBER. A view of the main vacuum chamber is shown in Figure 4-1. It was designed around a 24-inch diameter 16-inch high stainless steel cylinder with a 7/8-inch thick base. A 24-inch Wheeler flange welded to the top of the cylinder mates to a similar flange on the chamber top plate. For added flexibility, the Wheeler flange on the chamber was designed to accept an elastomer O-ring to seal to an aluminum top plate. This

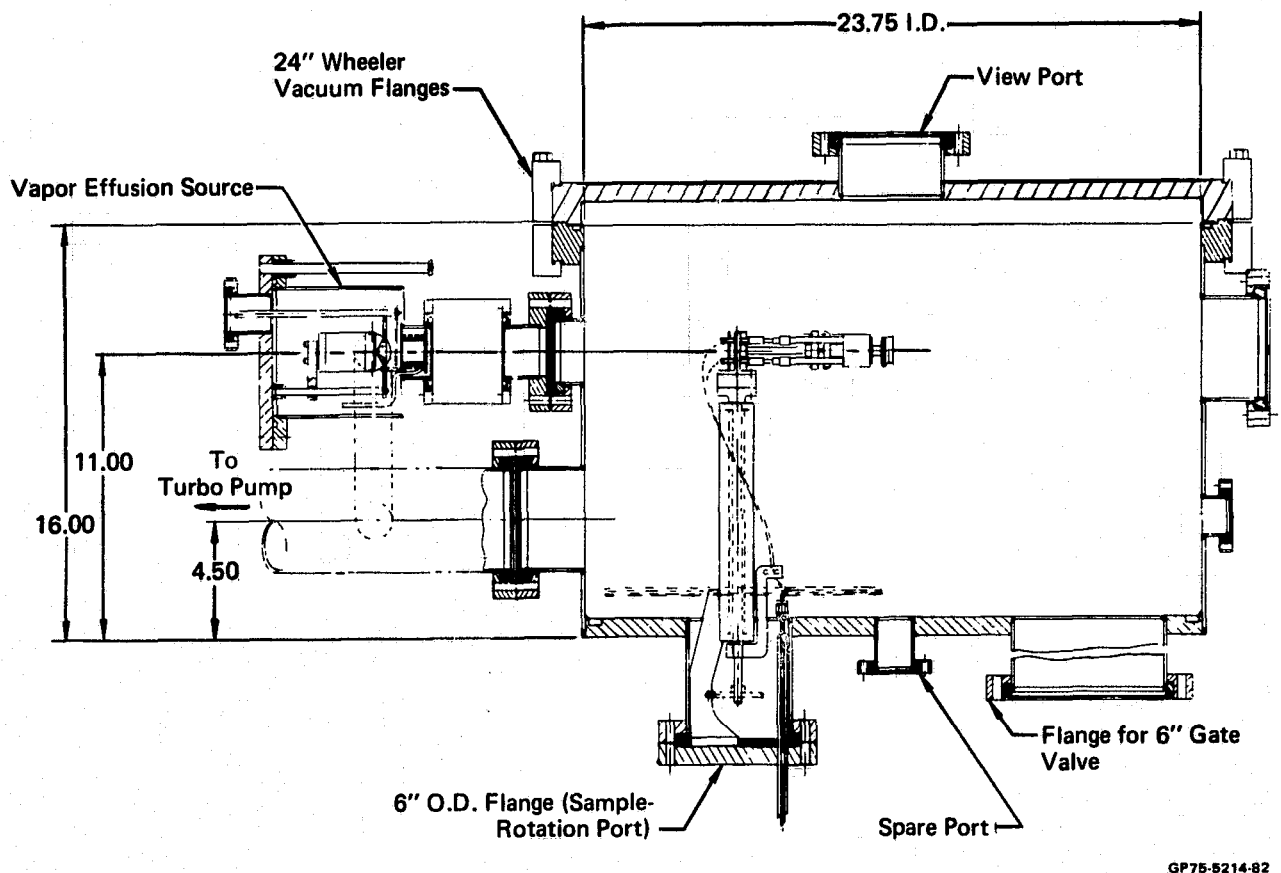

FIGURE 4-1 – SIDE ELEVATION VIEW OF WCA

feature provides for quick turnaround time at the expense of a decade or so of ultimate vacuum. A 6-inch diameter low profile viewing window is mounted on the chamber top plate.

Twenty penetrations are provided around the chamber wall and in the base of the chamber, for various pumping systems, for interfacing with other equipment and for miscellaneous instrumentation. Varian Conflat ™ flanges were selected to provide metal seals so that the system can be baked up to 350°C. The locations of the penetrations are shown in Figure 4-2.

4.2 PUMPING SYSTEMS. A combination of pumps are used to evacuate the WCA from atmospheric pressure to ultra-high vacuum. An overall view of the system is shown in Figure 4-3 and details of the roughing system are shown in Figure 4-4.

To reach the ultimate vacuum a gas aspirator pump is run to remove 80% of the gas load and reduce the system pressure to 150 torr. This allows the sorption pumps to be used in an efficient manner to further reduce the pressure to the 10^{-3} torr range.

The ion pump is isolated from the main chamber by a pneumatically operated gate valve so that the pump can be run continuously without troublesome starting procedures. To equalize the pump and chamber pressures prior to opening the valve, a low conductance bypass line is provided.

4.3 SAMPLE HOLDER. A multi-purpose sample holder was designed for the WCA. It features an electrically isolated, temperature controlled, instrumented sample mount which can be rotated through 270°. As shown in Figure 4-5, four sample positions are available as follows:

- Opposite the Vapor Effusion Source (VES) chamber for deposition of contaminant films.
- Over the vapor deposition boats for fabrication of optical coatings.
- Opposite the view port for simultaneous ellipsometric and vacuum ultraviolet reflectance measurements.
- Opposite the energetic radiation port for exposure to electrons, protons or solar radiation.

When the sample holder is in position for vapor deposition of optical film, the sample is tilted into the horizontal plane using a lever arm on a bellows pass thru.

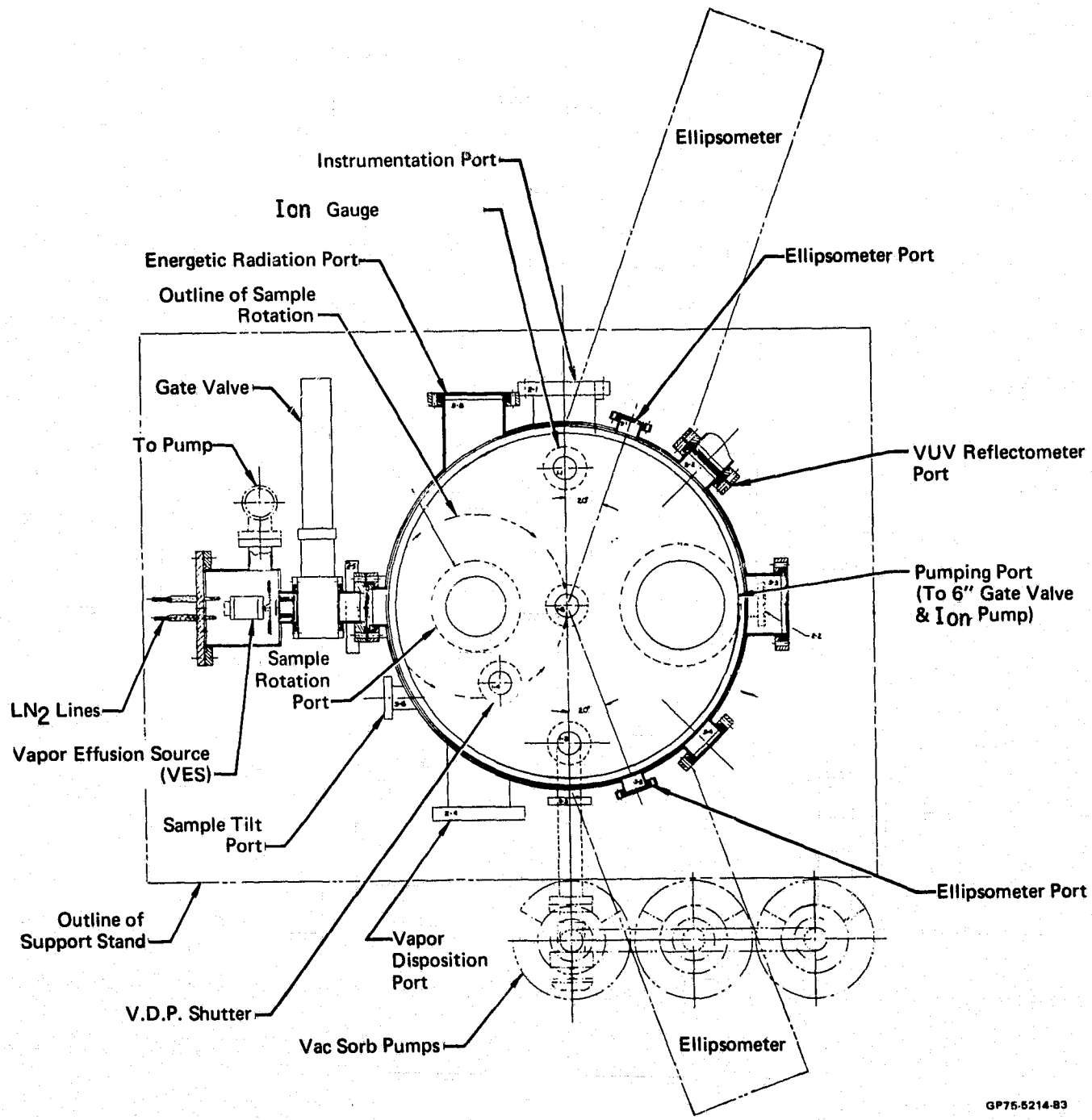

FIGURE 4-2 – PLAN VIEW OF THE WCA

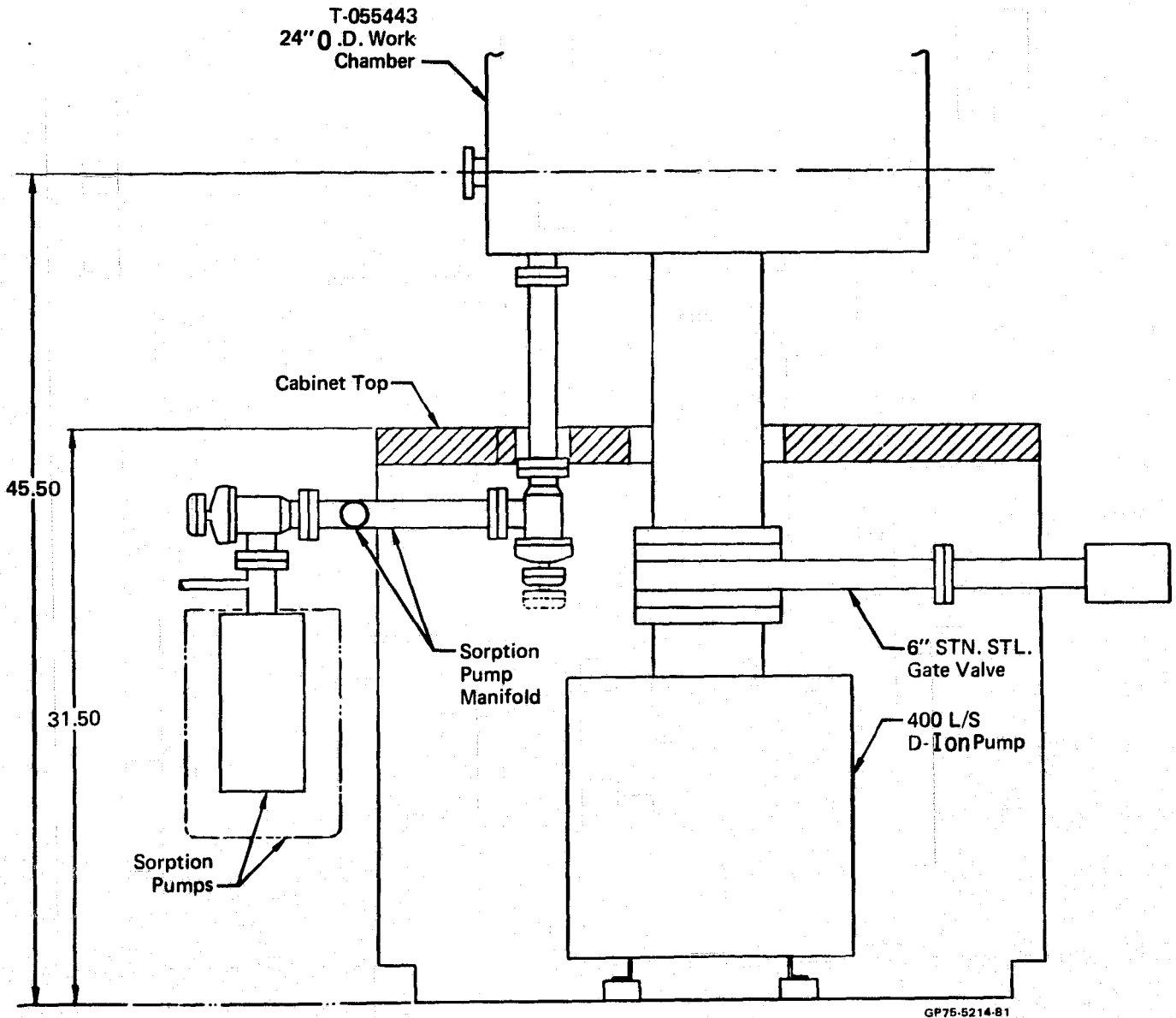

FIGURE 4-3 – VIEW OF PUMPING SYSTEMS

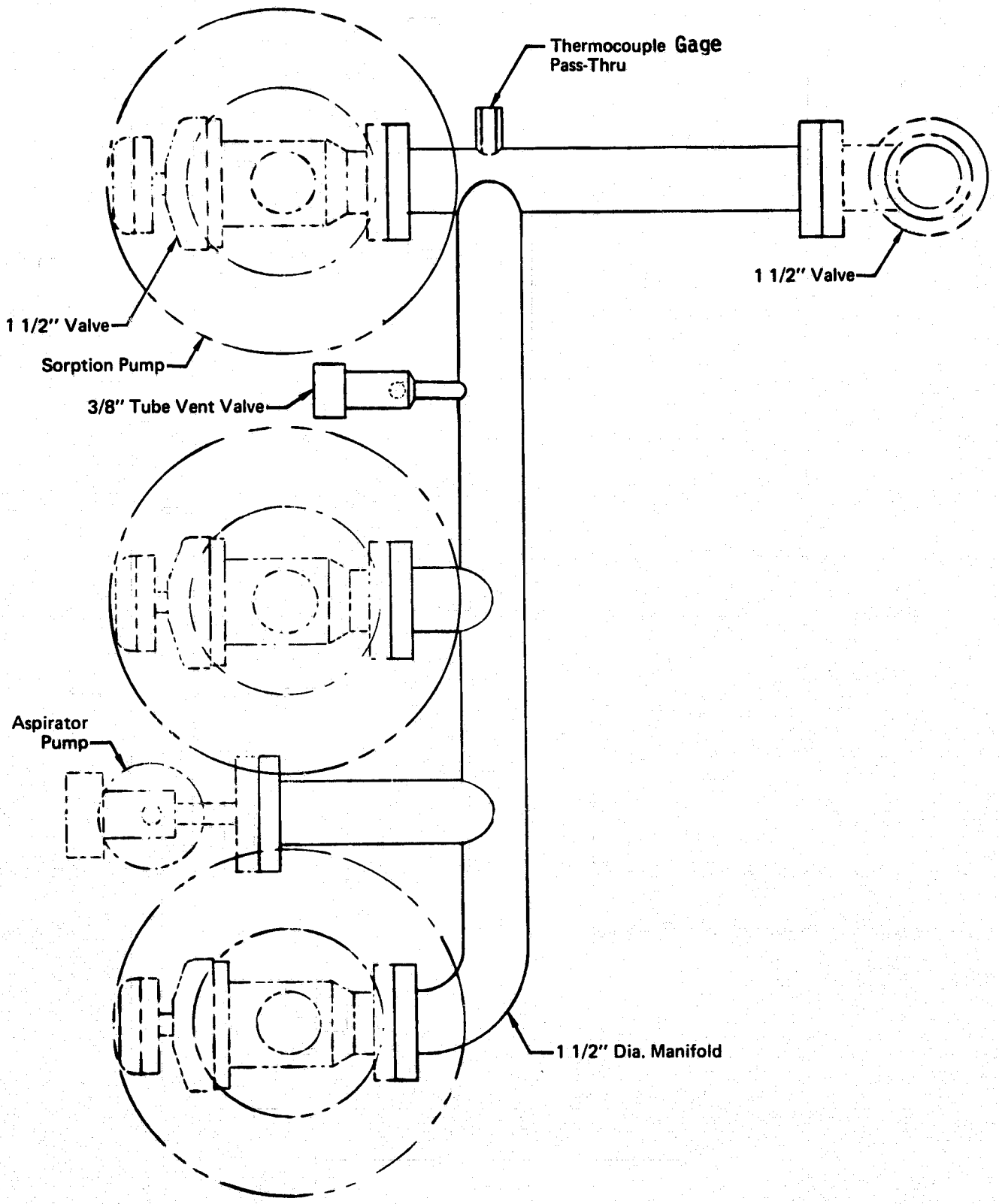

FIGURE 4-4 – SORPTION PUMP MANIFOLD

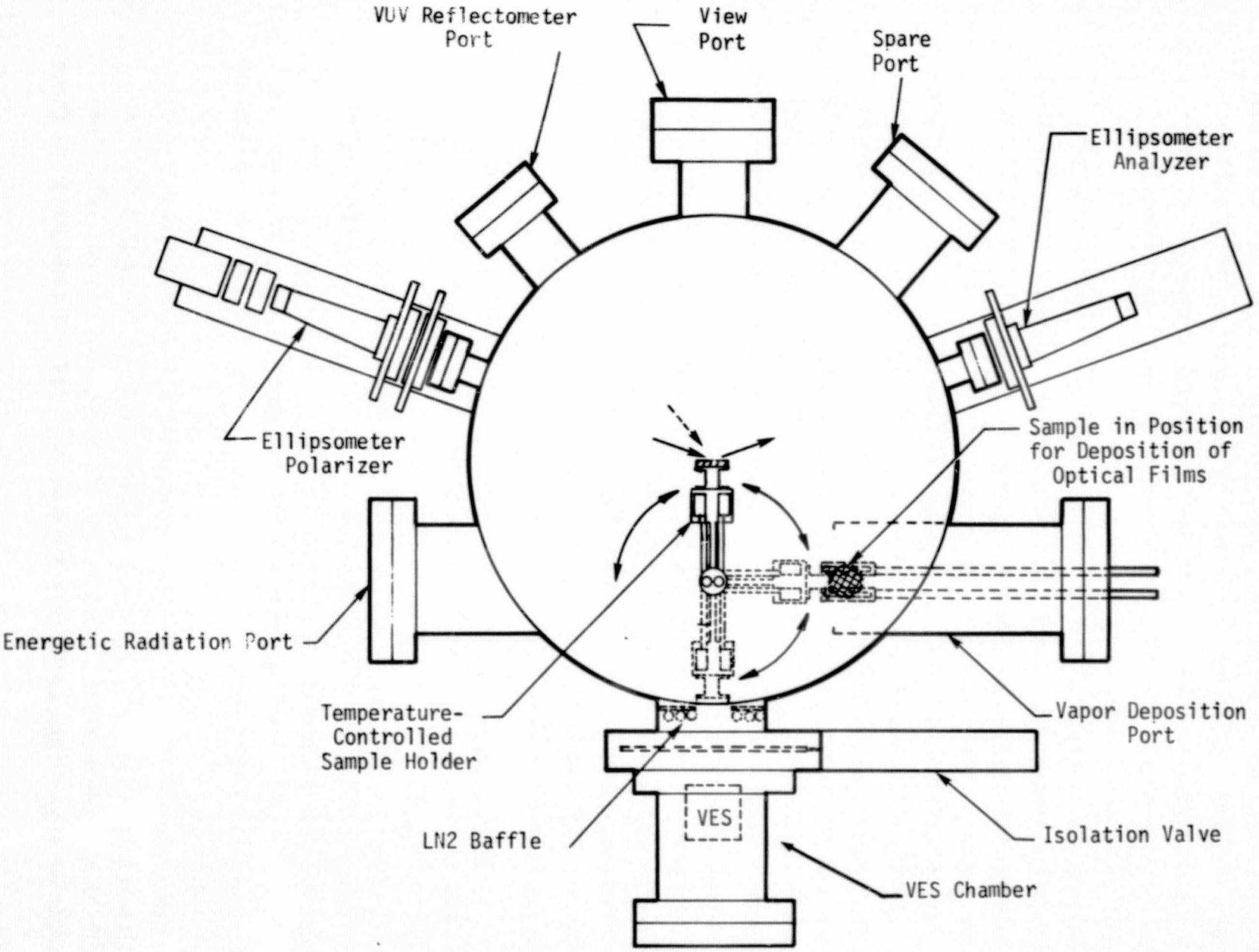

FIGURE 4-5 – WCA VIEW

The sample rotation assembly is shown in Figure 4-6. It is supported on two ball bearings and is driven by a worm gear through a bellows rotary feedthrough. The 100:1 reduction of the worm allows precision, repeatable positioning of the sample assembly. A mechanical counter mounted on the feedthrough registers each 1/10 of a revolution of the worm, equivalent to a movement of 20 arc minutes of the sample holder.

Also shown in Figure 4-6 are the liquid nitrogen connections to the sample coolant reservoir. Two 12-inch long 1/4-inch diameter stainless steel flexible bellows provide the coupling between the fixed input and exit tubes, and the rotating sample holder.

Details of the sample holder are shown in Figure 4-7. A one-inch diameter, 1/4-inch thick sample is mounted on a hinged section, in thermal contact with the temperature control system. The sample temperature is controlled between -150 and +100°C by balancing the power input to a small nichrome heater, against the cooling effect of liquid nitrogen circulating through the small reservoir. Experience with this technique has shown that sample temperatures can be controlled within ±0.5°C.

A ceramic insulator and two glass-to-metal transitions in the liquid nitrogen circulation system provide electrical isolation of the sample for glow discharge cleaning and other experiments. Miniature stainless steel bellows are included in the cooling lines to prevent damage to these transitions due to differential thermal expansions or contractions.

4.4 VAPOR EFFUSION SOURCE. The vapor effusion source, for deposition of molecular contaminant films is housed in an isolated annex to the main chamber. This VES Annex is illustrated in Figure 4-8.

The annex is attached to the main WCA vacuum chamber across a Consolidated Vacuum Corporation 2-inch gate valve. An 8-inch o.d. Varian Conflat flange, modified to include an elastomer seal, provides a removable end plate for the annex. All the internal fittings for the annex are supported on this end plate so that they can be removed easily for cleaning and recharging the VES.

The inclusion of the gate valve, connecting flanges and liquid nitrogen baffles result in an 8 1/2-inch separation between the VES nozzle and the sample to be contaminated. To limit the field angle of the molecular beam a single orifice nozzle and aperture system are used. A combination of three

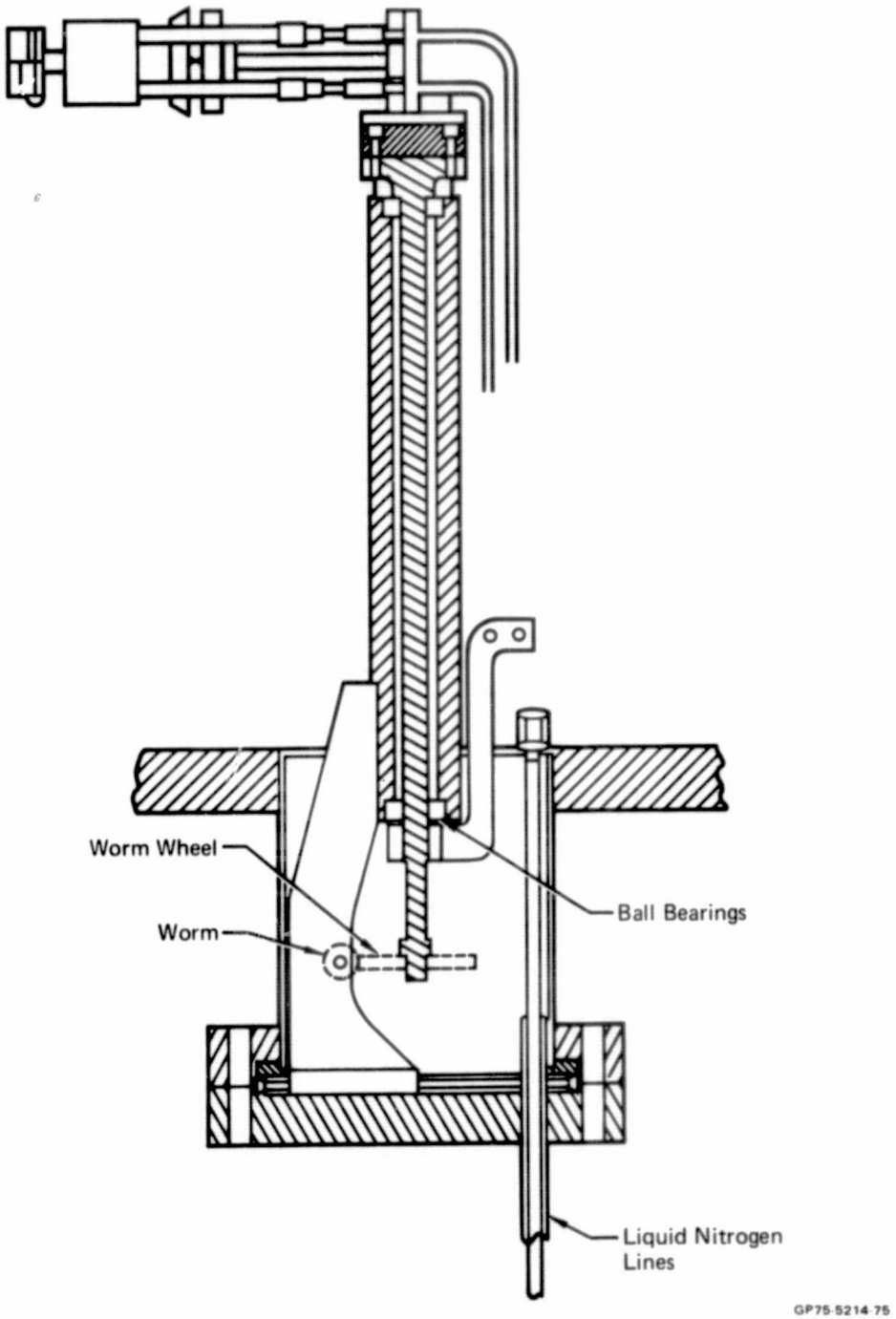

FIGURE 4-6 – DESIGN FOR SAMPLE ROTATION ASSEMBLY

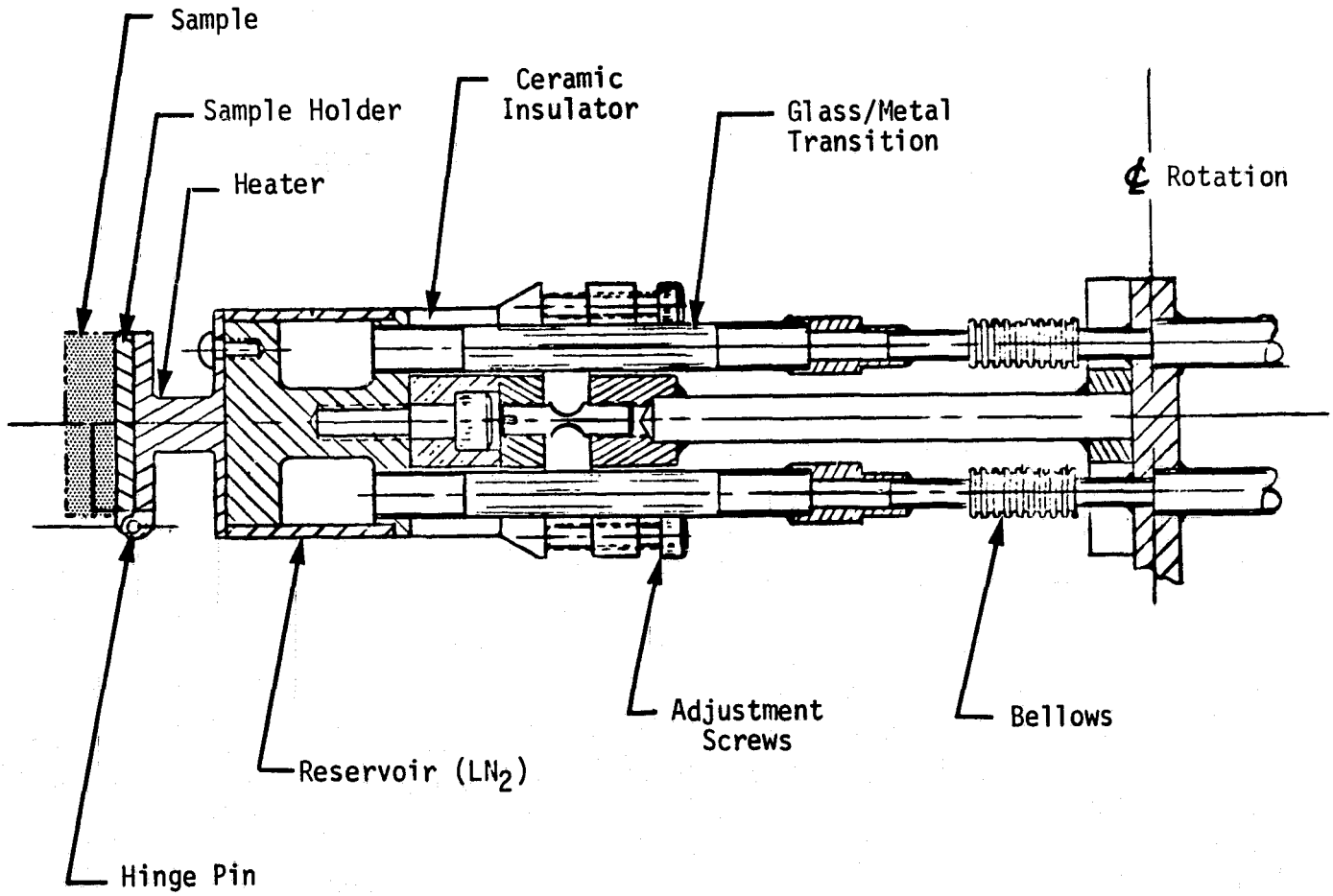

FIGURE 4-7 – DETAIL OF SAMPLE HOLDER ASSEMBLY SHOWING THERMAL CONTROL SYSTEM

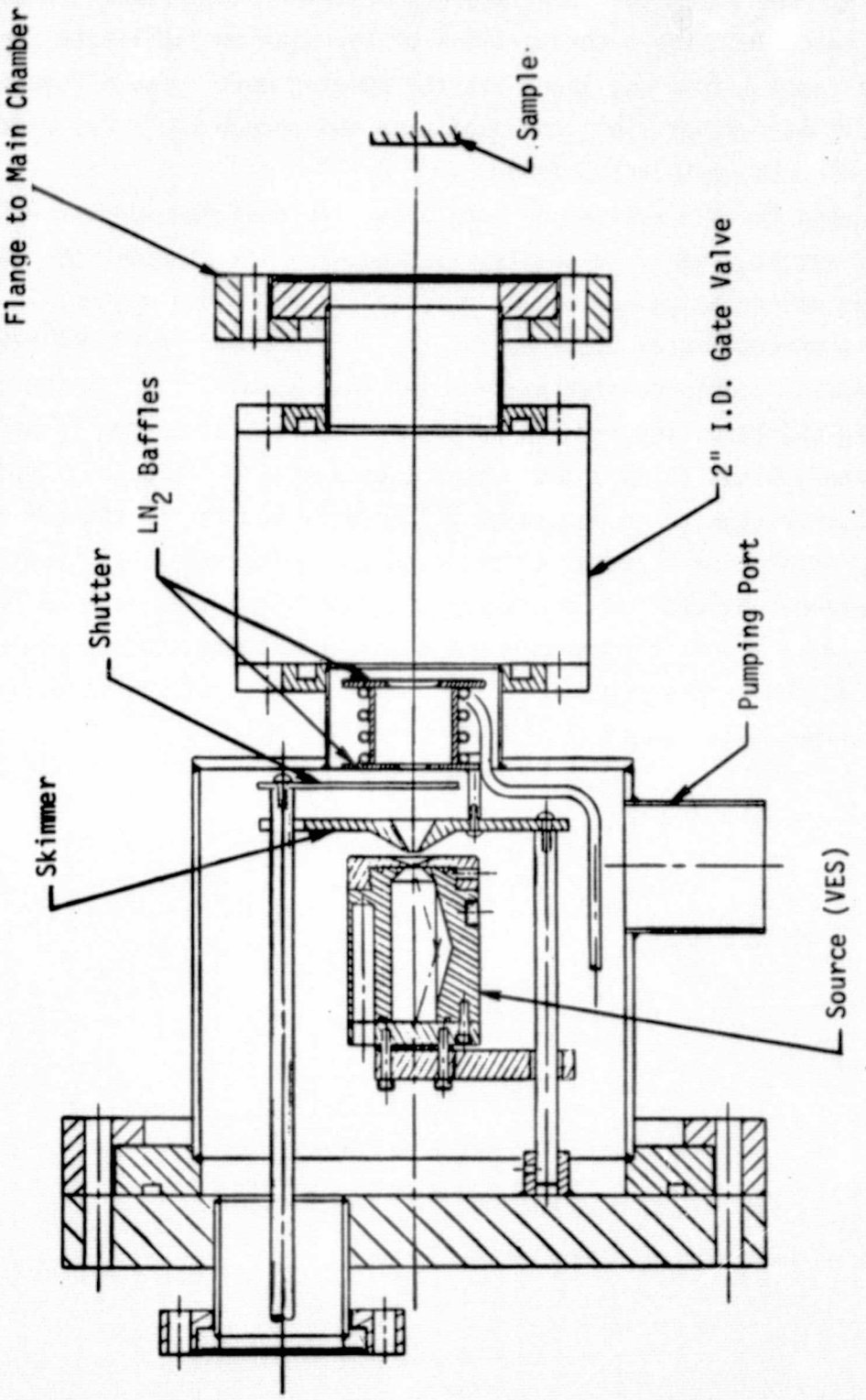

FIGURE 4-8 – VES ANNEX

apertures limit the cross section of the molecular beam to the diameter of the sample. The first aperture is a beam skimmer, the primary function of which is to deflect the outer portions of the beam to facilitate their immediate removal from the annex via the pumping port. Two cryogenically-cooled baffles further limit the beam area and reduce the stray contamination entering the main WCA chamber.

Although the VES system has been primarily designed for use with high molecular weight organic materials, it can, with slight redesign, be used with other molecular gases such as ammonia, nitrogen and oxygen.

The instrumentation provided for the VES is shown in Figure 4-9. Three thermocouples (copper-constantan) monitor the VES oven, the skimmer, and the LN_2-cooled aperture; and the six heaters on the VES are wired in series. All the connections to this instrumentation are wired through a Deutsch vacuum pass-through to an instrumentation panel mounted on the WCA support stand. A digital panel meter is provided to monitor the instrumentation, and a Deutsch connector is mounted on the panel to interface with the NASA-JSC Doric data acquisition system. Similar instrumentation channels are provided on the sample mount (Section 4.2) and these are integrated on the same instrumentation panel as the VES channels.

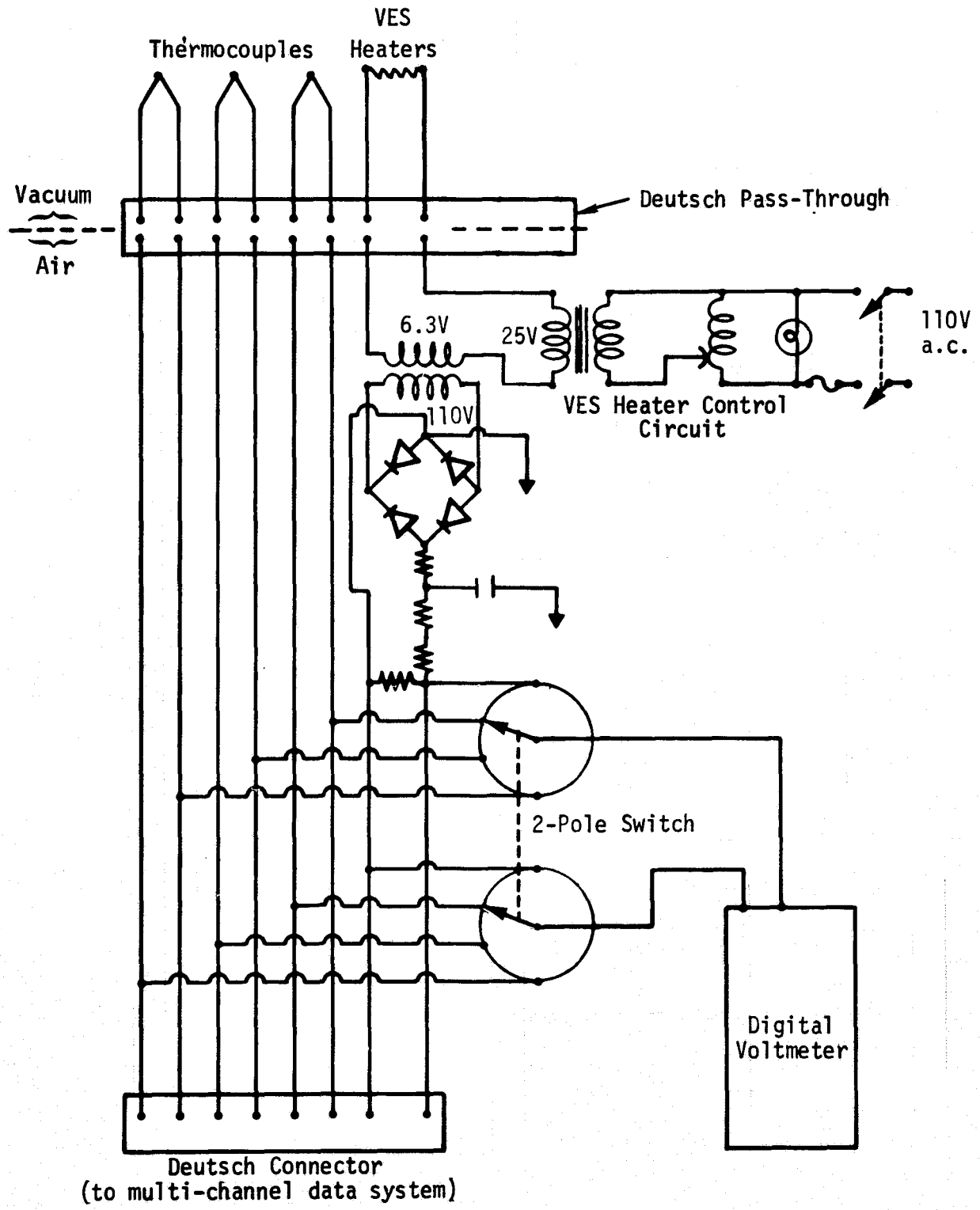

FIGURE 4-9 – VAPOR EFFUSION SOURCE INSTRUMENTATION

5.0 FABRICATION AND ASSEMBLY OF THE WORK CHAMBER ASSEMBLY

5.1 MAIN VACUUM CHAMBER. The 24-inch diameter Wheeler flange with an 18-inch skirt was fabricated by the Varian Vacuum Division, and the chamber was completed by welding the bottom plate to the skirt at MDAC-E. Varian Conflat™ flanges were then welded onto tubes and each of the tubes was carefully aligned and welded into penetrations machined in the wall and base of the chamber. Type 321 stainless steel was used throughout the fabrication of the vacuum chamber.

After welding, the chamber was cleansed by immersion in an organic solvent and then in an alkaline cleaning bath. To passivate the internal surfaces to reduce virtual leaks, the chamber was immersed in a 50% nitric acid bath. A final polished finish was given by hand, using a series of abrasive and buffing compounds.

The chamber was then sealed with blank flanges for helium leak testing as shown in Figure 5-1. It was leak checked with a Veeco MS9 helium-sensitive leak detector, which has a sensitivity of approximately 10^{-10} torr liters/sec. A detailed seal-by-seal check established that the system was leak tight and this was confirmed by completely enclosing the chamber in a helium-filled plastic bag for several hours.

After leak checking, the chamber was mounted on three legs and installed on a support stand. This stand was fabricated from welded 2-inch square section aluminum with a 1 1/2 inch plywood top covered in formica. The stand also included instrumentation racks for the ion pump power supply, ion gage and other instruments.

Once the pumps had been installed and the power, air and liquid nitrogen were plumbed into the stand a vacuum check was performed with the aluminum top plate installed on an elastomer "O"-ring seal. Only two of the sorption pumps were required to reduce the system pressure to 10 microns in 15 minutes. At this pressure, the ion pump was valved in, first via the bypass line, and then by activating the pneumatic gate valve. After 48 hours and a mild bake at 100°C the ultimate pressure was 5×10^{-8} torr.

5.2 SAMPLE HOLDER. A photograph of the completed sample holder is shown in Figure 5-2. All seals were brazed with great care to properly heat-sink the glass to metal transitions, thereby protecting them from fracturing

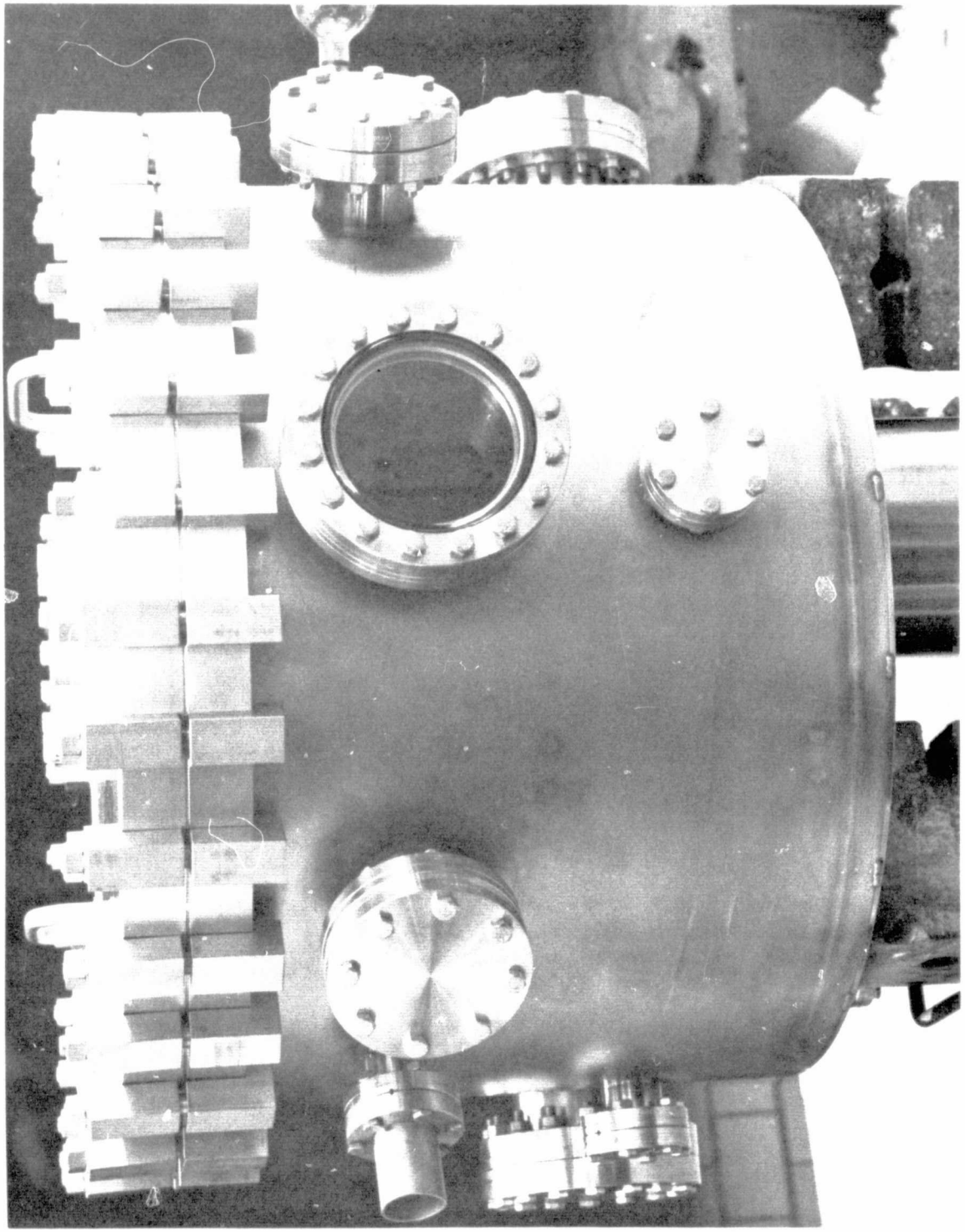

FIGURE 5-1 – WORK CHAMBER ASSEMBLY CONFIGURED FOR VACUUM LEAK TEST

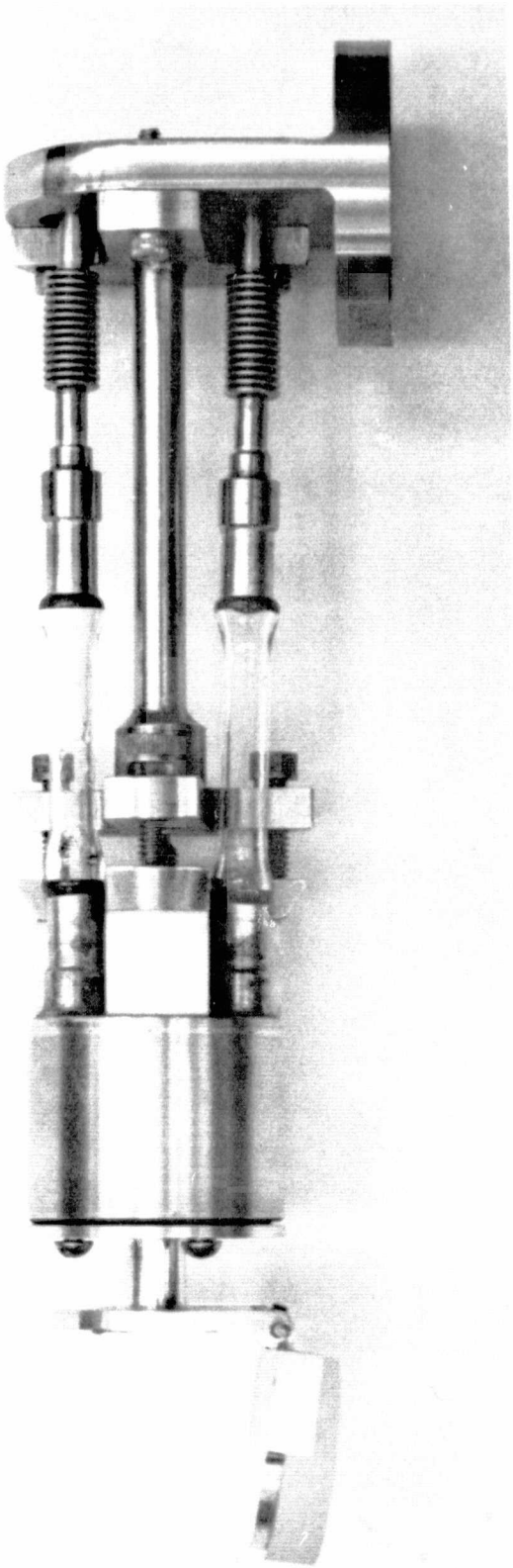

FIGURE 5-2 – ASSEMBLED SAMPLE HOLDER

by differential expansion. The entire assembly was helium leak checked, and then was installed in the main chamber.

5.3 VAPOR EFFUSION SOURCE. A photograph of the assembled VES complete with its housing, electrical and cooling connectors, and rotary feed through is shown in Figure 5-3.

The VES assembly was checked out on an auxiliary vacuum system using a Celesco Industries quartz crystal microbalance as a detector. Particular attention was paid to the temperature distribution of the beam apertures, and the contaminant fluxes generated at various VES temperatures.

The results of the first calibration run with DC-704 oil are shown in Table VI. These figures indicated that the skimmer temperature was well below the design value of approximately 25°C, while all the other temperatures were as predicted. Incident fluxes ranging from 74.5 Å min^{-1} to 3.86 Å min^{-1} were recorded.

Following this run, the VES assembly was modified to thermally isolate the skimmer from the LN_2-cooled aperture, and the experiment was repeated with DC-705 oil. Data from this second test is shown in Table VII. Apparently the modifications were successful and workable deposition rates of approximately 6 and 15 Å min^{-1} were generated. The VES was therefore concluded to be operating satisfactorily and was installed on the WCA.

5.4 VAPOR DEPOSITION SOURCE. A vapor deposition source for the preparation of optical coatings was fabricated on a 6-inch Varian flange. Two evaporation boats were supported on 3/8-inch diameter copper rods. The rods were mounted on Ceramaseal Corporation pass throughs which were welded into the flange. Inside the chamber, the rods were supported by a machinable ceramic mount attached to the flange by a stainless steel bar. A pass through was mounted on a 2 3/4-inch Varian flange to provide power and cooling to a Sloan quartz-cyrstal thickness monitor mounted above the evaporation boats, adjacent to the sample deposition position. Shielding was installed to prevent inadvertent coating of the chamber walls, sample holder, etc. A rotatable shutter was mounted over the boats, supported on a pass through from the chamber base.

5.5 INSTRUMENTATION. To provide for complete instrumentation of experiments to be conducted in the WCA an instrumentation flange was fabricated from a combination of standard Varian feedthrough components

FIGURE 5-3 – PHOTOGRAPH OF ASSEMBLED VES

TABLE VI
RESULTS OF VES CHECKOUT WITH DC-704

VES Temperature (°C)	Skimmer Temperature (°C)	Aperture Temperature (°C)	Chamber Pressure (torr)	Deposition Time (Minutes)	Deposition Rate (Å/Minute)
155	−90	−190	5.0×10^{-6}	8	74.5
145	−80	−185	5.2×10^{-6}	10	29.3
135	−73	−185	5.0×10^{-6}	5	4.86
135	−70	−185	5.0×10^{-6}	10	3.86

GP75-5214-86

Notes:
Nozzle Diameter 0.062 in.
Wall Thickness 0.040 in.
VES to Skimmer Distance 0.050 in.
VES to QCM Distance 9.500 in.

TABLE VII
RESULTS OF VES CHECKOUT WITH DC-705

VES Temperature (°C)	Skimmer Temperature (°C)	Aperture Temperature (°C)	Chamber Pressure (torr)	Deposition Time (Minutes)	Deposition Rate (Å/Minute)
155	18	−190	3.8×10^{-6}	10	15.5
155	19	−190	3.8×10^{-6}	10	14.7
155	20	−190	3.4×10^{-6}	10	15.8
145	15	−190	2.2×10^{-6}	10	6.04
145	15	−190	2.2×10^{-6}	10	6.54

GP75-5214-87

Notes:
Nozzle Diameter 0.062 in.
Wall Thickness 0.040 in.
VES to Skimmer Distance 0.050 in.
VES to QCM Distance 9.500 in.

welded into a blank flange. The arrangement of the feedthrough is illustrated in Figure 5-4 and the following connections were provided:

- Thermocouple 8 each
- Instrumentation 8 each
- High Voltage, 2 kV 4 each
- Medium Current - Ground 1 each

Copper-constrantan thermocouples were attached to both the sample holder and the VES, and were connected via Deutsch thermocouple feedthroughs to the WCA Control Unit. This unit was wired as shown in Figure 4-9 and the front panel is illustrated in Figure 5-5.

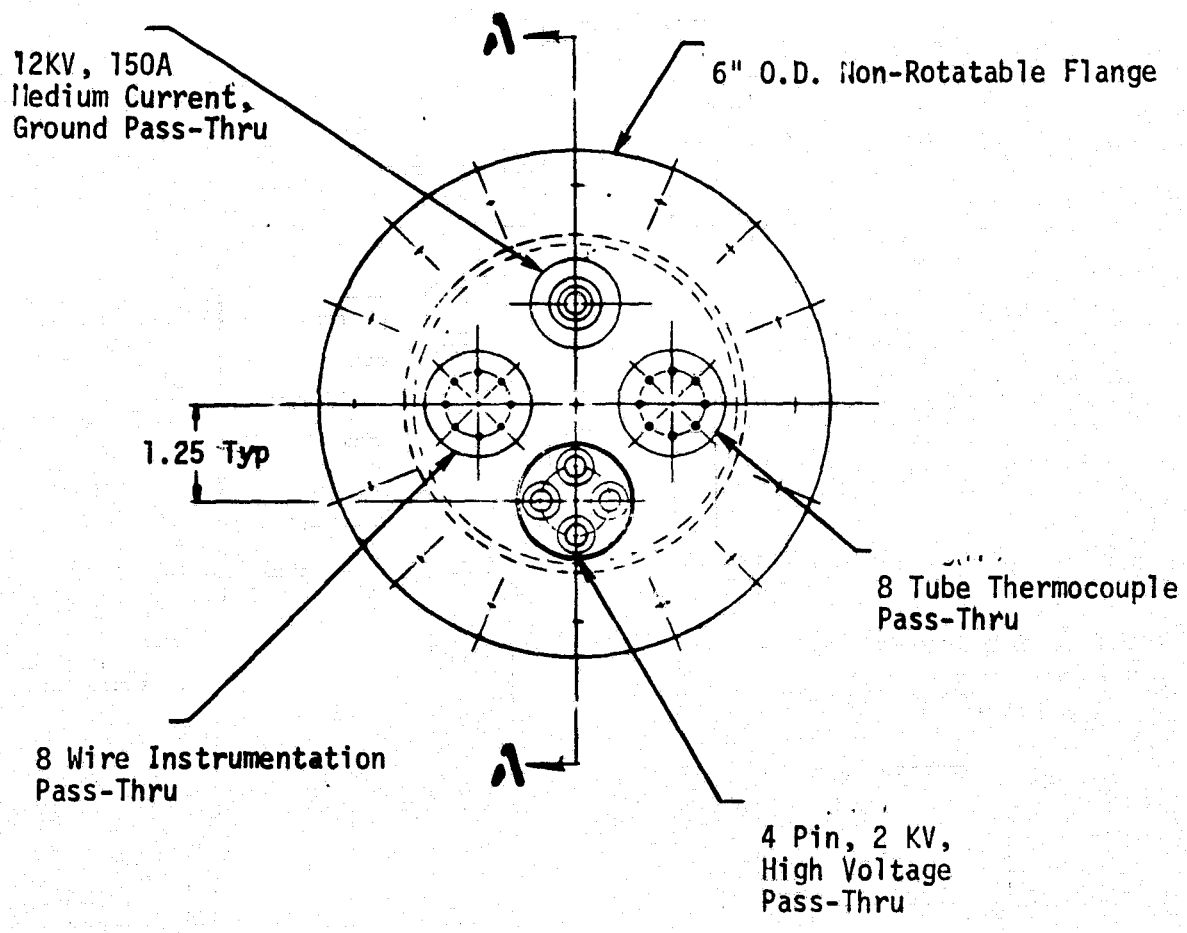

FIGURE 5-4 – DIAGRAM OF INSTRUMENTATION PORT

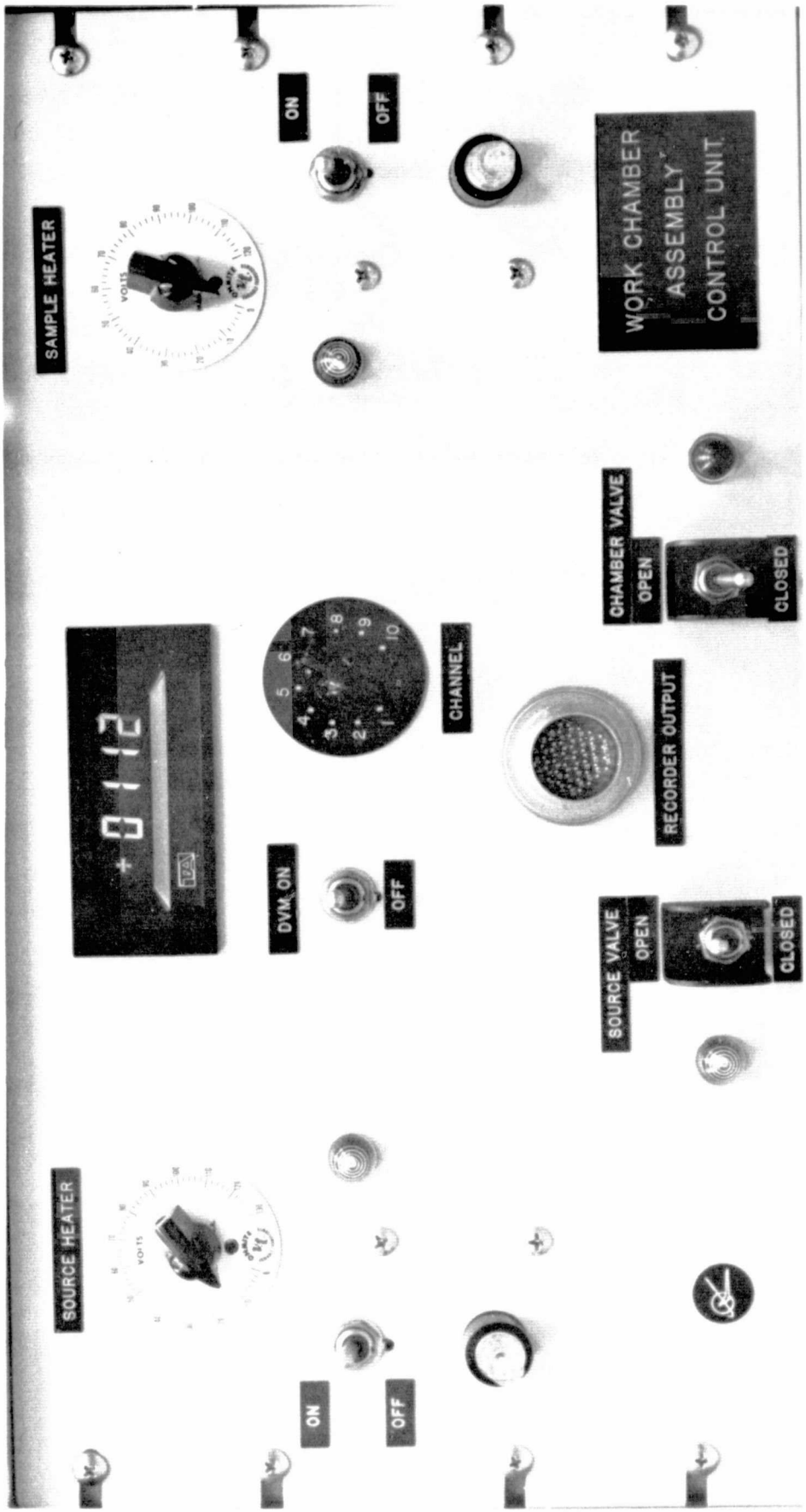

FIGURE 5-5 — FRONT PANEL OF WCA CONTROL UNIT

5.6 ELLIPSOMETER. Ellipsometry has been used extensively at MDAC-E for measuring the optical constants, n and K, of thin optical films and for determining the thickness of contaminant film on optical surfaces. Film thicknesses of several hundred angstroms can be readily measured with a precision of ±0.5Å.

To provide the capability for measuring thin film on samples in the WCA, standard Gaertner Scientific Corp. ellipsometer optics are mounted on a rigid platform attached to the chamber. A helium-neon laser, modulated at 800 Hz, illuminates the sample at 70° angle of incidence, and the reflected light is synchronously detected by a silicon detector monitored by a lock-in amplifier. An ellipsometer data reduction program, described in Section 6, permits rapid data reduction.

5.7 INSTALLATION. A photograph of the completed WCA is shown in Figure 5-6. The system was installed at NASA-JSC and its vacuum integrity verified. The sample holder was installed, instrumented and mechanically and optically aligned. Supports for the ellipsometer optics were then attached to the main chamber and support stand. The optics, mounted on dovetail slides, were then installed and aligned. Operation of the ellipsometer was demonstrated and the Ellipsometer Data Reduction Program (EDRP) was exercised on the HP-9830. The vacuum ultraviolet reflectometer (VUV) was assembled, its vacuum interface with Model 235 monochrometer completed, and it was then optically aligned. A system checkout was then performed to verify the operation of the VUV.

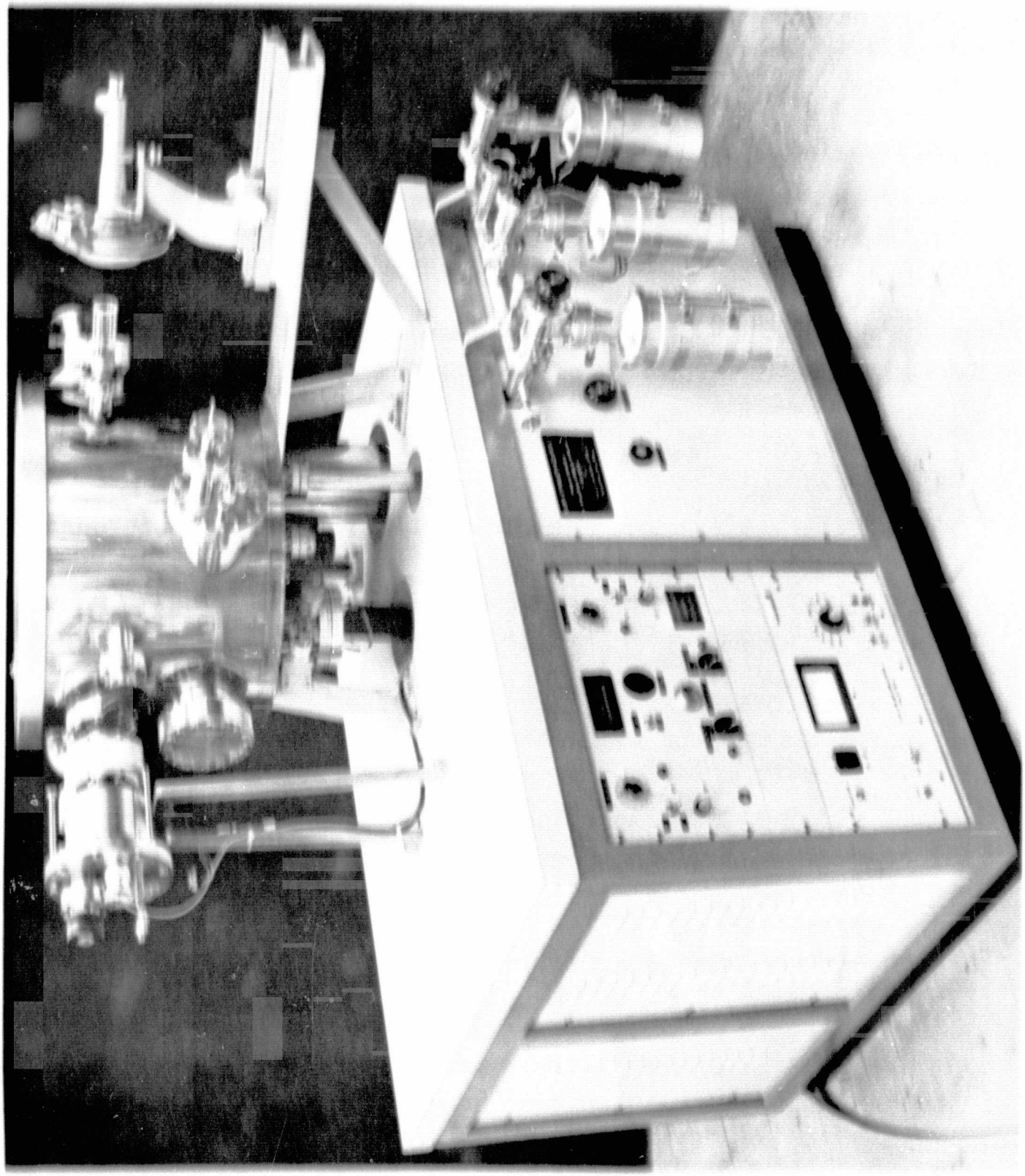

FIGURE 54 – COMPLETED WCA

6.0 ELLIPSOMETER DATA REDUCTION SYSTEM

To reduce the experimental data taken with the ellipsometer (the angles ψ and Δ) to determine the properties of surface films, it is necessary to find solutions to the primary ellipsometric equations. To facilitate easy solutions of these complex equations, an Ellipsometer Data Reduction System (EDRS) was assembled and checked out.

6.1 HARDWARE. The EDRS consists of selected hardware, the function of which is to permit adaptions of existing data reduction programs to be run in the laboratory without a dependence on remote computation facilities. After a detailed review of available components, a Hewlett-Packard Model 9830 Programmable Calculator was selected as the most appropriate system. The HP-9830 is a table-top unit which is easily transported. Table VIII lists the components which comprise the EDRS hardware.

TABLE VIII - EDRS HARDWARE

° HP-9830	Programmable Calculator with 8K words of memory and magnetic tape cassette mass storage
° HP-9866	Thermal Line Printer
° HP-11270B	Matrix Operations Read-Only-Memory (ROM)
° HP-271	Plotter Control Option
° HP-272	Extended Input/Output ROM
° HP-274	String Variables ROM
° HP-11279B	Advanced Programming Option

The principal features which recommended the HP-9830 to the present application are the programming language and the man-machine interface design. The HP-9830 is programmed in "keystroke BASIC", one of the most commonly used and widely known scientific programming languages. The user enters his BASIC program code via a built-in keyboard arranged in standard teletype format. Each program line is edited for proper syntax before the machine executes the instructions contained in the line. In this way the user is assured of a syntactically perfect program code (but not necessarily logically perfect). In addition, commands for storing and retrieving files of program code or data from the tape cassette mass storage are entered via the keyboard and can be included as programmed

commands.

6.2 ELLIPSOMETER DATA REDUCTION PROGRAM. An Ellipsometer Data Reduction Program (EDRP) was developed to facilitate rapid analysis of ellipsometric data. The EDRP is stored in several files on a magnetic tape cassette. In producing the EDRP two alternatives were considered: a) producing a new program in BASIC starting with the ellipsometric equation; or b) adapting an existing FORTRAN program to the HP-9830. The latter alternative was explored initially and it was found to be a straightforward task to make the translation to HP-9830 BASIC. Consequently, the EDRP, as detailed in Appendix C, is an adaptation of an extremely powerful FORTRAN code produced by Dow Chemical Company[6]. The BASIC EDRP version was economized somewhat compared to the FORTRAN version, and the capability for plotting calculated results via an x-y plotter (driven by the HP-9830) was added to the BASIC code. A complete description, listing and examples of output of the EDRP are contained in Appendix C.

7.0 VACUUM ULTRAVIOLET REFLECTOMETER

7.1 VACUUM ULTRAVIOLET REFLECTOMETER. The properties of highly reflective, optically smooth surfaces are particularly sensitive to contamination-induced degradation at ultraviolet and vacuum ultraviolet (VUV) wavelengths (400nm to 50nm), the effect being more pronounced at the shorter wavelengths. Such degradation was observed in the Reflectance Study discussed in Section 3.2 of this report. To provide the capability for further studies of these effects a bi-directional scanning VUV reflectometer was designed and fabricated to interface with the Work Chamber Assembly.

7.2 PRELIMINARY EXPERIMENTS. A series of experiments were performed in order to determine the operating parameters of the McPherson Model 235 Monochromator and the Model 630 Capillary Discharge Light Source. Knowledge of the spectral radiance levels was required prior to designing the reflectometer. The monochromator was mounted on an extension elbow attached to a 275 ls^{-1} turbomolecular pump. A mechanical pump was used to evacuate the first stage of the differential slit assembly. A McPherson-supplied 13-stage photomultiplier was freshly coated with sodium salicylate and its anode current was measured with a picoammeter.

Both helium and hydrogen were evaluated as lamp gases and the resultant spectra are shown in Figures 7-1 and 7-2. The hydrogen spectrum was obtained with a lamp pressure of 1.6 torr and a photomultiplier voltage of 900V, while the helium lamp pressure was 45 torr and the photomultiplier was operated at 1000V. The signal levels of the hydrogen spectrum are between a few tenths of a microamp and several microamps, with a dark current of 1.5×10^{-11}amp. An ultraviolet/visible scattered light background level of 1×10^{-8}amp exists in these spectra. Both spectra were recorded with 125 micron exit slits and 100 micron entrance slits.

7.3 REFLECTOMETER PUMPING SYSTEM. During the preliminary experiments a study of the pumping requirements for the monochromator was undertaken. The effective speed of the turbomolecular pumping system used was 150 ls^{-1} and the differential slit assembly was evacuated at an effective speed of 5 ls^{-1}. With this system and a helium pressure of 40 torr across 100 micron slits, the pressure in the monochromator rose to between 10^{-3} and 10^{-2} torr. A 6-inch pumping line between the monochromator and the

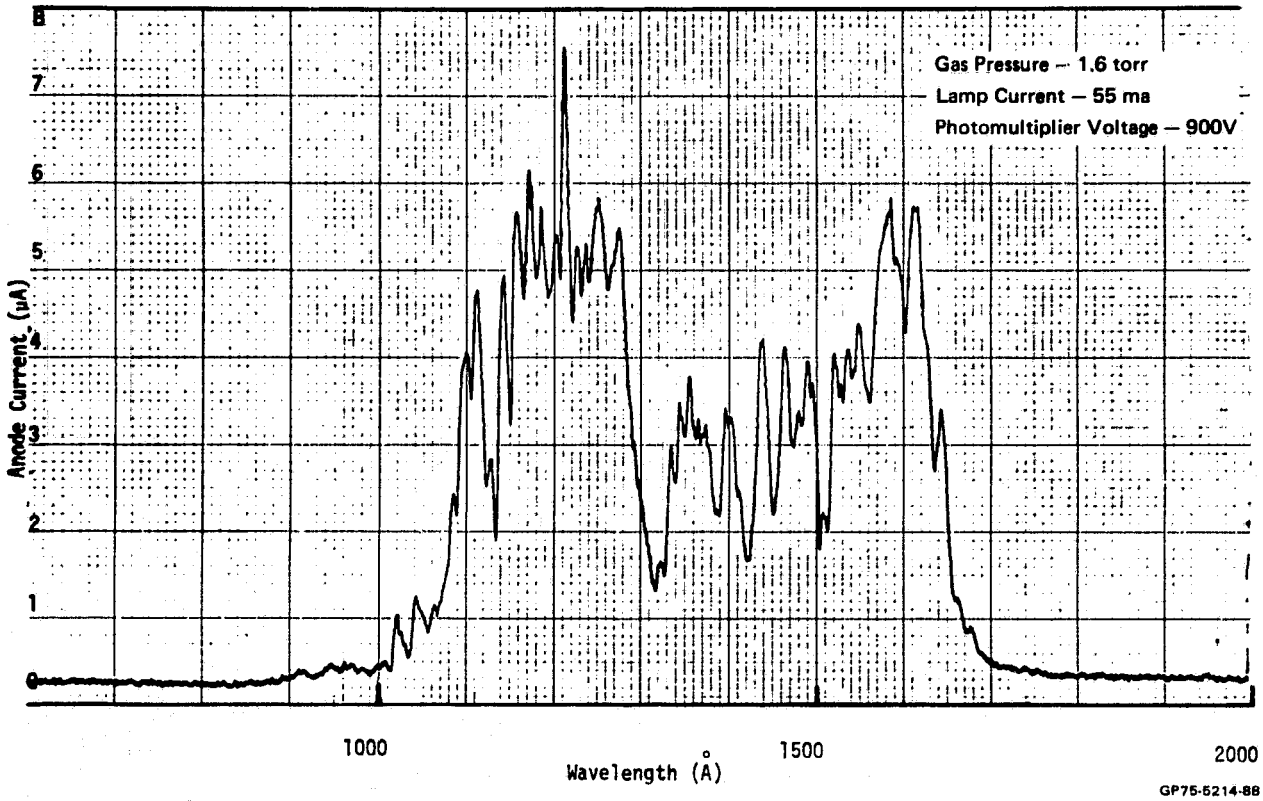

FIGURE 7-1 – SPECTRAL RADIANCE LEVEL OF THE HYDROGEN DISCHARGE

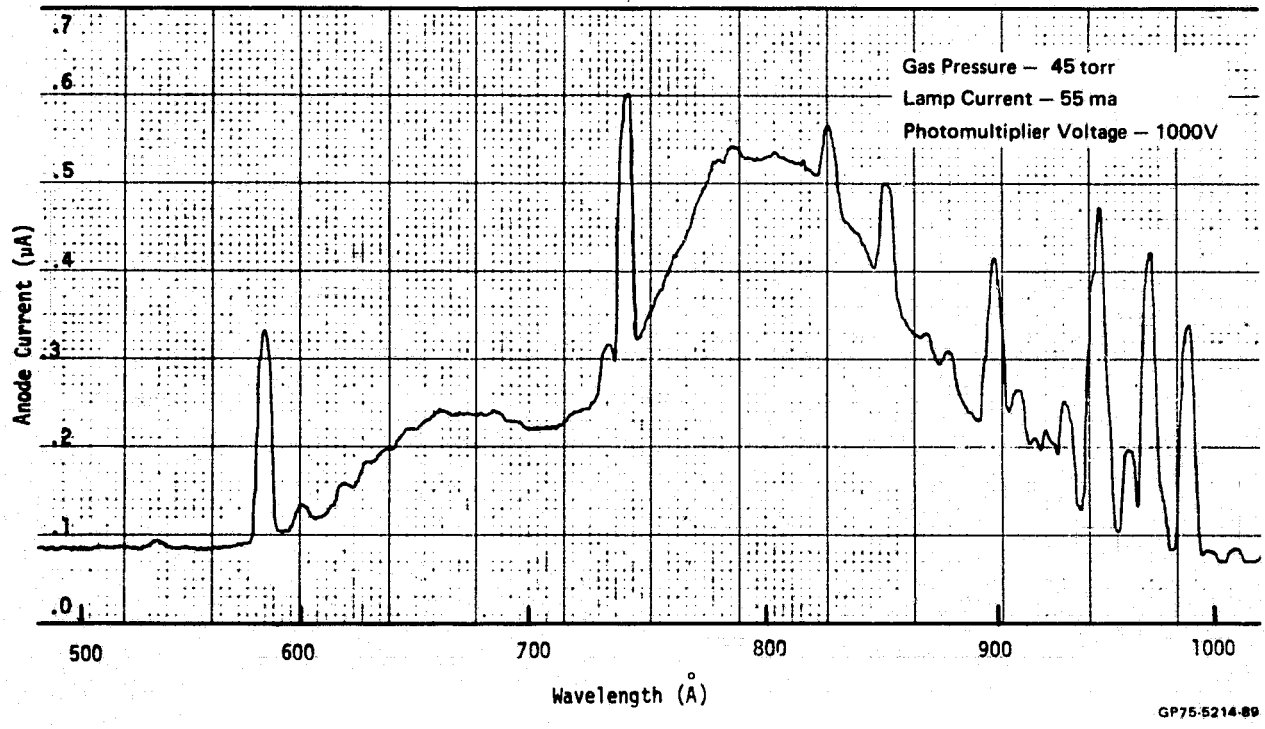

FIGURE 7-2 – SPECTRAL RADIANCE LEVEL OF THE HELIUM DISCHARGE

WCA would at best provide 150 ls^{-1} of pumping capacity in the Model 235, and the WCA ion pumps would then be exposed to damaging high pressures. This fact coupled with the inherently poor pumping efficienty of noble gases by ion pumps made it imperative that a separate high speed pumping system be provided for removing large helium and hydrogen gas loads. A Veeco Pumping Station equipped with a 6-inch diffusion pump was selected.

7.4 REFLECTOMETER DESIGN. The design goals were to develop a scanning, dual-channel reflectometer with a single detector operating between 50nm and 200nm. It was also required that the reflectometer output data be compatible with the McPherson Model 782 Logarithmic Ratiometer.

The optical design of the reflectometer is shown in Figure 7-3 and the key elements of the design are illustrated in Figure 7-4. Radiation from the monochromator passes through an order filter, a radiation baffle and a three-blade rotary chopper before illuminating a 1/2-meter focal length platinum-coated, split spherical mirror. This split mirror focusses the sample beam onto the sample and the reference beam onto the wall of the integrating sphere, wherein the two beams are alternately detected by a photomultiplier.

A key element is the three-blade rotating chopper that is driven by a 200 rpm synchronous motor through a bellows-sealed rotary pass thru in the base of the mirror chamber. As illustrated in Figure 7-5, this chopper successively blocks both beams, opens the reference channel, blocks both, then exposes the sample channel.

Another feature of the design is the fluorescent integrating sphere. A 4-inch diameter stainless steel sphere was first painted with an opaque coating of barium sulphate paint, chosen for its vacuum quality and its good diffuse reflectance throughout the visible spectrum. A coating of fluorescent para-terphenyl (~3mg cm^{-2}) was vacuum deposited onto the painted surface. An EMI 9635A photomultiplier is mounted in the bottom of the sphere.

The optical system results in a detector output like that shown in Figure 7-5. The detector current output is fed directly into the logarithmic ratiometer where it is synchronized with the electronic logic circuitry. Reference pulses at 6.6 Hz are generated by an optical switch coupled to the drive shaft of the three-blade chopper. The switch consists of a slotted circular plate attached to the drive shaft passing through a

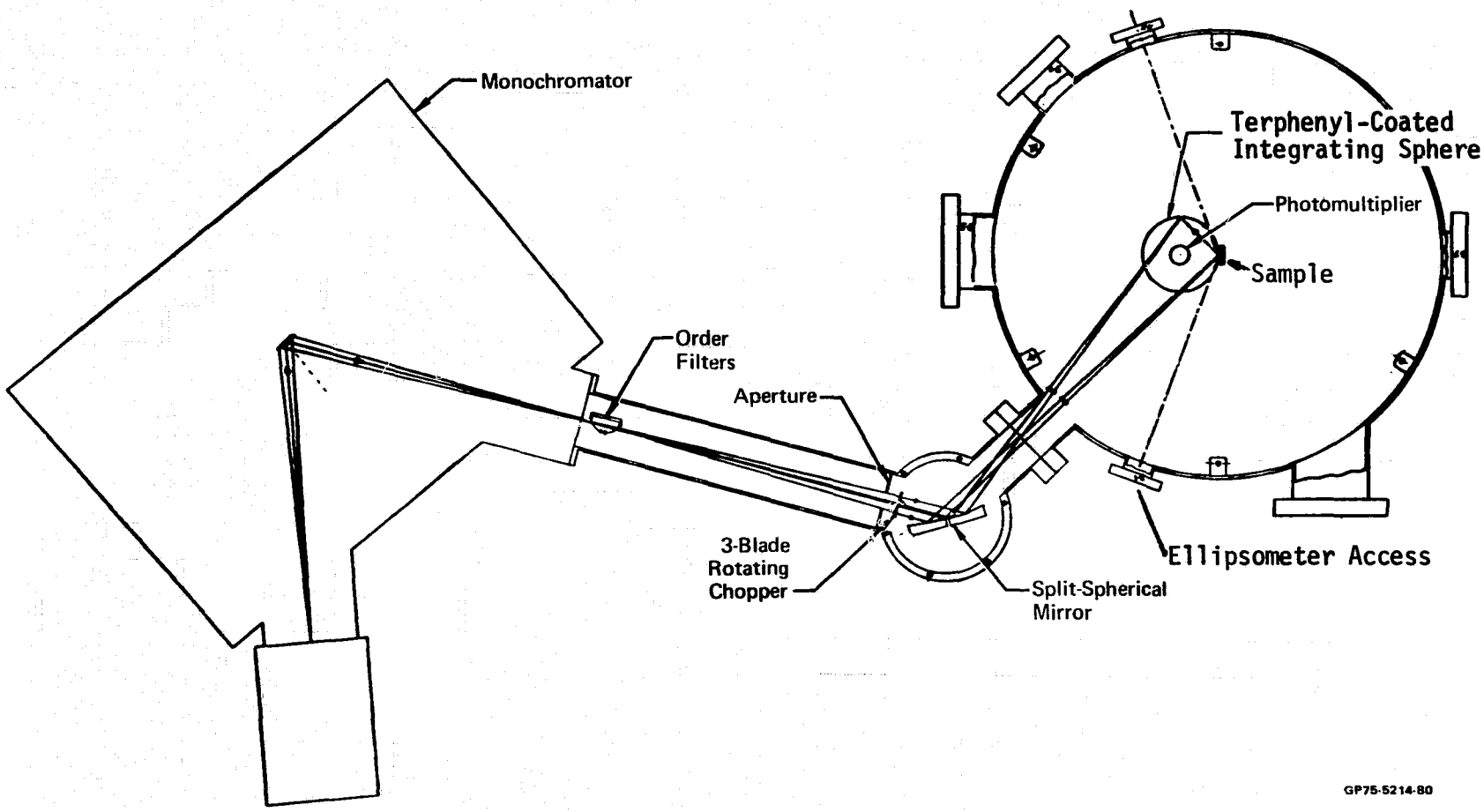

FIGURE 7-3 – LAYOUT AND OPTICAL DIAGRAM OF VUV REFLECTOMETER

Monsanto MCA-81 optical switch. Electronics designed to drive this switch with the ratiometer power supply and to interface the optical switch with the McPherson ratiometer logic are shown in Figure 7-6.

7.5 INTEGRATION OF THE REFLECTOMETER WITH THE WCA. The selection of the location for the reflectometer was dictated by the requirement to make hemispherical reflectance measurements on a sample, while maintaining the capability to perform ellipsometric measurements. This constraint, coupled with the need to preserve access to all the other components on the system, resulted in the arrangement illustrated in Figure 7-3. For VUV reflectance measurements, the sample is rotated to the centerline of the chamber, on the axes of the ellipsometer optics. The reflectometer optics are at an angle of 45° to the sample normal, compared to 70° for the ellipsometer. The reflectometer attachment was fabricated to fit between the VUV port on the WCA and the exit slit of the McPherson instrument, as shown in Figure 7-3. This attachment contains the reflectometer optics as well as coupling the two vacuum systems.

7.6 REFLECTOMETER CHECKOUT. In order to verify the performance of the VUV reflectometer without interfacing with the main vacuum chamber and pumping system, the optical components were assembled to simulate the actual testing configuration and reflectance measurements were made in air between 200nm and 300nm. Measurements in this range were a stringent check on the system performance as the output of the discharge lamp is extremely weak at these wavelengths.

The measured hemispherical reflectance of a magnesium fluoride overcoated aluminum mirror is shown in Figure 7-7 (the scale is inverted as the ratiometer measures absorptance). Shown also, for comparison, are the values for the specular reflectance of a similar mirror measured previously and reported in Section 3-2, and the reflectance spectra measured on a Beckmann DK-2A Spectrophotometer. It is evident that the measured reflectance is in quite good agreement with the other measured values, even on the expanded scale.

The measured transmittance of soda lime glass, compared to the values obtained with the Beckmann DK-2A is shown in Figure 7-8. Again the data recorded with the VUV reflectometer system agrees with that obtained from the other systems, the apparent difference between the two sets of data

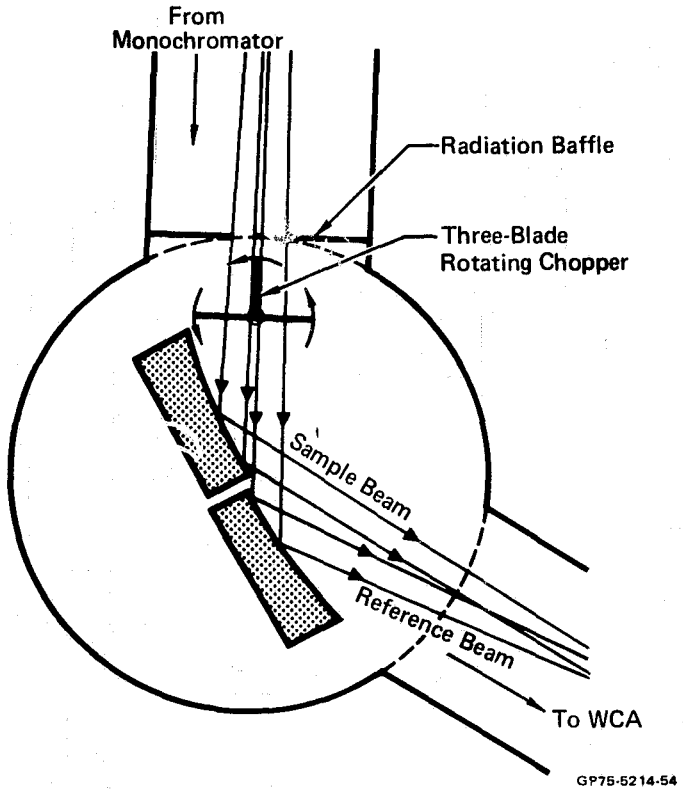

FIGURE 7-4 - KEY ELEMENTS OF THE VUV REFLECTOMETER OPTICAL SYSTEM

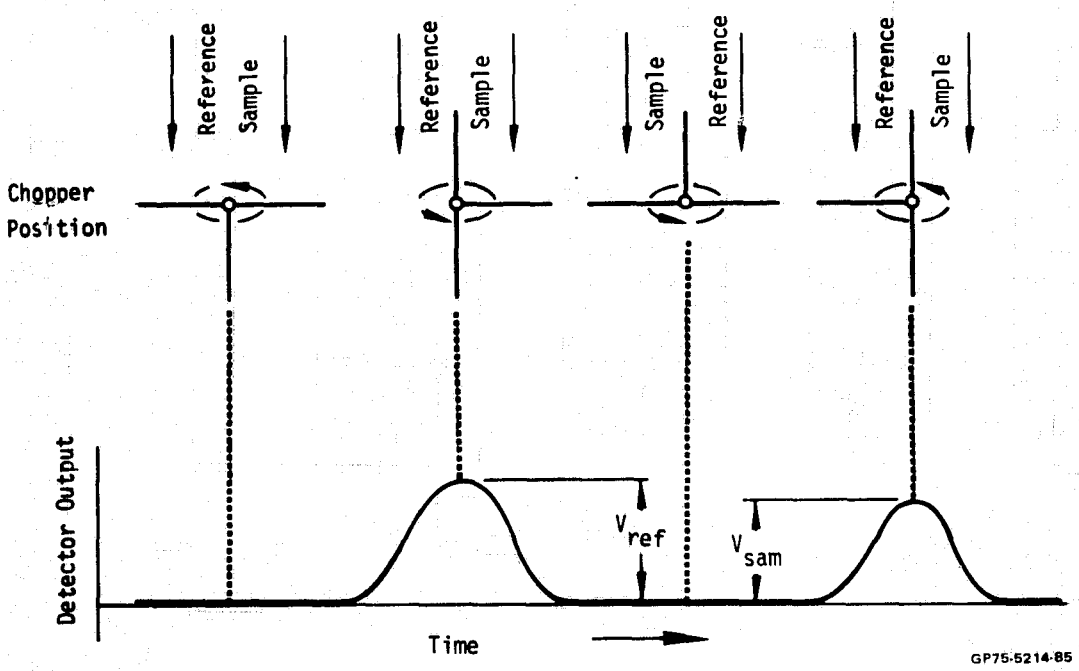

FIGURE 7-5 – OUTPUT OF VUV REFLECTOMETER DETECTOR FOR EACH POSITION OF ROTATING CHOPPER

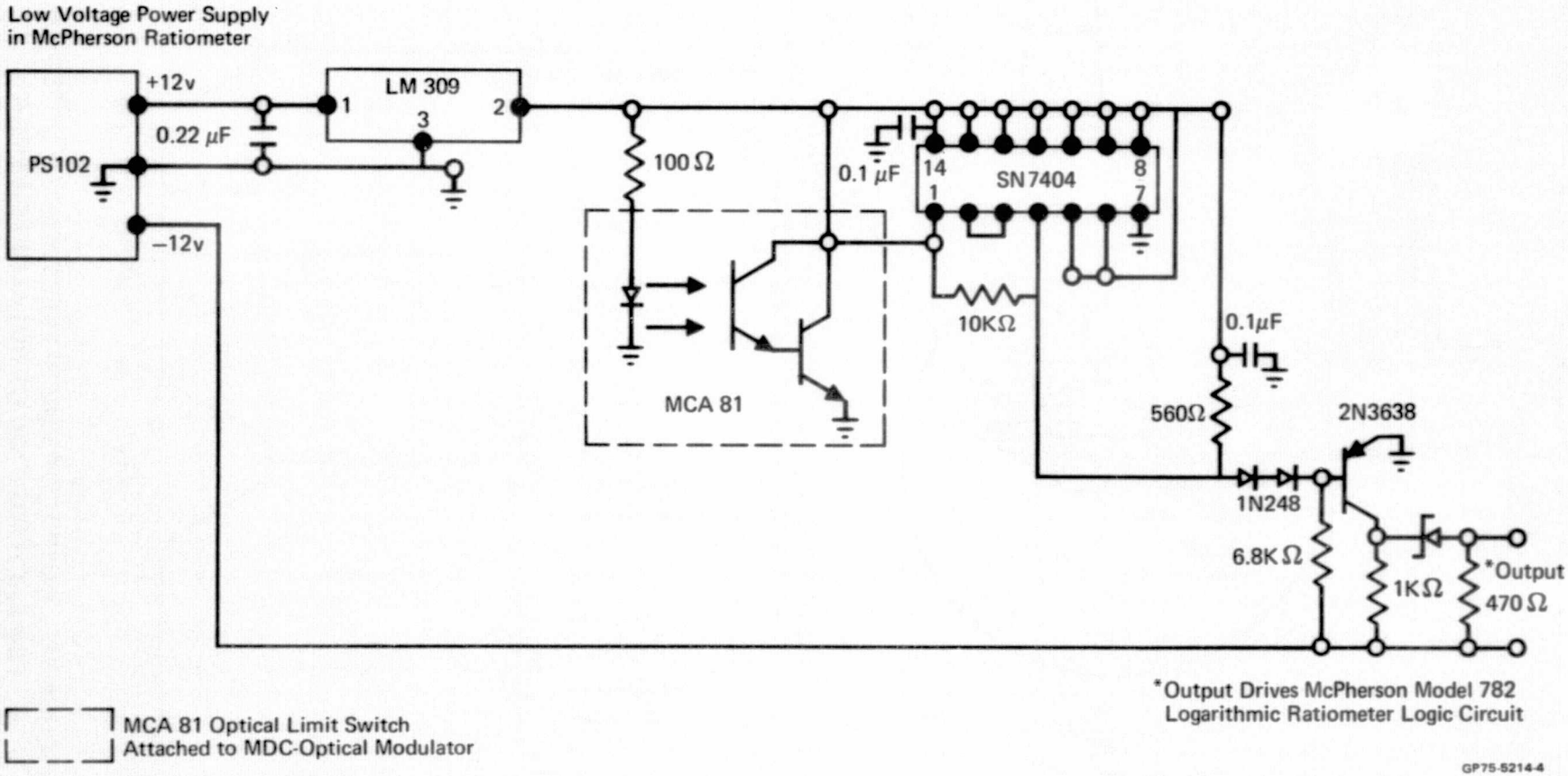

FIGURE 7-6 – ELECTRONIC INTERFACE BETWEEN THE VUV REFLECTOMETER AND THE MCPHERSON MODEL 782 LOGARITHMIC RATIOMETER

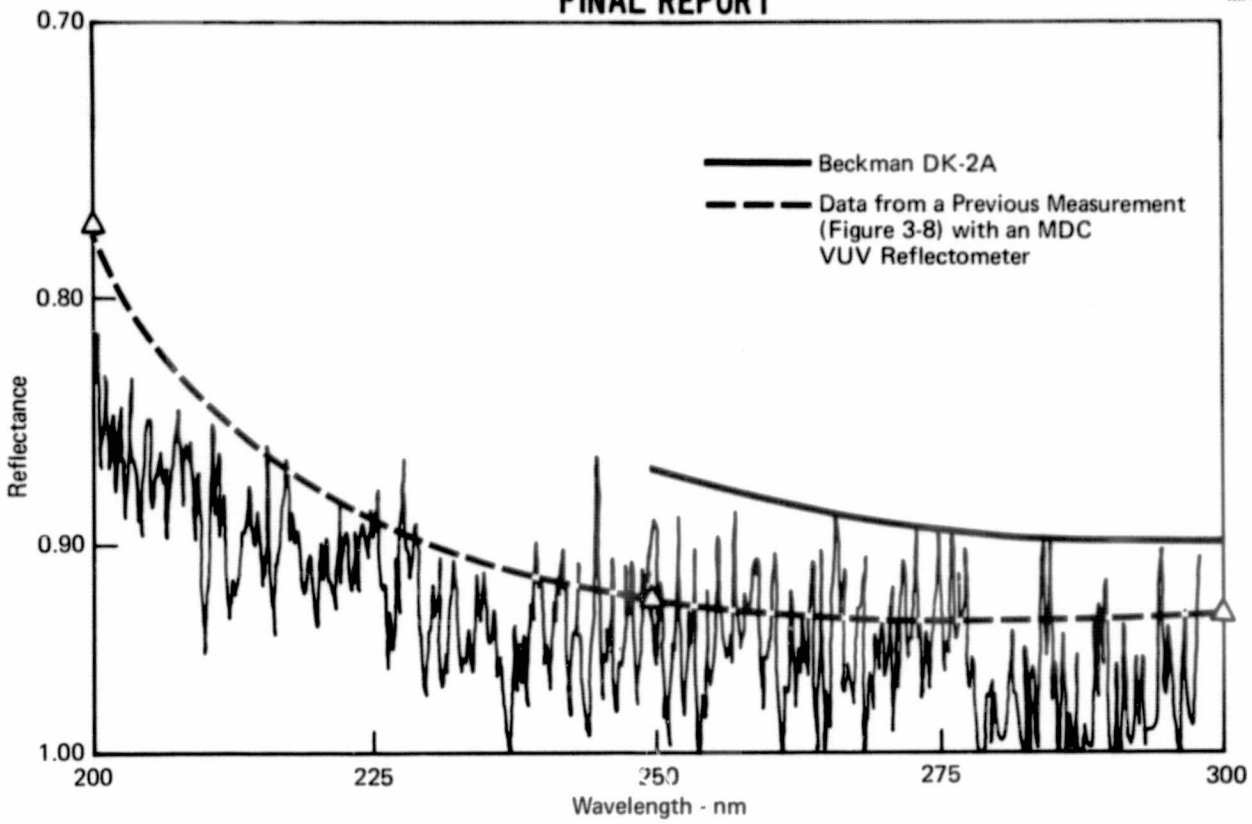

FIGURE 7-7 — REFLECTANCE OF A MAGNESIUM FLUORIDE OVERCOATED ALUMINUM MIRROR AS MEASURED WITH THE VUV REFLECTOMETER AND TWO OTHER SYSTEMS

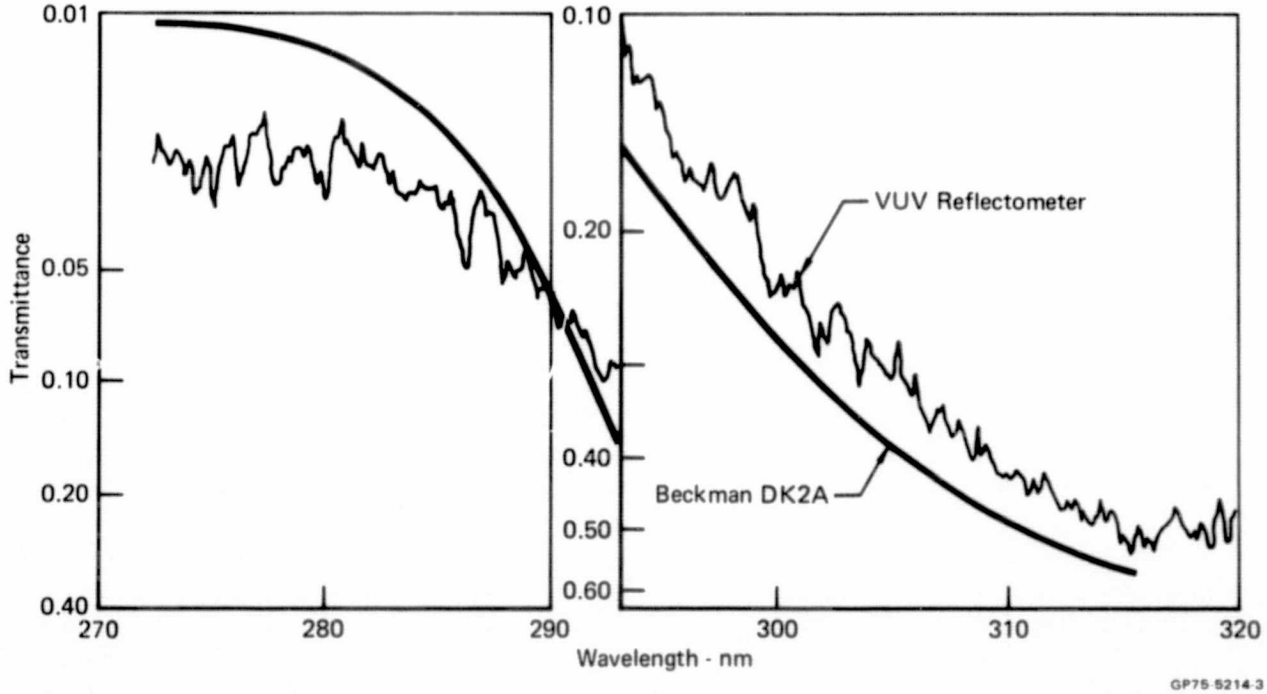

FIGURE 7-8- TRANSMITTANCE OF SODA LIME GLASS AS MEASURED ON THE VUV REFLECTOMETER AND A BECKMAN DK 2A SPECTROPHOTOMETER

being accentuated by the expanded scale. Moreover, it should be noted that wavelength inaccuracies in either system as small as 5nm could cause such a discrepancy.

A study was undertaken to determine the nature of the noise exhibited in the spectral scans. The Hinterregger discharge source was found to be the source of the noise. This was confirmed by observing the system output with a D.C. source inserted in place of the capillary lamp. With this noise-free source the spectral scans were correspondingly smooth.

8.0 CONCLUSIONS AND RECOMMENDATIONS

The completed Work Chamber Assembly successfully met all the design goals in almost every respect, and it should provide a versatile and valuable system for a variety of experimental studies. In particular, the combined ellipsometer/VUV reflectometer capability will lend itself to studies of the reflectance of both oxidized and contaminated surfaces, with precise measurements of the thickness and properties of the surface films. The use of the vapor deposition port in conjunction with the ellipsometer and the VUV relfectometer will facilitate the development of optimum deposition techniques for metallic mirror coatings. The combination of the VES and the temperature-controlled substrate will allow a variety of contamination experiments to be performed ranging from the study of contamination kinetics to the investigation of optical degradation mechanisms.

Although well equipped, the WCA has spare access ports for the addition of further instruments. A port has been included which permits the sample to be irradiated with electron, proton or solar fluxes and, when used with the VES and VUV reflectometer, provides a unique capability for investigating the effects of particulate and radiative fluxes on contaminated optical surfaces. For some applications a residual gas analyzer (RGA) would be valuable and several commerical RGAs are available that would mate with the WCA ports. The integration of many instruments such as ESCA or AES would be difficult, as the necessary adjustment and proximity of the sample to the electron analyzer would require extensive modifications to the chamber.

SECTION 9 - REFERENCES

(1) G. Hass and W. R. Hunter, Applied Optics 9, 9 (1970).

(2) R. W. Fane and W. E. J. Neal, J. Opt. Soc. Am. 60, 6 (1970).

(3) G. Hass, Optik 1, 2 (1946).

(4) G. Hass and J. E. Waylonis, J. Opt. Soc. Am. 51, 7 (1961).

(5) O. S. Heavens, Optical Properties of Solid Films, Dover Publications, Inc. New York, 1975.

(6) R. W. Loser and D. T. Larson, A.E.C. AT(29-1)-1106, 1969.

APPENDIX A

BIBLIOGRAPHY

1. SOURCES - ROCKET PLUMES

Moses, J.; Miller, E.; Zoller, L.: Contamination of Optical Surfaces by Solid Rocket Exhausts. NASA TN-P and VE-P-67-2, 22 May 1967.

Troester, R.: Star Sighting Problems Due to Light Scatter from RCS Plume Residue on Apollo Spacecraft Optics. NASA-CR-73509, 30 September 1968.

Borson, N.: Rocket Plumes as Contamination Sources. Optical Contamination in Space Symposium, Aspen, Colorado, 14 August 1969.

Martinkovic, P. J.: Monopropellant Exhaust Contamination Investigation Final Report. AFRPL-TR-69-72, 1969.

Martinkovic, P. J.: Bipropellant Attitude Control Rocket (ACR) Plume Effects on Solar Cells, Optics and Thermal Paint. AFRPL-TR-70-87, August 1970.

Spisz, E. W.: Effects of Exhaust Products from a Biopropellant Attitude Control Engine on Transmittance of Quartz. NASA TM X-2399, September 1971.

Jack, J. R.; Spisz, E. W.: The Effect of Rocket Plume Contamination on the Optical Properties of Transmitting and Reflecting Materials. AIAA Paper 72-56, January 1972.

Kemp, R. F.; Luedke, E. E.; Hall D. F.; Miller, W. D.: Effects of Electrostatic Rocket Material Deposited on Solar Cells. AIAA Paper 72-447, 1972.

Bowman, R. L.; Spisz, E. W.; Sommers, R. D.; Jack, J. R.: Skylab Plume Contamination Experiments. NASA SP-336, 1973.

Spisz, E. W.; Bowman, R. L.; Jack, J. R.: Effects of a Bipropellant Thruster Plume on Spacecraft Materials and Optical Components. NASA TM X-68212, March 1973.

2. SOURCES - ABLATORS

Steinberg, M.; Maiden, C. J.; Leak, W. R.; Hansen, C. F.: Preliminary Studies of the Effects of Ablation Contaminants on Radiation. ARPA Order 347-62, December 1962.

3. SOURCES - ORGANICS

Hearst, P. J.: Effect of Photodegratation on Organic Coatings. NBS Spec. Pub. 336, 1970.

Coulson, D. M.; Haynes, D. L.: Contamination Character of Materials in Space Technology Testing. AIAA Paper 72-267, April 1972.

Fleischauer, P. D.; Tolentino, L.: The Far Ultraviolet Photolysis of Polymethylphenysiloxane Films on Quartz Substrates. NASA SP-336, November 1973.

4. SOURCES - CRYODEPOSITS

Liu, C. K.; Tien, C. L.: Spectral Transmittance of Cryodeposits on a Transmitting Substrate. AIAA Paper 73-149, 1973.

5. SURFACES - OPTICAL SYSTEMS

Shapiro, H.; Contamination of Optical Surfaces. NASA Technical Note D-4612, June 1968.

Enlow, D. L.: Contamination Studies in a Space Simulated Environment. NBS Spec. Pub. 336, 1970.

Heinisch, R. P.: Light Scatter from Contaminated Spacecraft Windows. AIAA Paper 71-472, April, 1971.

Kruger, R.: A Contamination Experiment Investigating the Failure of the Nimbus IV Filter Wedge Spectrometer. NASA SP-298, 1972.

Leger, L. J.: APOLLO Experience Report - Window Contamination. NASA TN D-6721, March 1972.

Viehmann W.; Eubanks, A. G.: Effects of Surface Contamination on the Infrared Emissivity and Visible-Light Scattering of Highly Reflective Surfaces at Cryogenic Temperatures. NASA SP-298, 1972.

Bowman, R. L.; Spisz, E. W.; Jack, J. R.: Effects of Contamination on the Optical Properties of Transmitting and Reflecting Materials Exposed to a MMH/N_2O_4 Rocket Exhaust. NASA TM X-68204, March 1973.

Visentine, J. T.; Richmond, R. G.: Contamination Effects of Titanium Sublimation-Pumped Systems on Optical Surfaces. NASA SP-336, 1973.

6. SURFACES - SENSORS

Anspaugh, B. E.: ATS-5 Solar Cell Experiment After 699 Days in Synchronous Orbit. Record of the Ninth IEEE Photovoltaic Specialists Conference,Silver Spring, Maryland, 2-4 May 1972.

Moore, W. W., Jr.: Environmental Simulation Testing of Solar Cell Contamination by Hydrazine. NASA SP-298, 1972.

7. SURFACES - THERMAL CONTROL COATINGS

Wappaus, W.A.: The Photo-Response at an Alkaline Paint Interface W. Aluminum. NBS Spec. Pub. 336, 1970.

Sommers, P. D.: Optical Properties of Thermal Control Coatings Contaminated by MMH/N_2O_4 5-Pound Thruster in a Vacuum Environment with Solar Simulation. AIAA Paper 72-263, 10-12 Apr 72.

Sommers, P.D.; and Raquet, C.A.: Effect of Thruster Pulse Length and Thruster Exhaust Damage of S13G White Coatings. NASA TM X-68213, March 1973.

8. EXPERIMENTAL - MEASUREMENT TECHNIQUES

Dunipace, D.W.; Horr, K. S.; Jackman, R. W.; Poehlmann, H. C.; Reynolds, M. M.: A New, Sensitive, Rapid Materials Contamination Screening System. Sampe Journal, Vol. 5, 38, (1969).

Burns, G.L.; Moore, W. W., Jr.; Tashbar, P. W.: An Investigational Technique for the Behavior of a Contaminated Optical Surface in the Near Ultraviolet-Visible-Near Infrared. Applied Spectroscopy, 24, 457 (1970).

Chuan, R.L.: Particulate Contaminant Measurement by QCM. NBS Spec. Pub. 336, 1970.

Edwards, T. R.: An Approach to Contamination Identification. NASA-TM-X-64506, 1970.

Linton, R. C.: Measurement & Application of Contaminant Optical Constants. AIAA Paper 71-460, Apr 71.

Williams, J. R.: Holographic Analysis of Contaminant Deposits on Optical Surfaces. Proc. Instrumentation Soc. Am. 17, 154 (1971).

Zaun, N.: Ellipsometric Analysis of Contaminate Deposits on Optical Surfaces. Jour. Opt. Soc. Am. 61, 693 (1971).

Wallace, P.A.; Chuan, R. L.: The Use of a QCM and an Optical Reflectometer to Determine Contaminant Material Optical Constants. NAS SP-298, 1972.

Klingman, E.E.: Experimental Determination of Sticking Coefficients. NASA SP-298, 1972.

Williams, J. R.; Kurtz, R. L.: Holographic Analysis of Particle Size Distribution and Particle Velocities for Skylab Contamination Ground Test. NASA SP-298, 1972.

Dormant, L.: Use of Ellipsometry for the Quantitative Detection of Contaminants on Second Surface Mirrors. NBS SP-336, 1973.

Hamberg, O.: Photographic Measurement of Particulate Surface Contamination. NASA SP-336, 1973.

Hayes, J. D.; Richmond, R. G.; Chatterton, N. E.: Development of Techniques for Advanced Optical Contamination Measurement With Internal Reflection Spectroscopy. NASA SP-336, 1973.

Saylor, W. P.: Measurement of Condensate Film Contamination on Critical Surfaces by Charged Particle Excited X-Ray Fluorescence. NASA SP-336, 1973.

9. EXPERIMENTAL - CONTAMINATION MONITORING

Sawyer, R. R.: Potential AAP Cluster on Apollo Contamination Monitor in Support of ATM. Martin Marietta Corporation Report MCR-68-78, March 1968.

Zwiener, James M.: Ground Contamination Monitoring Devices for the Apollo Telescope Mount. AIAA Paper 71-458, April 1971.

Arnett, G. M.; Linton, R. C.: Integrated Real-Time Contamination Monitor: Optical Module. NASA SP-298, 1972.

Richmond, R. G.; Harmon, H. N.: An Instrument for Real-Time Detection of Contamination in Space Environmental Test Chambers. NASA SP-298, 1972.

McKeown, D.; Corbin, W. E., Jr.; Naumann, R. J.: Thermoelectrically-Cooled Quartz Crystal Microbalance. NASA SP-336, 1973.

Wallace, D. A.: Development of a Miniature Cryogenic QCM for Low Temperature Contamination Measurement. NASA SP-336, 1973.

10. EXPERIMENTAL-CLEANING TECHNIQUES

Carlson, G. L.; Gillette, R. B.; Hollahan, J. R.: Restoration of Optical Properties of Surfaces by Radiofrequency-Excited Oxygen. Journal of Vacuum Science and Technology, 7, 534 (1970).

Gibson, W. C.; Modisette, J. L.: A System for Removing Contaminants from Spacecraft Optical Systems. Journal of Spacecraft and Rockets, 1, 353 (1970).

Gillette, R. B.: Restoration of Degraded Spacecraft Surfaces Using Reactive Gas Plasmas. AIAA Paper 71-463, April 1971.

Baurer, T.; Goldstein, H. W.; Pikus, I. M.: Contaminant Removal from Optical Surfaces. NASA SP-298, 1972.

Beverly, W. D.; Gillette, R. B.; Cruz, G. A.: Removal of Hydrocarbon Contaminant Film from Spacecraft Optical Surfaces Using a Radiofrequency-Excited Oxygen Plasma. AIAA Paper 72-263, 1973.

Cruz, G. A.; Gillette, R. B.: Active Cleaning Technique for Removing Contamination from Optical Surfaces in Space, NASA-CR-127219 QPR-4, 1972.

11. THEORETICAL - ANALYTICAL TECHNIQUES

Klingman, E.: Analysis of a Two-Dimensional Mass Transport Problem in Contamination of Space Flight Experiments. NASA TM X-64581, 18 February 1971.

Naumann, R. J.: Design Principles for Contamination Abatement in Scientific Satellites. International Astronautical Federation, International Astronautical Congress, 23rd, Vienna, Austria, 8-15 October 1972.

12. THEORETICAL - CONTAMINATION KINETICS

Naumann, R. J.: Dynamics of Spacecraft Contamination. NASA SP-298, 1972.

13. GENERAL - SPACE RADIATION EFFECTS

Griffin, R. N.; Scannapieco, J. F.: Optical Surface Degradation from Combined Ultraviolet Radiation and Outgassed Materials. Journal of Vacuum Science and Technology, Vol. 6, 209 (1969).

Jones, P. F.: Radiation Effects on Contaminants from the Outgassing of Silastic 140 RTV. NASA SP-298, 1972.

Nicoletta, C. A.; Eubanks, A. G.: Effect of Simulated Space Radiation on Selected Optical Materials. Appl. Opt. 11, 1365 (1972).

McPherson, D. G.: Apollo Telescope Mount Extended Applications Study Program ATM Contamination Study. NASA CR-61173, May 1967.

Buffalano, A. C.: Optical Contamination in Space - A Program for Decision. NASA-CR-112653, 1970.

Cothran, C. A.; Greenberg, S. A.; McCargo, M.: A Survey of Contamination of Spacecraft Surfaces. AIAA Paper 71-457, 1971.

Sherman, A. L.: Evaluation of Orbital Optical Contamination Phenomena and its Effects on Astronomical Experiments. AIAA Paper 71-74, January 1971.

Smith, D. C.: Cleanliness Requirements for Space Borne Optical Sensors. AIAA Paper 71-471, April 1971.

APPENDIX B

INSTRUCTIONS FOR OPERATION OF VACUUM SYSTEM

HOT START. This pumping procedure should be used when the ion pump is isolated from the main chamber and already operating under vacuum.

(1) Check that the system is leak tight and all valves are closed. (By-Pass valve, manifold roughing valve, VES gate valve).
(2) Open the manifold roughing valve and rough pump the system with the air aspirator pump to 150 torr. Close air aspirator valve.
(3) Cool the cryo-sorption pumps with liquid nitrogen.
(4) Open the valve of the first cryo-sorption pump. The system should pump to 50 micron in about 15 minutes, at which time the valve should be closed and the second pump should be activated. The system should pump to about 10 microns.
(5) The by-pass valve may now be carefully opened, not allowing the pressure in the ion pump to exceed 5×10^{-5} torr.
(6) When the chamber pressure is below 1×10^{-3} torr the cryo-sorption pump, manifold roughing, and by-pass valves should be closed.
(7) Set the range selector switch on the ion pump power supply to the 10KV position and the START/RUN switch to START.
(8) Open the main chamber gate valve. The voltage may drop to 500 volts, but should climb back to about 4750 volts within a few minutes. Do not allow a low voltage condition to exist for over 10 minutes. If the voltage does not rise, close the main chamber gate valve and repeat this procedure.
(9) When the voltage reaches 4750 volts set the START/RUN switch to RUN and the power supply selector switch to TORR.

COLD START. This pumping procedure should be used when the ion pump and the main chamber are at atmospheric pressure.

(1) Open the main chamber gate valve and perform steps 1 through 4 of the Hot Start Procedure.
(2) Close the main chamber gate valve.
(3) Set the range selector switch on the ion pump power supply to the 10KV position and the START/RUN switch to START.

(4) Turn the unit on. The voltage will fall to about 500 volts. Do not allow this low voltage condition to exist for over 10 minutes. If it does, turn the power supply off, open the chamber gate valve and rough the system again to at least 10 microns.

(5) The voltage should climb to about 4750 volts in a few minutes. When it does, switch the range selector to Torr and perform stemps 5 through 9 of the Hot Start Procedure.

APPENDIX C

ELLIPSOMETER DATA REDUCTION PROGRAM

DESCRIPTION. THE ELLIPSOMETER DATA REDUCTION PROGRAM (EDRP) IS DESIGNED TO FACILITATE THE RAPID ANALYSIS OF ELLIPSOMETRIC DATA. THE EDRP IS WRITTEN IN H-P BASIC CODE AND IS INTENDED FOR USE WITH THE H-P9830 PROGRAMMABLE CALCULATOR. IT IS NOT NECESSARY THAT THE USER BE CAPABLE OF PROGRAMMING THE H-P9830. BY FOLLOWING THE DIRECTIONS PRESENTED BELOW, THE EDRP CAN BE SUCCESSFULLY RUN. THE EDRP IS AN ADAPTATION OF A FORTRAN PROGRAM WRITTEN BY ROBERT W. LOSER AND DONALD T. LARSON OF THE DOW CHEMICAL COMPANY, GOLDEN, COLORADO.

OPTIONS. THE EDRP ALLOWS THE USER TO SELECT THREE PROCESSING OPTIONS.

#1 COMPUTE THE COMPLEX REFRACTIVE INDEX OF THE SUBSTRATE MATL
#2 COMPUTE THE THICKNESS OF A THIN FILM ON A SUBSTRATE MATERIAL
#3 COMPUTE THE ELLIPSOMETRIC ANGLES PSI AND DEL FOR VARIOUS THICKNESSES OF A GIVEN FILM MATERIAL ON A GIVEN SUBSTRATE MATERIAL AND PLOT THE RESULTS ON AN X-Y PLOTTER.

THE USER WILL BE INTERROGATED REGARDING THE DESIRED OPTION. BY TYPING THE APPROPRIATE OPTION NUMBER (1,2,OR 3) THE USER ROUTES THE EDRP THROUGH THE PROPER PATH TO OBTAIN THE DESIRED OUTPUT

1. EDRP CASSETTE CONTAINS SEVEN FILES OF PROGRAM CODE. THE FILES ARE NUMBERED CONSECUTIVELY FROM 0 THROUGH 6 ON THE TAPE. THE FILE CONTENTS ARE DESCRIBED BELOW:

FILE NO.	CONTENTS
0	INTRODUCTION. THIS IS THE FILE BEING RUN NOW
1	EXECUTIVE FILE. THIS FILE IS LOADED INTO THE CALCULATOR NEXT TO BEGIN EXECUTION OF THE EDRP
2	OPTION #1 PROGRAM CODE. THIS FILE IS AUTOMATICALLY LOADED WHEN THE USER SELECTS OPTION #1.
3	OPTION #2 PROGRAM CODE. THIS FILE IS AUTOMATICALLY LOADED WHEN THE USER SELECTS OPTION #2
4	SUBROUTINE FOR CALCULATING PSI AND DEL FOR GIVEN FILM THICKNESSES & VICE-VERSA. THIS FILE CONTAINS THE PROGRAM CODE OF THE BASIC EQUATIONS OF ELLIPSOMETRY AND IS THE HEART OF THE ERDP
5	OPTION #3 PROGRAM CODE. THIS FILE IS AUTOMATICALLY LOADED WHEN THE USER SELECTS OPTION #3
6	EMPTY FILE. AVAILABLE FOR USER DEFINED USE.

EDRP EXECUTION IS BEGUN WITH THE FOLLOWING COMMAND:

```
LOAD 1 EXECUTE
```

TAPE FILL #1, THE EXECUTIVE PROGRAM WILL THEN BE LOADED INTO MEMORY. THE NEXT-STEP IS TO INPUT VIA THE KEYBOARD STARTING DATA FOR THE PROGRAM. THESE DATA ARE ENTERED USING BASIC DATA STATEMENTS NUMBERED BETWEEN 200 AND 998. DEPENDING UPON WHICH OPTION IS CHOSEN, THE FORMAT OF THESE DATA STATEMENTS WILL VARY. A 'DATA SET' REFERS TO THE ONE OR SEVERAL DATA STATEMENTS INPUT FOR THE SELECTED OPTION. THE FORMATS FOR EACH OF THE THREE TYPES OF DATA SET IS PRESENTED BELOW:

OPTION #1

```
200 DATA 'REFRACTIVE INDEX OF SURROUNDING MEDIUM','ANGLE OF
         INCIDENCE','NUMBER OF PAIRS OF PSI AND DEL TO BE PROCESSED'
201 DATA 'PSI1','DEL1'
202 DATA 'PSI2','DEL2'
203 DATA 'PSI3','DEL3'
 ...
 ...
998 DATA 'PSIN','DELN'
```

FOR EACH PSI, DEL PAIR, OPTION #1 COMPUTES THE COMPLEX REFRACTIVE INDEX OF THE BARE SUBSTRATE (NO FILM ON SUBSTRATE)

OPTION #2

```
200 DATA 'REFRACTIVE INDEX OF SURROUNDING MEDIUM','ANGLE OF
         INCIDENCE','WAVELENGTH OF LIGHT','REAL PART OF SUBSTRATE
         REFRACTIVE INDEX','IMAGINARY PART OF REFRACTIVE INDEX',
         'NUMBER OF PSI AND DEL PAIRS'
201 DATA 'REAL PART OF FILM REFRACTIVE INDEX','IMAGINARY PART OF
         FILM REFRACTIVE INDEX'
202 DATA 'PSI1','DEL1'
203 DATA 'PSI2','DEL2'
204 DATA 'PSI3','DEL3'
 ...
 ...
998 DATA 'PSIN','DELN'
```

FOR EACH PSI, DEL PAIR, OPTION #2 COMPUTES THE THICKNESS OF THE SURFACE FILM IN ANGSTROMS AND THE EXPECTED ERROR IN THE COMPUTED THICKNESS VALUE

OPTION #3

```
200 DATA 'REFRACTIVE INDEX OF SURROUNDING MEDIUM','ANGLE OF
         INCIDENCE','WAVELENGTH OF LIGHT','REAL PART OF SUBSTRATE
         REFRACTIVE INDEX','IMAGINARY PART OF SUBSTRATE REFRACTIVE
         INDEX'
```

```
201 DATA 'MINIMUM VALUE OF IMAGINARY PART OF FILM REFRACTIVE INDEX'
         'MAXIMUM VALUE OF IMAGINARY PART OF FILM REFRACTIVE INDEX',
         'INCREMENT IN IMAGINARY PART OF FILM REFRACTIVE INDEX'
202 DATA MINIMUM VALUE OF REAL PART OF FILM REFRACTIVE INDEX',
         'MAXIMUM VALUE OF REAL PART OF FILM REFRACTIVE INDEX',
         'INCREMENT IN REAL PART OF FILM REFRACTIVE INDEX'
203 DATA 'MINIMUM VALUE OF FILM THICKNESS','MAXIMUM VALUE OF FILM
         THICKNESS','INCREMENT IN FILM THICKNESS' (ALL IN ANGSTROMS)
```

OPTION #3 COMPUTES A PSI, DEL PAIR FOR EACH SPECIFIED FILM REFRACTIVE INDEX AND FILM THICKNESS

NOTE: IF DESIRED, SEVERAL DATA SETS CORRESPONDING TO THE SAME OR TO DIFFERENT OPTIONS CAN BE ENTERED USING CONSECUTIVELY NUMBERED DATA STATEMENTS. FOR EXAMPLE, A DATA SET FOR OPTION #1 NUMBERED 200 TO 210 & A DATA SET FOR OPTION #2 NUMBERED 211 TO 220

AFTER THE USER HAS ENTERED THE REQUIRED DATA SETS, THE COMMAND

```
RUN EXECUTE
```

IS ENTERED. THE EDRP RESPONDS...

```
NO. OF DATA SETS?
```

IF THE USER HAS PROPERLY ENTERED 3 DATA SETS, HE TYPES...

```
3 EXECUTE
```

THE EDRP RESPONDS...

```
OPTION NO.?
```

IF, FOR EXAMPLE, THE FIRST DATA SET CORRESPONDS TO OPTION #1 THE USER TYPES...

```
1 EXECUTE
```

THE EDRP WILL THEN LOAD THE APPROPRIATE TAPE FILE (FILE #2 FOR OPTION #1) AND WILL PRODUCE A HARD COPY OF THE COMPUTED OUTPUT

UPON COMPLETION OF THE CALCULATIONS FOR EACH DATA SET, THE EDRP WILL DISPLAY...

```
OPTION NO.?
```

THE DESIRED OPTION IS THEN ENTERED AS BEFORE AND THE CYCLE REPEATS

WHEN OPTION #3 IS CHOSEN THE CALCULATOR WILL LOAD THE PROPER FILE AND RESPOND...

```
WANT X-Y PLOTS? 1=YES, 2=NO
```

THE USER WILL ENTER EITHER 1 OR 2 ACCORDING TO HIS CHOICE
IF PLOTS ARE DESIRED, FURTHER QUESTIONS WILL BE ASKED TO DETERMINE
THE GRAPH LIMITS AND AXIS MARKINGS

THE H-P9862 PLOTTER WILL THEN PRODUCE THE OUTPUT IN THE FORM
OF A PLOT OF PSI VS. DEL

WHEN ALL DATA SETS HAVE BEEN PROCESSED, PRESS...

STOP EXECUTE

AND REWIND THE CASSETTE TO THE BEGINNING

TO BEGIN ERDP EXECUTION, TYPE...

LOAD 1 EXECUTE

PRINTER OUTPUT FORMAT
OPTION #1

DATA SET NO. 1

COMPUTING THE INDEX OF REFRACTION OF A CLEAN SURFACE

THE INDEX OF REFRACTION OF THE SURROUNDING MEDIUM IS 1
THE ANGLE OF INCIDENCE IS 70 DEGREES

	PSI PRIME	DEL PRIME	N31	N32
1	31.43	134.73	3.199898996	4.301208114

DATA SET NO. 2

COMPUTING THE INDEX OF REFRACTION OF A CLEAN SURFACE

THE INDEX OF REFRACTION OF THE SURROUNDING MEDIUM IS 1
THE ANGLE OF INCIDENCE IS 70 DEGREES

	PSI PRIME	DEL PRIME	N31	N32
1	31.43	134.73	3.199898996	4.301208114

PRINTER OUTPUT FORMAT
OPTION #2

INDEX OF REFR.OF SURROUNDING MEDIUM IS 1
ANGLE OF INCIDENCE IS 70 DEG
WAVEL OD LIGHT IS 5461 ANGSTROMS
INDEX OF REFR. OF SUBSTRATE IS N31= 3.2
AND N32= 4.3
VALUE OF N21 IS 2
VALUE OF N22 IS 1.5

QUADRANT	PSI	DELTA	THICKNESS	ERROR
1 4	31.43	134.73	-0.021835224	4.42602E-03
2 4	30.7	114.15	100.0008069	5.62464E-03
3 4	29.36	99.89	200.0082604	1.39471E-04
4 4	27.61	90.13	300.0813658	3.68481E-03
5 3	25.63	83.76	400.0729325	3.94224E-03
6 3	23.64	80.33	500.1145688	5.15467E-04
7 3	21.94	79.47	600.2264556	3.51184E-03
8 3	20.76	80.42	699.847096	2.62897E-03
9 2	20.12	82.16	799.5883976	3.04853E-03
10 2	19.9	83.88	899.8160719	2.12786E-03
11 2	19.95	85.15	1001.367083	0.025711167

PRINTER OUTPUT FORMAT
OPTION #3

X-AXIS LIMITS--DELTA 0 360
Y-AXIS LIMITS--PSI 0 90
OPTION NO. 3
INDEX OF REFR. OF SURROUNDING MEDIUM IS 1.003
ANGLE OF INCIDENCE IS 70
WAVEL OF LIGHT IS 5461
INDEX OF REFR OF SUBSTRATE IS N31= 3.24 N32= 2.7416
N21= 2.4 N22= 0.168

THICKNESS	PSI CALC	DEL CALC
0	65.86442124	307.5360682
40	65.35784928	297.1904193
80	64.79152449	287.3374379
120	64.16098424	277.9542275
160	63.44589779	268.9914948
200	62.60683767	260.362276
240	61.58283777	251.9164207
280	60.29411905	243.3941949
320	58.66328538	234.3552187
360	56.68642369	224.1077945
400	54.59736902	211.7655337
440	53.06723936	196.7420427
480	53.02791602	179.7583618
520	54.81443135	162.9751041
560	57.75525288	148.1643782
600	60.94901105	135.524227
640	63.89627009	124.3641056
680	66.45988944	113.9193107
720	68.65872395	103.6155957
760	70.54629169	93.06312604
800	72.16581993	82.00125236
840	73.53972805	70.26218477
880	74.67155610	57.76286512
920	75.55247205	44.5186963
960	76.17002811	30.66283487
1000	76.51769452	16.44676487
1040	76.60263379	2.201295472
1080	76.44871699	348.2624405
1120	76.09364	334.8965481

ELLIPSOMETER DATA REDUCTION PROGRAM
FILE 1

```
10 DIM A[160]
30 I1=1
40 DISP "NO. OF DATA SETS";
50 INPUT A[1]
60 DISP "OPTION NO.";
70 INPUT A[2]
80 GOTO A[2] OF 90,110,150,150,150
90 LINK 2,1000
100 GOTO 160
110 LINK 3,1000
120 GOTO 160
130 LINK 4,1000
140 GOTO 160
150 LINK 5,1000
160 GOSUB 1000
170 IF (I1-A[1])=0 THEN 9999
180 I1=I1+1
190 GOTO 60
```

ELLIPSOMETER DATA REDUCTION PROGRAM
FILE 2

```
1000 PRINT
1001 PRINT "DATA SET NO.";I1
1005 READ A[3],A[4],A[5]
1010 FOR I2=1 TO A[5]
1015 READ B[I2],C[I2]
1020 NEXT I2
1025 PRINT
1030 PRINT
1040 PRINT "COMPUTING THE INDEX OF REFRACTION OF A CLEAN SURFACE"
1045 PRINT
1050 PRINT "THE INDEX OF REFRACTION OF THE SURROUNDING MEDIUM IS"A[3]
1055 PRINT "THE ANGLE OF INCIDENCE IS";A[4];"DEGREES"
1060 PRINT
1065 PRINT "     ","PSI PRIME","DEL PRIME","N31","N32"
1070 A[6]=A[7]=0
1080 FOR I3=1 TO A[5]
1081 I=I3
1085 GOSUB 1300
1090 PRINT I3,B[I3],C[I3],A[6],A[7]
1100 NEXT I3
1105 GOTO 1400
1300 A[8]=SIN(A[4]/57.29578)
1305 A[9]=COS(A[4]/57.29578)
1310 A[10]=SIN(2*B[I]/57.29578)
1315 A[11]=COS(2*B[I]/57.29578)
1316 A[11]=A[11]↑2
1320 A[12]=SIN(C[I]/57.29578)
1325 A[13]=COS(C[I]/57.29578)
1330 A[14]=A[8]/A[9]
1335 A[15]=A[14]*A[14]*A[11]/((1+A[10]*A[13])↑2)
1340 A[16]=(A[3]↑2)*(A[8]↑2)*(1+A[15])
1345 A[17]=A[3]*A[14]*A[8]*A[10]*A[12]/(1+A[10]*A[13])
1350 A[18]=A[16]-(A[17]↑2)
1355 A[19]=(A[16]-(A[3]↑2)*(A[8]↑2))/A[16]
1360 A[20]=2*A[17]*SQR(A[16]*A[19])
1365 A[21]=SQR(A[18]*A[18]+A[20]*A[20])
1370 A[6]=SQR((A[21]+A[18])/2)
1375 A[7]=SQR((A[21]-A[18])/2)
1380 RETURN
1400 RETURN
9999 END
```

ELLIPSOMETER DATA REDUCTION PROGRAM
FILE 3

```
1000 LINK 4,2500
1001 READ A[3],A[4],A[22],A[6],A[7],A[5]
1005 READ D,E
1010 A[23]=A[24]=A[25]=A[26]=A[27]=0
1015 A[28]=A[29]=A[30]=A[31]=A[32]=A[33]=0
1020 A[34]=A[35]=A[36]=A[37]=A[38]=A[39]=0
1025 A[40]=A[41]=F=G=0
1030 A[42]=A[43]=2
1040 PRINT
1045 PRINT "INDEX OF REFR.OF SURROUNDING MEDIUM IS";A[3]
1050 PRINT "ANGLE OF INCIDENCE IS";A[4]"DEG"
1055 PRINT "WAVEL OD LIGHT IS";A[22];"ANGSTROMS"
1060 PRINT "INDEX OF REFR. OF SUBSTRATE IS N31=";A[6]
1065 PRINT "AND N32=";A[7]
1070 IF A[2]>2 THEN 1090
1075 PRINT "VALUE OF N21 IS";D
1080 PRINT "VALUE OF N22 IS";E
1090 PRINT
1095 PRINT "    ","PSI","DELTA","THICKNESS","ERROR","QUADRANT"
1100 PRINT
1105 FOR I2=1 TO A[5]
1110 READ K,L
1115 H=0
1120 GOSUB 2500
1125 A[44]=K-A[23]
1130 A[45]=L-A[24]
1135 M=SQR((A[44]↑2)+A[45]↑2)
1140 A[43]=3
1141 PRINT
1145 PRINT I2,K,L,F,M,G
1150 NEXT I2
1155 IF A[2]=2 THEN 1170
1160 PRINT "CALC. VALUE OF N21 IS";D;"WITH STD. ERROR";N
1165 PRINT "SELECTED VALUE OF N22 IS";E
1170 RETURN
```

ELLIPSOMETER DATA REDUCTION PROGRAM
FILE 4

```
2500 GOTO A[43] OF 2600,2600,3500,2600,5000
2600 A[46]=COS(A[4]/57.29578)
2605 A[47]=A[46]*A[46]
2610 A[16]=A[3]*A[3]
2615 A[48]=A[6]*A[6]
2620 A[49]=A[7]*A[7]
2625 A[50]=A[48]+A[49]
2630 A[51]=1-(A[16]*A[48]-A[16]*A[49]+A[47]*(A[16]*A[49]-A[16]*A[48]))/(A[50]↑2
2635 A[52]=(2*A[16]*A[6]*A[7]*(1-A[47]))/(A[50]↑2)
2640 A[53]=0
2645 IF A[51]=0 OR A[51]>0 THEN 2660
2650 A[53]=ATN(A[52]/A[51])-3.141593
2655 GOTO 2665
2660 A[53]=ATN(A[52]/A[51])
2665 A[53]=A[53]*0.5
2670 A[17]=(A[51]*A[51]+A[52]*A[52])↑0.25
2675 A[54]=A[17]*COS(A[53])
2680 A[55]=A[17]*SIN(A[53])
2685 A[56]=D*D
2690 A[57]=E*E
2700 A[58]=A[56]+A[57]
2705 A[59]=1-(A[16]*A[56]-A[16]*A[57]+A[47]*(A[16]*A[57]-A[16]*A[56]))/(A[58]↑2
2710 A[60]=(2*A[16]*D*E*(1-A[47]))/(A[58]↑2)
2715 A[61]=0
2720 IF A[59]=0 OR A[59]>0 THEN 2735
2725 A[61]=ATN(A[60]/A[59])-3.141593
2730 GOTO 2740
2735 A[61]=ATN(A[60]/A[59])
2740 A[61]=A[61]*0.5
2745 A[17]=(A[59]*A[59]+A[60]*A[60])↑0.25
2750 A[62]=A[17]*COS(A[61])
2755 A[63]=A[17]*SIN(A[61])
2760 A[64]=D*A[63]+E*A[62]
2765 A[15]=D*A[62]-E*A[63]
2770 A[16]=A[64]*A[64]+A[15]*A[15]
2775 A[17]=-A[22]/(4*3.141593)
2780 A[65]=A[64]/A[17]
2785 A[66]=A[15]/A[17]
2790 A[67]=A[3]*A[46]-D*A[62]+E*A[63]
2795 A[68]=A[3]*A[46]+D*A[62]-E*A[63]
```

FILE 4 (CONT'D)

```
2800 A[69]=D*A[63]+E*A[62]
2805 A[70]=D*A[46]-A[3]*A[62]
2810 A[71]=E*A[46]-A[3]*A[63]
2815 A[72]=D*A[46]+A[3]*A[62]
2820 A[73]=E*A[46]+A[3]*A[63]
2825 A[74]=D*A[62]-E*A[63]-A[6]*A[54]+A[7]*A[55]
2830 A[75]=D*A[62]-E*A[63]+A[6]*A[54]-A[7]*A[55]
2835 A[76]=A[6]*A[55]+A[7]*A[54]-D*A[63]-E*A[62]
2840 A[77]=A[6]*A[55]+A[7]*A[54]+D*A[63]+E*A[62]
2845 A[78]=A[6]*A[62]-A[7]*A[63]-D*A[54]+E*A[55]
2850 A[79]=A[6]*A[62]-A[7]*A[63]+D*A[54]-E*A[55]
2855 A[80]=D*A[55]+E*A[54]-A[6]*A[63]-A[7]*A[62]
2860 A[81]=D*A[55]+E*A[54]+A[6]*A[63]+A[7]*A[62]
2865 A[82]=(A[67]*A[68]-A[69]*A[69])/(A[68]*A[68]+A[69]*A[69])
2870 A[83]=(A[67]*A[69]+A[69]*A[68])/(A[68]*A[68]+A[69]*A[69])
2875 A[84]=(A[70]*A[72]+A[71]*A[73])/(A[72]*A[72]+A[73]*A[73])
2880 A[85]=(A[70]*A[73]-A[71]*A[72])/(A[72]*A[72]+A[73]*A[73])
2885 A[86]=(A[74]*A[75]-A[76]*A[77])/(A[75]*A[75]+A[77]*A[77])
2890 A[87]=(A[74]*A[77]+A[76]*A[75])/(A[75]*A[75]+A[77]*A[77])
2895 A[88]=(A[78]*A[79]-A[80]*A[81])/(A[79]*A[79]+A[81]*A[81])
2900 A[89]=(A[78]*A[81]+A[80]*A[79])/(A[79]*A[79]+A[81]*A[81])
2905 GOTO A[43] OF 3500,3500,5000,5000
3500 A[11]=COS(K/57.29578)
3505 A[10]=SIN(K/57.29578)
3510 A[90]=A[10]/A[11]
3515 A[91]=SIN(L/57.29578)
3520 A[92]=COS(L/57.29578)
3525 A[93]=A[84]*A[86]*A[88]*A[92]*A[90]-A[85]*A[86]*A[88]*A[91]*A[90]
3530 A[93]=A[93]-A[84]*A[86]*A[89]*A[91]*A[90]-A[85]*A[86]*A[89]*A[92]*A[90]
3535 A[93]=A[93]-A[84]*A[87]*A[88]*A[91]*A[90]-A[85]*A[87]*A[88]*A[92]*A[90]
3540 A[93]=A[93]-A[84]*A[87]*A[89]*A[92]*A[90]+A[85]*A[87]*A[89]*A[91]*A[90]
3545 A[93]=A[93]-A[82]*A[86]*A[88]+A[82]*A[87]*A[89]+A[83]*A[87]*A[89]
3550 A[93]=A[93]+A[83]*A[86]*A[89]
3555 A[94]=A[84]*A[86]*A[88]*A[91]*A[90]+A[85]*A[86]*A[88]*A[92]*A[90]
3560 A[94]=A[94]+A[84]*A[86]*A[89]*A[92]*A[90]+A[84]*A[87]*A[88]*A[92]*A[90]
3565 A[94]=A[94]-A[85]*A[86]*A[89]*A[91]*A[90]-A[85]*A[87]*A[88]*A[91]*A[90]
3570 A[94]=A[94]-A[84]*A[87]*A[89]*A[91]*A[90]-A[85]*A[87]*A[89]*A[92]*A[90]
3575 A[94]=A[94]+A[83]*A[87]*A[89]-A[83]*A[86]*A[88]-A[82]*A[86]*A[89]
3580 A[94]=A[94]-A[82]*A[87]*A[88]
3585 A[95]=A[86]*A[92]*A[90]-A[87]*A[91]*A[90]+A[82]*A[84]*A[88]*A[92]*A[90]
3590 A[95]=A[95]-A[82]*A[85]*A[89]*A[92]*A[90]-A[83]*A[84]*A[89]*A[92]*A[90]
3595 A[95]=A[95]-A[83]*A[85]*A[88]*A[92]*A[90]-A[82]*A[84]*A[89]*A[91]*A[90]
3600 A[95]=A[95]-A[82]*A[85]*A[88]*A[91]*A[90]-A[83]*A[84]*A[88]*A[91]*A[90]
3605 A[95]=A[95]+A[83]*A[85]*A[89]*A[91]*A[90]-A[82]*A[84]*A[86]
3610 A[95]=A[95]+A[83]*A[85]*A[86]+A[83]*A[84]*A[87]+A[82]*A[85]*A[87]
3615 A[95]=A[95]-A[88]
3620 A[96]=A[87]*A[92]*A[90]+A[86]*A[91]*A[90]+A[82]*A[84]*A[89]*A[92]*A[90]
3625 A[96]=A[96]+A[82]*A[85]*A[88]*A[92]*A[90]+A[83]*A[84]*A[88]*A[92]*A[90]
3630 A[96]=A[96]-A[83]*A[85]*A[89]*A[92]*A[90]+A[82]*A[84]*A[88]*A[91]*A[90]
3635 A[96]=A[96]-A[82]*A[85]*A[89]*A[91]*A[90]-A[83]*A[84]*A[89]*A[91]*A[90]
3640 A[96]=A[96]-A[83]*A[85]*A[88]*A[91]*A[90]-A[83]*A[84]*A[86]
3645 A[96]=A[96]-A[82]*A[85]*A[86]-A[82]*A[84]*A[87]+A[83]*A[85]*A[87]
3650 A[96]=A[96]-A[89]
3655 A[97]=A[82]*A[92]*A[90]-A[83]*A[91]*A[90]-A[84]
3660 A[98]=A[83]*A[92]*A[90]+A[82]*A[91]*A[90]-A[85]
```

ORIGINAL PAGE IS
OF POOR QUALITY

FILE 4 (CONT'D)

```
3665 A[99]=A[95]*A[95]-A[96]*A[96]-4*A[93]*A[97]+4*A[94]*A[98]
3670 A[100]=2*A[95]*A[96]-4*A[93]*A[98]-4*A[94]*A[97]
3675 A[101]=0
3680 IF A[99]=0 OR A[99]>0 THEN 3695
3685 A[101]=ATN(A[100]/A[99])-3.141593
3690 GOTO 3700
3695 A[101]=ATN(A[100]/A[99])
3700 A[101]=A[101]*0.5
4000 A[102]=(A[99]*A[99]+A[100]*A[100])↑0.25
4005 A[103]=2*(A[93]*A[93]+A[94]*A[94])
4010 A[104]=A[102]*(A[93]*COS(A[101])+A[94]*SIN(A[101]))
4015 A[105]=(-A[93]*A[95]-A[94]*A[96]+A[104])/A[103]
4020 A[106]=(-A[93]*A[95]-A[94]*A[96]-A[104])/A[103]
4025 A[107]=A[102]*(A[93]*SIN(A[101])-A[94]*COS(A[101]))
4030 A[108]=(A[94]*A[95]-A[93]*A[96]+A[107])/A[103]
4035 A[109]=(A[94]*A[95]-A[93]*A[96]-A[107])/A[103]
4040 A[110]=LOG(SQR(A[105]*A[105]+A[108]*A[108]))
4045 A[111]=LOG(SQR(A[106]*A[106]+A[109]*A[109]))
4050 IF A[2]>2 THEN 4300
4055 A[112]=A[113]=0
4065 X1=A[108]
4070 X2=A[105]
4075 X3=A[112]
4080 X4=A[113]
4085 X5=A[25]
4090 X6=A[26]
4095 X7=A[35]
4100 GOSUB 5500
4105 A[108]=X1
4110 A[105]=X2
4115 A[112]=X3
4120 A[113]=X4
4125 A[25]=X5
4130 A[26]=X6
4135 A[35]=X7
4140 A[114]=A[115]=0
4145 X1=A[109]
4150 X2=A[106]
4155 X3=A[114]
4160 X4=A[115]
4165 X5=A[27]
4170 X6=A[28]
4175 X7=A[41]
4180 GOSUB 5500
4185 A[109]=X1
4190 A[106]=X2
4200 A[114]=X3
4205 A[115]=X4
4210 A[27]=X5
4215 A[28]=X6
4220 A[41]=X7
4230 GOTO 4700
4300 A[112]=A[113]=0
4305 X1=A[108]
```

FILE 4 (CONT'D)

```
4310 X2=A[105]
4315 X3=A[112]
4320 X4=A[113]
4325 X5=A[25]
4330 X6=A[26]
4335 X7=A[29]
4340 X8=A[30]
4345 X9=A[31]
4350 Y1=A[32]
4355 Y2=A[33]
4360 Y3=I2
4365 Y4=A[34]
4370 Y5=A[35]
4377 GOSUB 6000
4380 A[108]=X1
4385 F[105]=X2
4390 A[112]=X3
4400 A[113]=X4
4405 A[25]=X5
4410 A[26]=X6
4415 A[29]=X7
4420 A[30]=X8
4425 A[31]=X9
4430 A[32]=Y1
4435 A[33]=Y2
4440 I2=Y3
4445 A[34]=Y4
4450 A[35]=Y5
4455 A[114]=A[115]=0
4460 X1=A[109]
4465 X2=A[106]
4470 X3=A[114]
4475 X4=A[115]
4480 X5=A[27]
4485 X6=A[28]
4490 X7=A[36]
4495 X8=A[30]
4500 X9=A[37]
4505 Y1=A[38]
4510 Y2=A[39]
4515 Y3=I2
4520 Y4=A[40]
4525 Y5=A[41]
4530 GOSUB 6000
4535 A[109]=X1
4540 A[106]=X2
4545 A[114]=X3
4550 A[115]=X4
4555 A[27]=X5
4560 A[28]=X6
4565 A[36]=X7
4570 A[30]=X8
4575 A[37]=X9
4580 A[38]=Y1
4585 A[39]=Y2
4590 I2=Y3
4595 A[40]=Y4
4600 A[41]=Y5
4700 A[116]=(A[64]*A[110]+A[15]*A[112])/A[16]
```

C-2

FILE 4 (CONT'D)

```
4705 A[117]=(A[64]*A[111]+A[15]*A[114])/A[16]
4710 A[118]=(A[64]*A[112]-A[15]*A[110])/A[16]
4715 A[119]=(A[64]*A[114]-A[15]*A[111])/A[16]
4720 A[120]=A[17]*A[116]
4725 A[121]=A[17]*A[117]
4730 A[122]=A[17]*A[118]
4735 A[123]=A[17]*A[119]
4740 IF (ABS(A[122])-ABS(A[123]))>0 THEN 4800
4745 F=A[120]
4750 G=A[113]
4755 H=A[122]
4760 GOTO 4850
4800 F=A[121]
4805 G=A[115]
4810 H=A[123]
4850 GOTO A[43] OF 5300,5000,5000
5000 A[124]=EXP(A[65]*F)*COS(A[66]*F)
5005 A[125]=EXP(A[65]*F)*SIN(A[66]*F)
5010 A[126]=A[84]+A[88]*A[124]-A[89]*A[125]
5015 A[127]=A[85]+A[88]*A[125]+A[89]*A[124]
5020 A[128]=1+A[84]*A[88]*A[124]-A[84]*A[89]*A[125]-A[85]*A[88]*A[125]
5021 A[128]=A[128]-A[85]*A[89]*A[124]
5025 A[129]=A[84]*A[88]*A[125]+A[84]*A[89]*A[124]+A[85]*A[88]*A[124]
5026 A[129]=A[129]-A[85]*A[89]*A[125]
5030 A[130]=(A[126]*A[128]+A[127]*A[129])
5031 A[130]=A[130]/(A[128]*A[128]+A[129]*A[129])
5035 A[131]=(A[127]*A[128]-A[126]*A[129])
5036 A[131]=A[131]/(A[128]*A[128]+A[129]*A[129])
5040 A[132]=A[82]+A[86]*A[124]-A[87]*A[125]
5045 A[133]=A[83]+A[86]*A[125]+A[87]*A[124]
5050 A[134]=1+A[82]*A[86]*A[124]-A[82]*A[87]*A[125]-A[83]*A[86]*A[125]
5051 A[134]=A[134]-A[83]*A[87]*A[124]
5055 A[135]=A[82]*A[86]*A[125]+A[82]*A[87]*A[124]+A[83]*A[86]*A[124]
5056 A[135]=A[135]-A[83]*A[87]*A[125]
5060 A[136]=(A[132]*A[134]+A[133]*A[135])/(A[134]*A[134]+A[135]*A[135])
5065 A[137]=(A[133]*A[134]-A[132]*A[135])/(A[134]*A[134]+A[135]*A[135])
5070 A[138]=(A[130]*A[136]+A[131]*A[137])/(A[136]*A[136]+A[137]*A[137])
5075 A[139]=(A[136]*A[131]-A[130]*A[137])/(A[136]*A[136]+A[137]*A[137])
5080 A[140]=SQR(A[138]*A[138]+A[139]*A[139])
5085 A[23]=ATN(A[140])*57.29578
5090 A[91]=A[139]/A[140]
5095 A[92]=A[138]/A[140]
5100 A[141]=0
5105 IF A[92]<0 THEN 5150
5110 IF A[91]<0 THEN 5200
5115 A[141]=ATN(A[91]/A[92])
5120 GOTO 5230
5150 A[141]=ATN(A[91]/A[92])+3.141593
5155 GOTO 5230
5200 A[141]=ATN(A[91]/A[92])+6.283186
5230 A[24]=A[141]*57.29578
5300 RETURN
5500 IF X2=0 OR X2>0 THEN 5550
5505 X3=ATN(X1/X2)-3.141593-X5
5510 X4=2
```

FILE 4 (CONT'D)

```
5515 X7=4
5520 GOTO 5600
5550 X3=ATN(X1/X2)-X5
5555 X4=3
5560 IF X1=0 OR X1>0 THEN 5650
5565 X4=X4+1
5570 IF (X4-X7)<0 OR (X4-X7)>0 THEN 5750
5575 IF (X4-X7)=0 THEN 5700
5600 IF X1<0 THEN 5565
5605 IF X1=0 OR X1>0 THEN 5750
5650 X4=1
5655 A[142]=X4-1+X6
5660 IF A[142]=0 OR A[142]>0 THEN 5800
5700 X5=X5+6.283186
5705 X6=0
5710 X7=0
5720 GOTO 5550
5750 X6=-1
5800 RETURN
6000 IF (X8-1)>0 THEN 6010
6005 Y4=1
6010 IF X2=0 OR X2>0 THEN 6030
6015 X3=ATN(X1/X2)-3.141593-X5
6020 X4=2
6025 GOTO 6070
6030 X3=ATN(X1/X2)-X5
6035 X4=3
6040 IF X1=0 OR X1>0 THEN 6100
6045 X4=X4+1
6050 IF X6<0 THEN 6300
6055 IF X6=0 OR X6>0 THEN 6250
6070 IF X1<0 THEN 6045
6075 IF X1=0 OR X1>0 THEN 6250
6100 X4=1
6105 A[142]=X4-1+X6
6110 IF A[142]<0 THEN 6140
6115 IF A[142]=0 THEN 6300
6120 IF A[142]>0 THEN 6250
6140 X5=X5+6.283186
6145 X6=1
6150 IF (X8-1)>0 THEN 6170
6160 X9=2
6165 GOTO 6030
6170 IF Y4<0 OR Y4=0 THEN 6030
6175 Y1=2
6180 GOTO 6030
6250 IF (Y3-1)<0 OR (Y3-1)=0 THEN 6300
6255 X6=-1
6300 IF (X8-Y2)<0 OR (X8-Y2)>0 THEN 6360
6305 IF (Y1-X8)<0 THEN 6330
6310 IF (X4-1)<0 OR (X4-1)=0 THEN 6330
6315 Y2=0
6320 Y1=0
6325 GOTO 6390
6330 X3=X3+6.283186
6335 X7=X7-6.283186
6340 Y2=0
```

FILE 4 (CONCLUDED)

```
6345 X9=2
6350 Y5=4
6355 GOTO 6390
6360 IF (X9-X8)<0 OR (X9-X8)=0 THEN 6390
6365 IF (X4-1)<0 OR (X4-1)=0 THEN 6390
6370 X3=X3-6.283186
6375 X7=X7+6.283186
6380 Y2=2
6385 X9=0
6390 IF (X4-Y5)<0 OR (X4-Y5)>0 THEN 6400
6395 X3=X3-6.283186
6400 IF ((X8-1)*Y4)<0 OR ((X8-1)*Y4)=0 THEN 6410
6405 Y4=0
6410 RETURN
9999 END
```

ELLIPSOMETER DATA REDUCTION PROGRAM
FILE 5

```
1000 LINK 4,2500
1005 READ A[3],A[4],A[22],A[6],A[7]
1010 READ A[143],A[144],A[145]
1015 READ A[146],A[147],A[148]
1020 READ F1,F2,F3
1025 DISP "WANTX-Y PLOT?1=YES,2=NO";
1030 INPUT A[152]
1035 IF A[152]=2 THEN 1105
1040 DISP "INPUT DEL-MIN,DEL-MAX";
1045 INPUT H1,H2
1050 PRINT "X-AXIS LIMITS--DELTA";H1;H2
1055 DISP "INPUT PSI-MIN,PSI-MAX";
1060 INPUT V1,V2
1065 PRINT "Y-AXIS LIMITS--PSI";V1;V2
1070 SCALE H1,H2,V1,V2
1075 DISP "INPUT X-AXIS TIC INTERVAL";
1080 INPUT H3
1085 XAXIS V1,H3
1090 DISP "INPUT Y-AXIS TIC INTERVAL";
1095 INPUT V3
1100 YAXIS H1,V3
1102 A[153]=180
1105 K=L=G=H=A[23]=A[24]=A[25]=0
1110 A[26]=A[27]=A[28]=A[29]=A[30]=A[31]=0
1115 A[32]=A[33]=A[34]=A[35]=A[36]=A[37]=0
1120 A[38]=A[39]=A[40]=A[41]=0
1125 PRINT "OPTION NO. 3"
1130 PRINT "INDEX OF REFR. OF SURROUNDING MEDIUM IS";A[3]
1135 PRINT "ANGLE OF INCIDENCE IS"A[4]
1140 PRINT "WAVEL OF LIGHT IS";A[22]
1145 PRINT "INDEX OF REFR OF SUBSTRATE IS N31=";A[6];"N32=";A[7]
1150 E=A[143]
1155 D=A[146]
1160 PRINT "N21=";D;"N22=";E
1165 PRINT
1175 PRINT "THICKNESS","PSI CALC","DEL CALC"
1180 A[43]=4
1181 F=F1
1185 GOSUB 2500
1190 A[43]=5
1193 IF A[24] <= 350 THEN 1195
1194 A[24]=A[24]-360
1195 PRINT F,A[23],A[24]
1196 IF A[152]=2 THEN 1240
1197 IF A[153]>90 OR A[24]<270 THEN 1200
1198 PEN
1199 GOTO 1205
1200 IF A[153]<270 OR A[24]>90 THEN 1205
1201 PEN
1205 PLOT A[24],A[23]
1210 CPLOT -0.3,-0.3
1220 LABEL (*) "+"
```

```
1230  IPLOT 0,0
1235  A[153]=A[24]
1240  F=F+F3
1245  IF (F-F2)<0 OR (F-F2)=0 THEN 1185
1246  IF A[152]=2 THEN 1250
1247  PEN
1248  PLOT H2,V2,0
1250  D=D+A[148]
1255  IF (D>A[147]) THEN 1270
1260  GOTO 1160
1270  E=E+A[145]
1275  IF (E>A(141)) THEN 1290
1280  GOTO 1155
1290  RETURN
```